Interface Failure Under Local Normal and Shear Stress Conditions: Initiation and Propagation

by

Clarence Chui

B.S. in Mechanical Engineering
University of Michigan, Ann Arbor (1992)

Submitted to the Department of Mechanical Engineering
in partial fulfillment of the requirements for the degree of

Master of Science in Mechanical Engineering

at the

MASSACHUSETTS INSTITUTE OF TECHNOLOGY

January 1995

Author _____
Department of Mechanical Engineering
January, 1995

Certified by _____
Mary Boyce
Associate Professor of Mechanical Engineering
Thesis Supervisor

Accepted by _____
Professor Ain Sonin
Chairman, Departmental Committee on Graduate Students

Interface Failure Under Local Normal and Shear Stress Conditions: Initiation and Propagation

by

Clarence Chui

Submitted to the Department of Mechanical Engineering
in partial fulfillment of the requirements for the degree of
Master of Science in Mechanical Engineering

Abstract

The direct stiffness and kinematic constraint descriptions are two techniques which are studied numerically via finite element analysis for use in interface flaw initiation and propagation modeling. The advantages and the conditions required for the validity of each technique have been explored and their resulting behavior is compared to observed failure in particle filled epoxy tension specimens as well as epoxy thin film indentation samples. The direct stiffness description has an advantage in that phenomenalogically relevant parameters such as characteristic lengths and surface/interface energies can be explicitly incorporated but suffers due to its numerical instability when applied to systems with large interface to constituent stiffness ratios. The kinematic constraint description allows for the direct implementation of stress based interface failure criteria and offers numerical stability, but lacks the versatility of the former method and often produces physically unrealistic interface stresses due to the constraint conditions it imposes near the interface crack tip.

Acknowledgments

I would like to thank Professor Boyce for her patience, understanding, and excellent management style for which I have a difficult time believing she obtained from MIT. She has been hands on enough so that I actually get some things done(no matter how little) but laid back enough so that I can explore with a great amount of creativity. A big thanks to Simona for her introduction to the wonderful world of user element hell(getting those damn elements to "pop" is a pain). Without her help and notes I think I'd still be thumbing through the ABAQUS manuals. Also a very appreciative nod to Apostolos for his tip on resolving sudden singularities in the stiffness matrix(without that hint I would have been dead for the qualifier!). A big ol' thanks to the mechanics of materials crew and especially Christine Allan for helping me figure out all of the 2.30 lab problems and not giving me a hard time when a screwed up by crushing somebody's hand, foot, head, tongue, etc. in the Instron. Thanks to Srihari for our late night abstract talks which always made me think there was no hope to understand anything(it always started with, "what is force, really?"). Thanks to John, Ganti, Lin, Shjung, Lisa, Debbie, Hyung Yil, Vasily, Leo, Hong,, Jian, Alex, and (whoever I've left out 'cause I'm tired) for keeping me insane, by reminding me that no matter how esoteric our discussions became, someone could always say something more obscure.

Thanks to my roomates,young Brian(pasta and cheese boy), Dave(Poker freak, OREO addict, tomato soup worshipper with no neck), and John(I'm never home) Leung. Thanks for not being around the apartment much 'cause I like having the TV to myself and going through your stuff.

I would like to thank my parents who've put up with my sporadic moments of caring and selfishness. Without your love and support I may have ended up working for Graebel Van Lines for the rest of my life, not knowing how truly cool it is to thumb through books which cost more than what I can get for donating a cornea. I've always had the highest respect for you and hope you can continue giving me sage advice as I head on in life.

Finally, I'd like to thank Noma for coming into my life just at the right time to make it frantic and interesting just when I thought work could keep me busy enough. I'll never forget how hectic quals were with all the traveling every weekend and late night phone calls during the week. I think we own half of AT&T and the Peter Pan bus line. I hope we'll always be as close as we are now and I look forward to a bright future with you.

CONTENTS

Chapter 1: Introduction

1.1 Motivation

The desire to modify materials to serve highly specific functions requires a fundamental understanding of the basic processes that determine their behavior. One method of obtaining these desired features is by creating composite systems which utilize the best properties of various materials. However, the behavior of such multiphase systems, such as polymer composites, can be highly dependent on the state of the interfaces and the micro-processes occurring in their vicinity. These processes may include phenomena ranging from microscopic damage accumulation of the constituent materials near the interface to the migration of impurities such as surfactants from the bulk material to the interface surfaces. Understanding the direct effects of these interfacial processes, which may include debonding and fracture, can aid in the development of materials with controllable properties favorable for use in numerous small and large scale applications. The possible settings for these materials can vary from indentation resistance in multi-layer paint coatings to electrical/thermal insulation as well as micro-scale adhesion or lubrication. For example, the behavior of the interface contributes a great deal to the performance of integrated circuits where the thermal mismatch between the substrate and circuit can create conditions at the interface which eventually lead to its separation. Also, impact/shock loading of protective coatings can create high stress levels at the interface leading to the initiation of interface flaws which can propagate and hence negate the effectiveness of the coating. Finally, separation of the interface between a matrix and toughness/stiffness enhancing filler particles in composites creates voids in the material which serve as nucleation sites for bulk material fracture.

1.2 Scope of Work

The objective of this work is to investigate the applicability of several approaches to modeling interface failure in polymer composite systems and to assess the relative importance of relevant phenomena. Specifically, the work focuses on interface failure criteria derived from predominantly elastic systems and is limited to analysis as performed within the finite element framework. Other approaches(i.e. molecular dynamics, boundary integral equations, etc.) are not employed.

A brief review of the relevant works in interface mechanics and energetics is provided in chapter 2. The review primarily considers basic energy concepts as first proposed by Griffith and surveys the related advances in fracture mechanics and their application to interface fracture.

Chapter 3 proposes three methods of modeling the interface: a purely energy based approach, a stress based approach, and a hybrid stress-energy approach. The advantages and disadvantages of each approach as well as their formulation are discussed.

The goal of chapter 4 is to use the information gathered from experimental observations of epoxy tensile test specimens filled with glass beads to deduce an interface failure criteria. The experimental results allow for an indirect estimation of the interface energy through a finite element simulation of the experiment. This energy is directly incorporated in the hybrid stress-energy model and several interface traction-displacement functions are investigated. The feasibility of each of these functions is discussed in detail and the conditions under which the approach is applicable are determined. Finally, the estimated interface energy is indirectly used to deduce an interface stress failure criteria via energetic feasibility arguments. The sensitivity of this criteria to location of stress measurement, crack tip constraint, interface element density, and apparent stiffness of the surrounding material is discussed and a relationship between all of these parameters is established.

Chapter 5 attempts to determine the validity of the stress failure locus derived in chapter 4 by comparing the amount of energy released from interface failure during plane strain biaxial tension simulations to the interface energy previously calculated. Finally, the failure locus is applied in an indentation simulation and its results are compared to observations obtained from dead load indentation experiments. The discrepancies between the two results are noted and several mechanisms to explain their differences are proposed.

Chapter 2: Overview of Interface Mechanics

There has been extensive work done on the energetics and mechanics of the interface. The main developments are briefly presented. The discussion is restricted to systems where the amount of energy dissipated through inelastic deformation is negligible compared to the amount of elastic strain energy stored in the system. References are provided for a more extensive treatment.

2.1 Energetics

The global energy theory of Griffith[1,2] has been recognized as one of the basic governing principle's of interface fracture. In order to understand how the theory applies to bimaterial systems(i.e. the interface), the theory as it applies to homogeneous material systems is reviewed. Essentially, Griffith postulated that a material would fail in the event that it became energetically feasible to create a failure. The basic problem considered by Griffith was an infinite plate in tension with a finite sized crack normal to the axis of loading(fig.2-1). By calculating the energy potential of the body, the effect of advancing the crack on the body's potential could be calculated as, for example, discussed in Broek[16]:

$$\pi = U_{strain} - U_{work} + U_{surf}$$

where

$\pi \equiv$ energy potential of the body
$U_{strain} \equiv$ elastic strain energy stored in the body
$U_{work} \equiv$ work done by the externally applied forces
$U_{surf} \equiv$ surface free energy of the crack surfaces

When the rate at which the mechanical energy(strain energy and external work) could be released from the body exceeded the energy required to create new surfaces, the crack was postulated to advance.

i.e.,

$$\frac{\partial \pi}{\partial a} = \frac{\partial [U_{strain} - U_{work}]}{\partial a} + \frac{\partial U_{surf}}{\partial a} = 0$$

or

$$\frac{\partial [U_{work} - U_{strain}]}{\partial a} = \frac{\partial U_{surf}}{\partial a} \quad \text{during fracture}$$

For Griffith's analysis, the energy required to create the new surfaces only considered the surface free energy of the material. Strictly speaking, the analysis applies only for ideally brittle materials where the vast majority of energy dissipated during fracture is spent on surface free energy. Unfortunately, all materials dissipate some energy through inelastic deformation during fracture. As a result, the energy releases observed during fracture are much higher than the theoretical values, even for materials where the inelastic deformation is confined to a very small region near the crack tip(small scale yielding). Consequently, the energy release rate observed during fracture includes the contributions of all phenomena which are active during propagation and has been termed the critical energy release rate, G_c.

Orowan[3] proposed that the contributions of plastic deformation and surface free energy could be partitioned to provide a more accurate representation of the fracture phenomena:

$$\frac{\partial [U_{work} - U_{strain}]}{\partial a} = \frac{\partial U_{surf}}{\partial a} + \frac{\partial U_{diss}}{\partial a} = G_c$$

where

$U_{diss} \equiv$ energy absorbed by dissipative processes

Although this form of the energy balance equation is informative, in practice, the contribution of plastic dissipation to the fracture process is impossible to determine a priori. Thus there has been a great debate over the differences between intrinsic and apparent energy for fracture. The consequences of considering these differences are discussed later in this section.

The Griffith criteria basically states that fracture occurs when it becomes more energetically feasible to release energy from the body by creating new surfaces(which may

activate other dissipative mechanisms simultaneously) than to continue storing the energy in the body(fig.2-2).

The above arguments are also applicable to fracture of bimaterial systems, or interface fracture. The only difference is that the intrinsic energy of fracture of the interface considers the surface free energies of both materials and the interface free energy during adhesion. Specifically, the intrinsic energy of the interface is the sum of the surface free energies of the constituent materials minus the interface free energy of their combination[4].

i.e.,

$$W_{ad} = \gamma_a + \gamma_s - \gamma_{as}$$

where

$W_{ad} \equiv$ work of adhesion
$\gamma_a \equiv$ surface free energy of the adhesive
$\gamma_s \equiv$ surface free energy of the substrate
$\gamma_{as} \equiv$ interfacial free energy of the adhesive/substrate combination

This energy is also known as the work of adhesion[5]. The energy arguments directly apply to bimaterial systems. Again, the interface is assumed to fracture, or continue fracturing when the amount of energy released during crack propagation exceeds the amount required to create the new surfaces. Experiments have shown[6,7] that the amount of energy actually released during fracture far exceeds the theoretical work of adhesion(fig.2-3). There are two main reasons for the discrepancy. The first reason is the same one as stated for fracture of homogeneous materials. That is, the energy released during propagation is channeled simultaneously into inelastic deformation near the crack tip and surface creation. The second reason concerns the nature of the bonding at the interface. For many bimaterial systems, strong or primary bonds are formed at the interface or interface diffusion of the constituents creates a region where the materials are "interlocked". For these interfaces, the intrinsic fracture energy far exceeds the theoretical work of adhesion since it only accounts for the formation of secondary(van der Waals) bonds[8]. Hence intrinsic energy estimates should account for the types of bonds formed at the interface and the type of interface present.

Again, it should be stated that the difference between intrinsic and apparent energy is more than a matter of semantics. Intrinsic energy is defined as the energy required just to break the bonds of the interface to create the new surfaces. The apparent energy is the amount of energy

observed to be released during flaw propagation and can include the effects of many dissipative processes in addition to the work of breaking bonds[5,8]

Intrinsic energy is postulated to be unique to a material system and is independent of macroscopic geometry and loading type. The same is not generally true for the apparent energy. A more detailed look into the mechanisms that affect the apparent fracture energy of interfaces is discussed later in the context of stress analysis.

2.2 Stress Approaches

The problem of determining the stress field in a body with a Griffith crack(see fig) was initially approached by Williams[14] and Westergaard[15] and is reviewed in many texts. Williams solved the problem by using a real eigenfunction expansion of the governing biharmonic equation. By arguing that the energy at the crack tip should be finite, a series solution was determined where the first term in the series dominated the solution near the crack tip. Westergaard's complex variable approach using analytic functions eventually led to the same solution. The basic result of their analysis was that near the crack tip, the dominance of the first term of the solution implied that the behavior near the tip depended only on that term and hence the corresponding coefficient or stress intensity factor, K, determined the intensity or severity of the apparent stress singularity near the crack tip. This observation led to the notion of similitude of the crack tip stress fields. Similitude meant that the stress intensity factor(coefficient of the first term of the stress solution) was the sole determinant of the near crack tip stress fields. In other words, as long as the stress intensities for different loading situations and geometries were the same, the stress fields at the crack tips were identical. Different types loading configurations or "modes"(fig.2-4) of loading gave different stress intensities. The definition of these modes is developed in great detail in many basic fracture mechanics texts[16,17]. Since the analysis was based on elastic systems, the solutions obtained from different modes of loading could be superposed, giving rise to the idea of "mixed mode" loading situations where the contributions of different farfield loads to the near crack tip stress field could be unambiguously partitioned. As will be discussed in later sections, this is not necessarily true for bimaterial systems.

In practice, the determination of the energy state of a body requires a knowledge of the stress and strain fields present. General stress analysis of composite material systems(i.e. materials which have phases with different properties) has been performed by numerous authors. In the context of elastic analysis, contributors include Michel, Timoshenko and Goodier, Love,

Michel, Sokolnikoff[9,10,11,12] to mention only a few. The work of Dundurs[13] deserves special acknowledgment for it was his work that helped characterize interface fracture problems. Dundurs's work showed that for bimaterial plane stress or plane strain problems, the material mismatch at the interface could be characterized by two constants, α and β , defined as:

$$\alpha = \frac{\mu_1(\kappa_2+1)-\mu_2(\kappa_1+1)}{\mu_1(\kappa_2+1)+\mu_2(\kappa_1+1)}$$

$$\beta = \frac{\mu_1(\kappa_2-1)-\mu_2(\kappa_1-1)}{\mu_1(\kappa_2+1)+\mu_2(\kappa_1+1)}$$

where

$\mu_i \equiv$ shear modulus of material i
$\kappa_i \equiv$ bulk modulus of material i

α essentially measures the plane or tensile modulus across the interface and β measures the mismatch in the shear moduli across the interface. Figure 2-5 displays the values of α and β found for several common material combinations. Of the two parameters, only the shear modulus mismatch parameter, β, has a significant effect on the near interface stress fields. That is, the value of β determines the amount of shear/tension coupling at the interface. For example, non zero values of β in a bi-material system subjected to farfield tension will produce shear stresses at and near the interface, a condition not affected by the values of α, the tensile modulus mismatch parameter.

The work of the authors mentioned above implicitly assumed that the interfaces between the different constituents behaved ideally(i.e. continuity of stress across the interface and zero relative displacement/zero slip condition) The desire to determine the effect of cracks on the stress fields in previously simply connected bodies led to the development of modern fracture mechanics. Before discussing the implications of these stress analyses to the problems of interface fracture, several concepts of stress analysis in cracked homogeneous bodies is reviewed. The discussion is limited to systems with negligible inelastic deformation.

2.3 Connection Between Stress Intensity and Energy Release Rate

It was the work of Irwin[18] which made the connection between the stress intensities of Williams and Westergaard's stress fields and the energy release rates of Griffith's energy theory. In fact, he was able to show that the two approaches were equivalent and that the stress intensities and energy release rates were related by:

$$G = \frac{K_I^2}{E'} + \frac{K_{II}^2}{E'} + C\frac{(1-\nu)K_{III}^2}{E} \text{ for plane problems}$$

where

G = energy release rate

K_i = stress intensity for mode i

C = 0 for plane stress, 1 for plane strain

$E' = E$ for plane stress, $\frac{(1-\nu^2)}{E}$ for plane strain

This meant that critical stress intensities could be used to characterize the fracture behavior or "fracture toughness" of a material instead of the energy release rate. However, the toughness measurement determined from the stress intensity only gave an indication of the apparent toughness of the material. Hence different energy release rates could be observed when different modes of loading were applied. The role of "mode mixity" during fracture is reviewed by Hutchinson[19]. For plane problems, the relative contributions of farfield normal stress(mode I) and in-plane shear stress(mode II) are grouped into the mode mixity parameter, ψ, which is defined as:

$$\psi = \tan^{-1}\left(\frac{K_{II}}{K_I}\right)$$

By using crack growth in a direction parallel to the plane of the crack to determine a reference energy release rate, energy release rates for cracks growing in directions not parallel to the plane of the crack could be calculated[20]. Different values of mode mixity produced different crack angles at which the energy release rate would be maximized(fig.2-6). For these elastic systems, it was found that these "kinking" directions which maximized the energy release rates corresponded to crack tip conditions which were absent of any local mode II contribution. This observation led to interesting questions about the nature of interface behavior which will be addressed shortly.

2.4 The J-Integral

A major breakthrough in the fracture mechanics field occurred upon the observation of Rice[22] that by using the energy momentum tensor as defined by Eshelby[23], a path independent contour integral around a crack tip could be used to uniquely define the state of the crack tip under certain conditions. The integral was termed the J-integral and defined by(fig.2-7):

$$J = \int_{\Gamma} \left(w\, dy - \tilde{T} \cdot \frac{\partial \tilde{u}}{\partial x} ds \right)$$

where

w = strain energy density
u = displacement field
T = tractions along the contour

The J-integral was found to be uniquely defined for linear and non-linear elastic materials, hence allowing its use to be extended to deformation theory materials subject to proportional loading. Under these conditions, Rice was able to show that the J-integral was equivalent to the energy release rate concepts developed in linear elastic fracture mechanics. For elastic systems, the J-integral was also rigorously shown to be equal to the rate of change of the system's potential energy with respect to the rate of change of the crack length[17]. Hence the J-integral represented a significant generalization of the basic tenets of fracture mechanics by allowing the calculation of changes in potential energy with respect to crack growth regardless of the macroscopic composition of the system(i.e. composites, film/substrate systems, etc.) for elastic materials and deformation theory materials undergoing proportional loading.

2.5 Analysis of Bi-material Systems

Shortly after the pioneering work of Williams, Westergaard, and Irwin, the analysis of cracks in bimaterial systems was approached by Williams[21]. Again, by using an eigenfunction technique to solve the governing equation for a dual domain(fig.2-8), he was able to determine

the stress fields near the crack tip. However, the solutions did contain some interesting features. The stress and displacement fields along the interface displayed oscillatory behavior near the crack tip. The solutions suggested that the two materials interpenetrated one another an infinite number of times very near the crack tip which was physically impossible. Also, the stress field solutions showed that normal stress and shear stress were very strongly coupled provided the elastic mismatch of the materials was significant and that the amount of coupling depended on the distance at which the "farfield" stress was applied. Here, we mean that in the presence of a farfield tensile stress, the crack tip will have significant tensile and shear opening stresses. For mixed mode problems, this implied that the mode mixity was dependent on the distance which was chosen for its measurement. These difficulties, made the notions of similitude and mode mixity rather ambiguous.

Other bimaterial geometries were solved by Erdogan[24] and England[25] with similar observations concerning crack tip oscillations. It was noticed[26,27] that the Dundurs parameters which quantified the compatibility of the materials composing the interface could be directly used in crack tip solutions. Specifically, the crack plane shear compatibility parameter(β), gave an indication of the strength of the tension/shear coupling.

Comninou[27] modified the conditions of the original bimaterial crack problem as posed by Williams. Specifically, she altered the original crack face conditions which stated that the crack faces should be traction free. Instead, she allowed a small portion of the crack faces to come in contact while transmitting non zero normal tractions(fig.2-9). The result of this slight modification was to produce stress fields which exhibited the conventional $\frac{1}{\sqrt{r}}$ singularity observed in homogeneous body solutions.

The work of Rice[28] attempted to circumvent the difficulty the oscillatory behavior produced by determining the conditions under which the distance at which the oscillations initiated was much smaller than the crack length. The notation introduced by Rice, reduces the bimaterial solutions to the conventional ones(i.e. homogeneous system) in the absence of the material mismatch. By defining an oscillation parameter ε, a function of β,the interface plane shear mismatch parameter of Dundurs, and by introducing the complex stress intensity factor, the results from analysis of other interface problems could be reduced to a single compact notation where

$$\varepsilon = \frac{1}{2\pi} \ln\left(\frac{1-\beta}{1+\beta}\right)$$

$$\hat{K} \equiv \text{complex stress intensity factor} = \wedge T\sqrt{L}\, \exp\left[-i\,\varepsilon \ln\left(\frac{L}{r}\right)\right] = K_I + iK_{II}$$

where

$\wedge$ = complex number dependent on the mode mixity

T = applied traction

$i = \sqrt{-1}$

L = characteristic geometric length which scales with crack length

r = distance from the crack tip

Rice argued that for a fairly large range of ε, the size of the oscillation region was so much smaller than that of the crack that the behavior and its consequences could be ignored. Rice also addressed the problem of the mode mixity dependence on measurement distance. He suggested that a specific and convenient length away from the crack tip be chosen for evaluation of the complex stress intensity and that the length be a constant for a given material combination. Hence similitude was defined with respect to a specific distance. For example, the stress fields near the crack tips for two different geometries with different far field loadings were considered to be identical when the complex stress intensities were the same for both configurations at a fixed distance away from the crack tip.

With these definitions, the energy release rates for a crack propagating could be easily calculated[29]:

$$G = \frac{(1-\beta)}{E_*}(K_I^2 + K_{II}^2)$$

where

$$\frac{1}{E_*} = \frac{1}{2}\left(\frac{1}{\bar{E}_1} + \frac{1}{\bar{E}_2}\right)$$

$$\bar{E}_i = \frac{E_i}{(1-\nu^2)} \text{ for plane strain, } E_i \text{ for plane stress}$$

This reduces to the expression found by Irwin in the absence of mode III loading when β=0. As with homogeneous fracture, the energy release rates for a crack propagating out of the interface were analytically determined. Using the release rate during propagation along the interface as a standard measure, the angles of crack kinking which would maximize the energy release rates for various values of mode mixity were determined. The results suggested that the path traveled by an interface crack was determined not only by the direction in which the energy release rate was maximized but also by the relative fracture energies of the various possible paths. If the interface

toughness was sufficiently low, the crack would continue propagating along the interface even though the energy release rates might be higher if the crack turned into the matrix or the substrate.

Experiments by Evans et al[30] confirmed that this "competition" among possible crack paths was indeed determined by the relative toughness of the interface, matrix, and substrate. For relatively weak interfaces where crack propagation was confined to the plane of the interface, experiments indicated that the apparent energy release rates during crack propagation were much higher than theoretical predictions. Although the intrinsic fracture toughness of the interface was assumed to be invariant, it was shown that the observed energy release rate depended very strongly on the mode mixity even under conditions where small scale yielding was valid(fig.2-10). This strong effect of mode mixity during small scale yielding was partially addressed by Zywicz and Parks[31] through analysis of the effect of mode mixity on the development of interface crack tip plastic zones. Their work found that the shape of the plastic zone was significantly affected by variations in mode mixity, leading to the suggestion that the interface crack could be characterized by both the complex stress intensity factor defined by Rice and the interfacial load-phase angle(ILPA), a parameter which roughly determines the plastic zone shape and plastic zone boundary tractions.

Analysis by Fraisse and Schmit[32] and others[33,34] of adhesive joints using the J-integral attempted to verify its path independent nature and its utility in identifying the local mode I and mode II components[32]. Their work suggested that the J-integral could be used most effectively to determine an adhesive failure criteria under certain conditions which included a small adhesive thickness to crack length ratio, the use elastic materials or deformation theory materials subjected to proportional loading, and the use of an integral contour which enclosed the adhesive as well as part of the constituent materials(fig.2-11).

2.6 Possible Mechanisms Contributing to Discrepancies in Energy Release Rate

There have been many attempts to explain this discrepancy in the release rates and its dependence on mode mixity. In all cases, the authors explain the difference as being due to the presence of some energy dissipating mechanism which acts during the fracture process. Gent and Kinloch[31] provided a phenomenological explanation for polymer systems. They attempted to correlate the viscoelastic dissipation to the observed increase. Their formulation showed that in the absence of viscoelastic dissipation, the energy release rate of the system reduced to the intrinsic energy of the interface. The variation due to changes in mode mixity was explained as being a result of the changes in local stress state induced by varying far field loads.

Ballarini and Plesha[36] and Evans and Hutchinson[37] attempted to explain the difference as being due to asperity crack tip shielding. They suggested that the roughness of the interface surfaces act to bare a significant portion of the local loading, hence increasing the level of stress intensity required to further propagate the cracks (fig.2-12). Evans and Hutchinson claim that the amount of asperity shielding increases greatly as the mode of loading changes from a purely tensile to one of pure shear, similar to the phenomena a crack closure observed in fatigue experiments. Ballarini and Plesha suggested that the roughness behind the crack tip not only acts to shield the crack but also acts to dissipate energy through some sort of frictional work. They also show that as the severity of the asperities grow, the apparent energy release rates increase with an increase in farfield shear. Their calculations along with Evans and Hutchinson's are consistent with experimental observations.

Ungsuwarungsri[38] credited the effect of crack tip shielding due to micro scale damage ahead of the crack tip for increasing the apparent energy release rate. Micro scale damage of the matrix and/or substrate material ahead of the crack tip changes the compliance of the material in the crack tip region, hence relieving a significant portion of the local stresses and making it much more difficult to propagate the flaw(fig.2-13).

Liang and Liechti[39] also admitted the possibility that electro static forces behind the crack tip might be responsible for the discrepancy. The strength of these forces were calculated to be of the same order as the intrinsic strength of the interface.

Finally, Hutchinson and Tvergaard[40] explored the role of small scale plastic deformation. They found that the amount of energy dissipated through plastic deformation could be up to several times more than the intrinsic energy of the interface, thus producing steady state releases which were consistent with experimental observations. However, they did find that the amount of dissipation was rather sensitive to the parameters of their interface model. They also suggested that the sensitivity of the apparent steady state energy release rate to the mode mixity was due to the difference in sizes of the plastics zones for various modes of loading. For example, loading in farfield shear produced a larger plastic zone than one produced during pure tension. The larger plastic zone facilitated more energy dissipation, making it more difficult to propagate the crack.

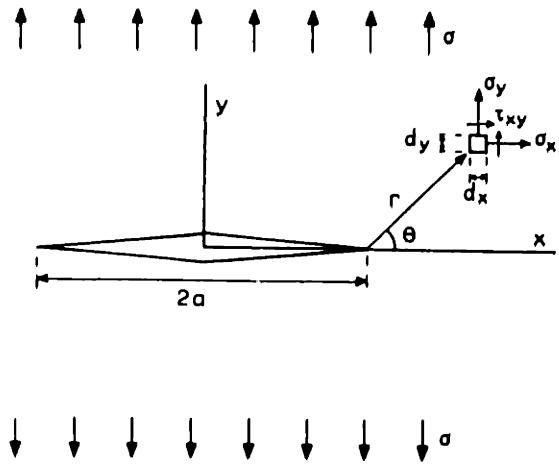

figure 2-1: Definition of a Griffith crack subjected to farfield tension

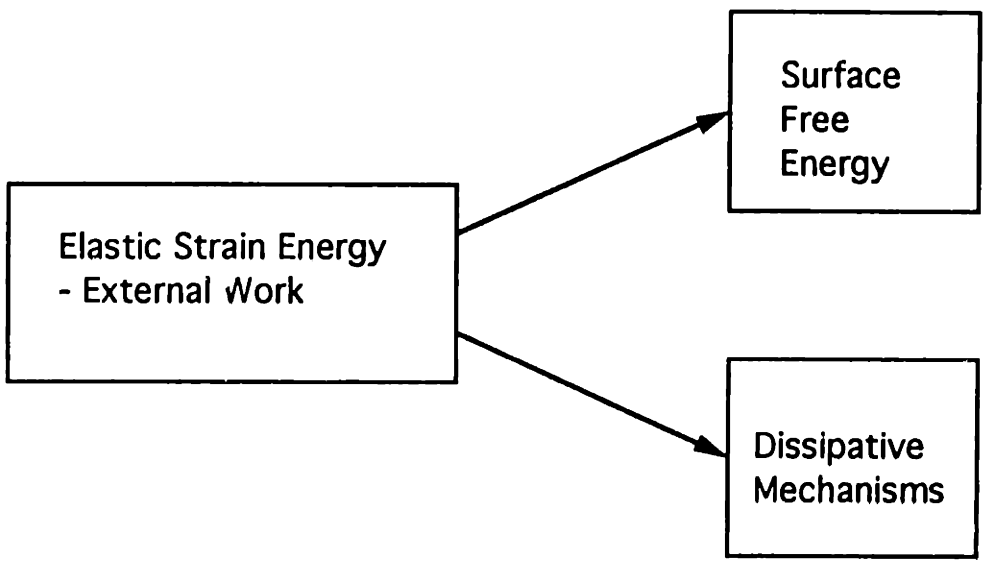

figure 2-2: Energy released during crack propagation is channeled into two directions: surface creation and dissipative processes. The portion channeled to surface creation is the intrinsic fracture energy

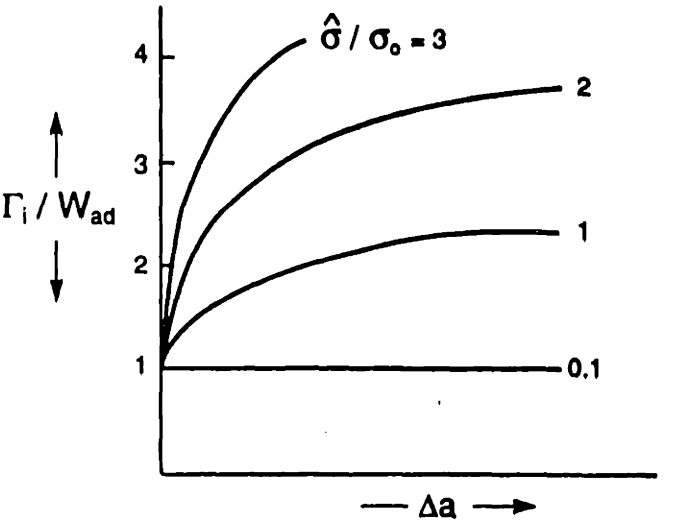

figure 2-3: Effect of yield strength on the interface fracture energy: σ_0 is the yield strength, $\hat{\sigma}$ the bond strength of the interface, and Δa the crack extension. Γ_i is the measure fracture energy and W_{ad} is the work of adhesion(intrinsic strength).

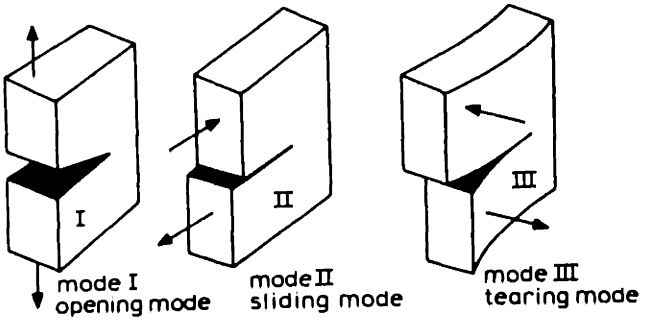

figure 2-4: Definition of the three basic fracture modes

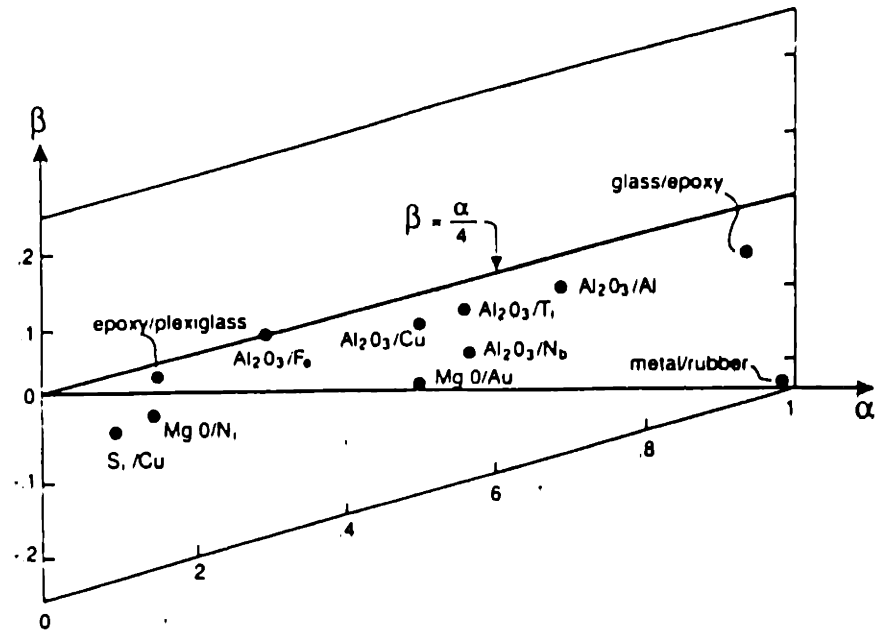

figure 2-5: Values of Dundurs parameters for several common material combinations.

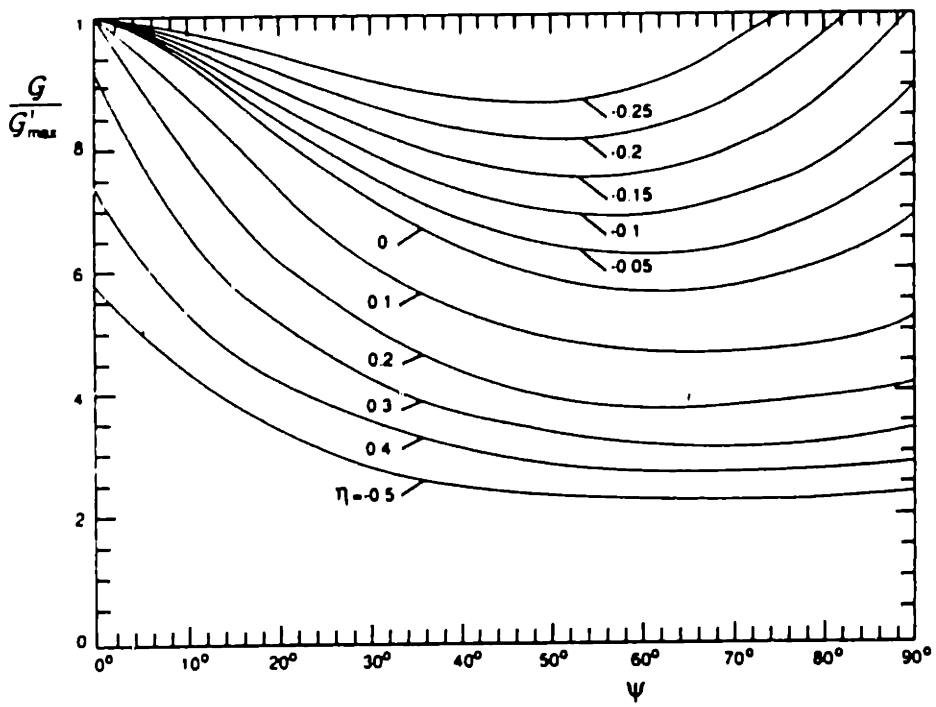

figure 2-6: Ratio of energy release rate for straight-ahead advance to maximum energy release rate for a kinked crack as a function of mode mixity, ψ. η is a measure of the T - stress.

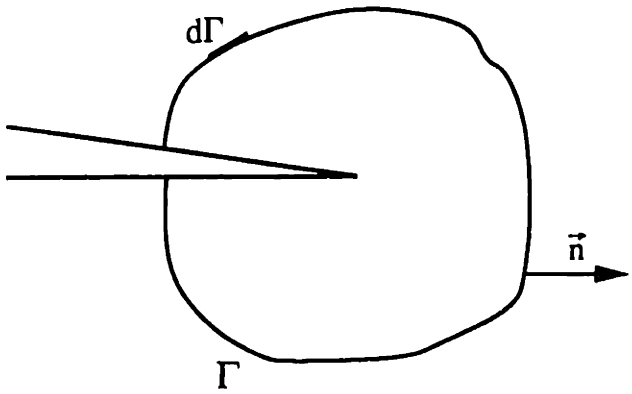

figure 2-7: Definition of the J-integral contour.

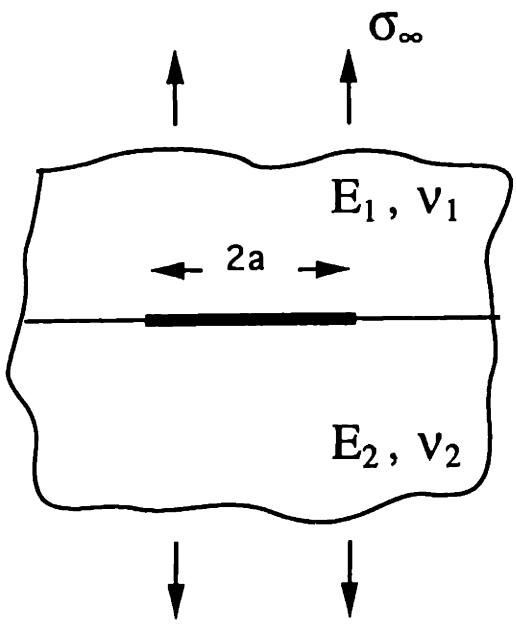

figure 2-8: Schematic of a bimaterial Griffith crack subjected to farfield tension.

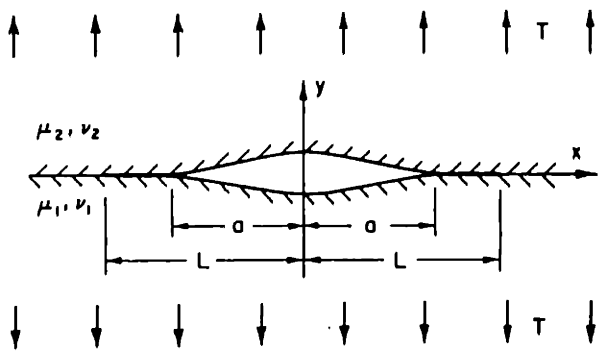

figure 2-9: The bimaterial crack formulated by Comninou. L is the true crack length and (L-a) is the length of the contact zone.

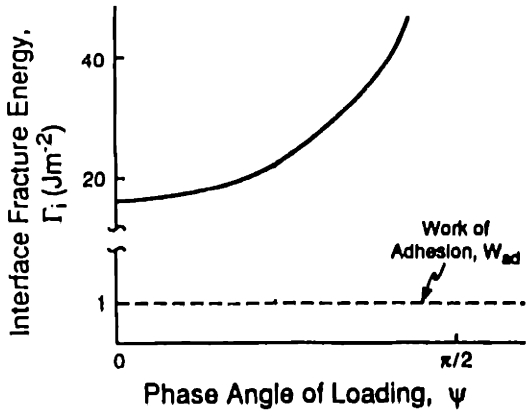

figure 2-10: Sensitivity of the apparent energy release rate to mode mixity, ψ.

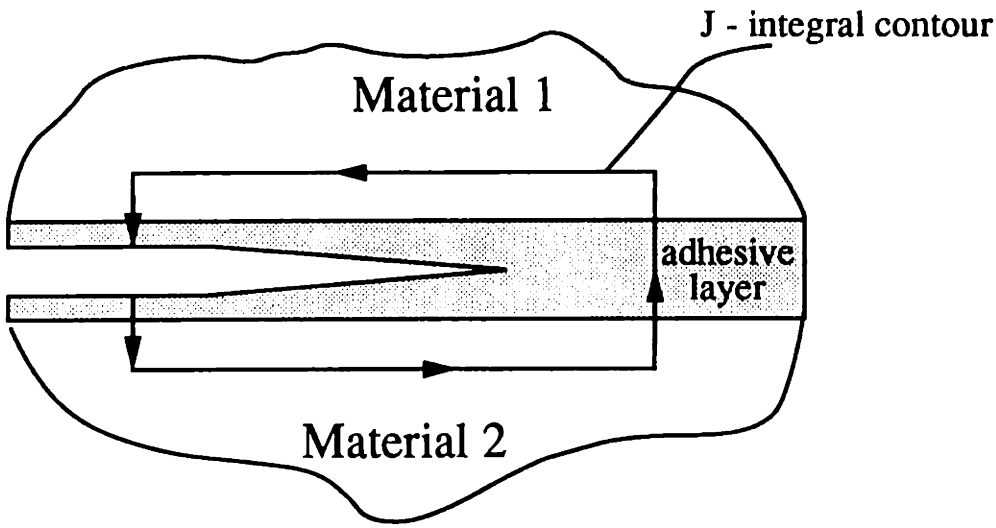

figure 2-11: Contour required for use of J-integral on adhesive joint.

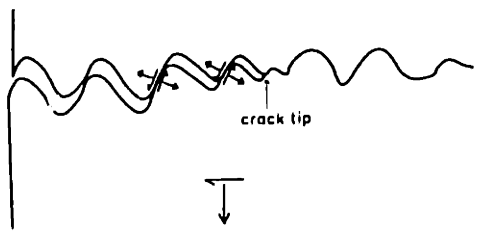

figure 2-12: Schematic of crack asperity shielding of the crack tip. The load carried by the asperities reduces the load at the crack tip.

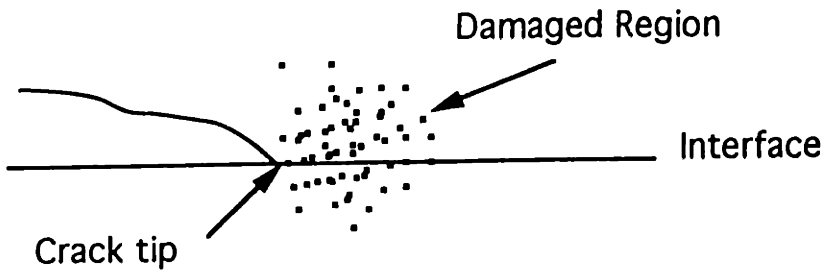

figure 2-13: - The damaged material in front of the crack tip shields it from the applied stress intensity

Chapter 3: Modeling Approaches

Various approaches for modeling interface failure are presented in this chapter. Specifically, three continuum formulations of interface behavior in the context of finite element analysis are discussed: purely energy based, local stress based, stress-energy based. Each of these formulations emphasizes different aspects of the interface behavior which can be exploited to create various interface failure criteria.

3.1 Assumptions

Developing a plausible interface failure criteria requires the acknowledgment of several basic assumptions. For all of the circumstances to be investigated below, three basic assumptions are made. First, the interface is assumed to be an inherent region of weakness, which implies that flaws nucleate and propagate on and along the interface only. The consequences of constituent fracture are not considered. Secondly, the interphase region, or material in the vicinity of the interface where the important mechanical properties may be some combination of the constituent properties, is assumed to be of negligible thickness, thereby eliminating the effects of property gradients or ,at most, lumping them into some continuum interface potential. Finally, the interface properties are assumed to remain constant, or independent of the state of deformation of the surrounding materials.

For polymer systems, this last assumption is in accord with the nature of the deformation mechanisms. Since constituent plastic deformation near the interface crack tip is primarily due to the rotation, sliding, and stretching of polymer chains and the interface bond is attributed to surface energy compatibility and possible mechanical interlocking, the amount of damage to the interface boundaries for polymer systems may be significantly less than those for metal systems where the primary mechanism of plastic deformation is dislocation motion. For metals, this defect motion may significantly alter the integrity of the interface by decreasing the local material density, thus reducing the local effective interface contact area. Under these assumptions, a suitable interface failure criteria is developed through three basic approaches.

The goal of this section is to create a numerical tool, based on presented approaches, that allows for an observation of the possible local and global causes and consequences of interface

failure. For this purpose, implementation of an appropriate model in the framework of finite element analysis is a first step towards exploring the relevant processes. By posing the models in a continuum form, the essential components of various relevant mechanisms, which may include polymer chain motion and diffusion, the effects of topology on the stress and/or strain state at the micro level, etc, are unfortunately "averaged" in that they are not explicitly taken into account. Although the actual processes affecting the interface behavior are inevitably tied to events occurring at the micro or atomic scales, for which a continuum method such as FEA is incapable of explicitly describing, general trends and globally observed behavior can be represented with reasonable accuracy through the imposition of kinematic constraints that allow imitation of interface behavior, the implementation of interface traction-displacement laws which may qualitatively mimic those found from atomic level simulations, or through the calculation of macroscopic energies.

Three basic approaches to modeling the interface are presented: energy based, stress based, and a mixed stress-energy based approach. Each of these approaches has advantages which can be exploited to help determine the relevance of various phenomena to the interface failure process. This information is then used to construct an applicable and phenomenological accurate representation of interface failure criteria.

3.2 Purely Energy Based Approach

By assuming that the majority of the interface toughness is attributed to the compatibility of the surface energies of the constituent materials, this approach dictates that interface failure occurs when interface energy is available. In other words, by obtaining a proper measure of the interface energy per unit area, an interface flaw can nucleate or an existing flaw can propagate when it becomes more feasible to release energy by creating new interface crack area than to continue storing or dissipating it as strain energy, plastic work, and other processes. By probing all possible deformation histories and allowing only the energetically feasible ones, a physically consistent failure history or "failure event sequence" can be constructed[41].

For the general case of possible constituent and interface fracture in an arbitrary geometry, this approach is inapplicable since all possible failures and all their consequences require exploration. Another difficulty arises when attempting to determine flaw initiation sites. Although it may be intuitively attractive to assume interface failure or failure initiation occurs when the strain energy density for a predominantly elastic system reaches a critical value in the

vicinity of the interface, this may not be entirely true and in the spirit of the global energy theory of Griffith[42]. It is possible that two very different modes of deformation (for example, local tension and local compression) produce the same value of local strain energy density yet have very different energy relief characteristics specifically during flaw initiation or propagation in these critical regions. However, for very special geometries, where the flaw initiation site and propagation history are constrained to follow a specific path, this approach of assuming a critical interface energy failure criterion can be used to deduce the local stress and strain histories during failure as will be shown in Chapter 4. This information may then be used in a more practical approach to develop a suitable model. A further explanation of this is presented later.

Numerical implementation

The purely energy based approach is appealing in that it follows one guiding physical principle: The system always acts to minimize its energy during various processes including elastic deformation, plastic dissipation, and interface failure. However, practically speaking, this is very difficult to explicitly implement in finite element analysis since it is unknown ahead of time when and where failures initiate and propagate[41]. A great amount of work has been done using the energetics of fracture on specific problems in elastic systems with pre-existing flaws[17]. Many of these solutions and their corresponding models can reasonably predict the onset of crack propagation. But again, the difficulty is in modeling the initiation and initiation to propagation transition behavior. For arbitrary geometries, where the site of flaw initiation is unknown, the required probing of all possible histories becomes unreasonably computationally intensive and time consuming.

3.3 Local Stress Based Approach

A seemingly more practical and applicable approach hypothesizes that interface failure initiates and/or propagates when the interface stress state(normal and shear) attains some critical values or combination of values[43]. By assuming stress to be the sole criteria for failure, the presence of other physical features and processes is implicitly assumed. It is implied that all "microscopic" material dimensions of the system (diffusion and interphase thicknesses, polymer chain lengths, surface roughness, etc) are so much smaller than other relevant geometric lengths (particle diameter, initial flaw size, interface and crack length), that the energetics are necessarily satisfied when the required stresses are attained[43]. Physically, this means that (1)the amount of strain energy and dissipative relief created by atomic or molecular scale separations is small

relative to the total amount of strain energy present in the system during failure's, and that (2)flaw initiation and propagation are clearly defined processes which are both locally governed by the same critical stress state. This last statement simply implies that the contribution of build up is not significant or influential to the occurrence of flaw initiation/propagation(i.e. discrete areas of interface surfaces are suddenly created). The interface flaw is either fully bonded or completely separated. Thus locally unstable growth is the only type of growth allowed[43].

Although this method seems very easy to implement, the main difficulty is in obtaining a suitable stress or stress state for failure which is energetically consistent. For example, although the interface can fail(flaw initiation or propagation) while subjected to various stress states(i.e. pure shear, pure tension, mixed loading), the total amount of energy released(elastic strain energy minus dissipation) during the process should be sufficient to create the new interface crack surfaces. Finally, there is the difficulty in determining exactly where the interface stresses should be measured(i.e. at what distance from the crack tip in the case of crack propagation). This difficulty arises because of the ambiguity at the microscopic scale as to where the near crack tip material can be considered a continuum and where it must be explicitly treated as a non-continuum system(i.e. there may be processes such as damage accumulation and impurity diffusion near the crack tip which may significantly influence the interface behavior but cannot be adequately describe through a continuum model). The assumed location of the non-continuum material can have a significant affect on the continuum behavior. With the above restrictions in mind, it seems that this approach is limited to large scale systems and is inappropriate for use in studying atomic level phenomena[48].

Numerical implementation

In this method, the interface behavior is not explicitly dictated by energy considerations and hence a stiffness description of the interface is not required. Instead, the interface is held together via a kinematic constraint enforced by Lagrange multipliers. The Lagrange multipliers not only maintain numerical stability of the system but also physically represent the interface tractions required to enforce the constraint[44].

The formulation is as follows:

Assuming a domain consists of two different materials joined at an interface boundary(fig.3-1), the interface surfaces are denoted by Γ_1 and Γ_2.

Equilibrium is stated as,

$$\frac{\partial \sigma_{ij}}{\partial x_j} = 0$$

A kinematic constraint is introduced where the displacement of one interface surface is written as a function of the displacement of the opposite interface surface -

$$u_{\Gamma_1} = f(u_{\Gamma_2})$$

These two residuals are posed in integral form:

$$\int_{Vol} \sigma_{ij} \frac{\partial \delta u_i}{\partial x_j} dV = \int_{Surf} n \cdot (\sigma_{ij}\, \delta u_i)\, dS$$

$$\int_{Vol} \lambda\, (u_{\Gamma_1} - f(u_{\Gamma_2}))\, dV = 0$$

where λ is a Lagrange multiplier introduced to enforce the constraint residual

Posing them in discretized form gives[45]:

$$\begin{bmatrix} [K] & \vec{e}_i \\ \vec{e}_i^T & 0 \end{bmatrix} \begin{bmatrix} \vec{u} \\ \vec{\lambda} \end{bmatrix} = \begin{bmatrix} \vec{F} \\ \vec{f}(u_{\Gamma_2}) \end{bmatrix}$$

$[K] \equiv$ system stiffness

$\vec{F} \equiv$ externally applied forces

$\vec{e}_i \equiv$ vector corresponding to the ith λ. All of its components equal zero except for the ith one, which equals 1

For the present analysis, the sole constraint function considered is $u_{\Gamma 1} = u_{\Gamma 2}$ (the closed interface). Interface failure occurs when λ or a function of λ reaches a critical value. At that point, the constraint is relaxed and the interface is allowed to separate. In order to enhance the numerical stability during the process, a very small residual stiffness is allowed between the two interface boundaries to eliminate the effects of the unavoidable singularity appearing in the

global stiffness matrix immediately after release. The main difficulties include construction of a suitable stress failure criterion, the method's inability to model micro or atomic scale systems as previously mentioned, and the excessive amount of constraint that the Lagrange multipliers introduce to the interface. In the presence of a crack tip singularity, this "pinning" of the crack may produce artificially high crack tip stresses which are sensitive to mesh size effects, thus degrading the reliability of the model.

3.4 Stress-Energy Based Approach

Finally, a combined stress-energy based approach explicitly accounts for energy and stress requirements simultaneously. This is possible by describing the interface as having an energy state or potential where the equilibrium position is achieved when the interface is fully bonded. Any relative displacement of the interface from this position immediately forces the system out of equilibrium, hence generating normal and shear tractions along the interface that attempt to restore equilibrium[46]. In the event that the amount of work done to separate the interface exceeds a critical value, the interface is allowed to debond. All interface displacements prior to the attainment of this failure criteria are fully recoverable. The approach allows for an explicit calculation of the work done on the interface, and hence a measure of interface energy, as well as a calculation of corresponding tractions(normal and tangential).

The approach implies that all size scales are subject to analytical/numerical investigation merely by changing the characteristic lengths embedded in the formulation of the potential[46]. Atomic level size scales as well as macroscopic size scales such as characteristic topological and diffusion lengths are easily incorporated. Also, the effects of the specific form of the interface potential and tensile/shear behavior coupling effects are readily explored. Unfortunately, the actual form of the interface potential and its corresponding characteristic lenghts are currently not directly measurable quantities. However, for a given form of potential, it is possible to deduce the lengths from estimates of interface energies and critical stresses[46]. Finally, due to the complexity of the formulation(i.e. the interface Jacobian needs to be continuously computed) and the poor physical conditioning of the system(i.e. the typically high interface to matrix stiffness ratio leads to poor numerical conditioning of the finite element stiffness matrix), the approach is difficult to implement.

Numerical implementation

This method's versatility and fairly comprehensive coverage of relevant phenomena make it an appealing choice for modeling interface behavior.

The finite element implementation of this approach, first formulated by Needleman[46] and used by several others[47], is briefly summarized:

Needleman proposes that an energy state or potential, ϕ, be used to determine the character of the interface. In finite element form, this potential is implemented in each element along the interface and is a function solely of the relative normal and tangential interface displacements(fig.3-2).

Tractions induced to restore the interface to equilibrium are determined by the gradient of the potential with respect to the two displacement components which are non-zero away from equilibrium. There are an infinite number of choices for potentials. For example, one of the most common ones is the Lennard-Jones potential which is described by the function, $\phi(u) = \phi_o \left[\left(\frac{u_o}{u}\right)^{12} - 2\left(\frac{u_o}{u}\right)^{6} \right]$ where ϕ_o and u_o are the minimum potential energy and equilibrium distance values respectively (fig.3-3a). The corresponding traction-displacement curve is given in figure 3-3b and is found by differentiating the potential with respect to the displacement. By truncating the effective distance of this potential, the functional form can be used to describe the energy state of an interface. The defining parameters of this truncated function include a characteristic length(i.e. truncating distance), δ, and the peak traction, T_{max}, for the traction-displacement curve. Debonding occurs and all interface tractions are set to zero when a critical amount of work on the interface is exceeded. The derivation is shown below. The stiffness of the interface is found by calculating the Jacobian or linearized stiffness which corresponds to the potential:

$$\phi = f(u_n, u_t) \text{ with defining parameters, } \delta_n, \delta_t, T_{n_{max}}, T_{t_{max}}$$

$$T_n = \frac{\partial \phi}{\partial u_n}$$

$$T_t = \frac{\partial \phi}{\partial u_t}$$

where T_n = normal traction on the interface

T_t = shear traction on the interface

The components of the Jacobian are then calculated by:

$$J_{ij} = \frac{\partial T_i}{\partial u_j}$$

The Jacobian and calculated tractions are directly implemented into finite element analysis with the Jacobian as the element stiffness and the computed tractions as interface nodal reaction forces with interface displacements being incorporated as solution variables.

i.e.

$$\begin{bmatrix} \frac{\partial T_n}{\partial u_n} & \frac{\partial T_n}{\partial u_t} \\ \frac{\partial T_t}{\partial u_n} & \frac{\partial T_t}{\partial u_t} \end{bmatrix} \begin{bmatrix} u_n \\ u_t \end{bmatrix} = \begin{bmatrix} \sigma_n \\ \sigma_t \end{bmatrix}$$

↑ corresponds to Jacobian

↑ corresponds to nodal forces

This method's biggest disadvantage originates from the relative stiffness of the interface and the surrounding material. Essentially, since the characteristic distances of the polymer interface are on the order of chain lengths(hundreds of nanometers), the corresponding interface stiffness becomes many orders of magnitude greater than the stiffness of the surrounding material, leading to difficult numerical convergence. For example, using the truncated potential proposed by Needleman[46], $\phi(u) = \frac{27}{8} T_{max} \delta \left(\frac{u}{\delta}\right)^2 \left[1 - \frac{4}{3}\left(\frac{u}{\delta}\right) + \frac{1}{2}\left(\frac{u}{\delta}\right)^2\right]$ with T_{max} on the order of 100Mpa and ϕ_{crit} on the order of .1J/m^2, produces a characteristic length on the order of 1 nm which corresponds to an initial interface area stiffness on the order of 1 x 10^8 GPa/m. By characterizing the matrix material geometry by a length of 100 μm(i.e. particle diameter or coating thickness), an epoxy matrix with a Young's modulus of 3GPa can have an effective area stiffness on the order of 1 x 10^3 GPa/m, hence producing an interface to matrix stiffness ratio of approximately 10000 to 1 Also, since interface failure is determined by an energy parameter, the elements may be required to debond while supporting large tractions. This sudden debonding in the presence of large tractions leads to instantaneous and dramatic changes in the global stiffness which further hinder "computational smoothness". The number of parameters required

(characteristic lengths, peak stresses, critical energy) as well as the unknown form of the potential make it especially difficult to ensure reasonably accurate behavioral predictions. Finally, as stated earlier, several of these quantities(form of potential, characteristic lengths) are currently not directly measurable[5]. Instead, they must be inferred from macroscopic observations. In spite of these difficulties, with suitable modifications, the method can still be useful for modeling the interface as will be shown later.

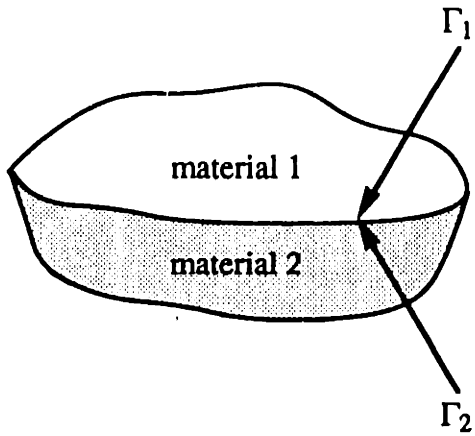

figure 3-1: Two materials joined at a common boundary

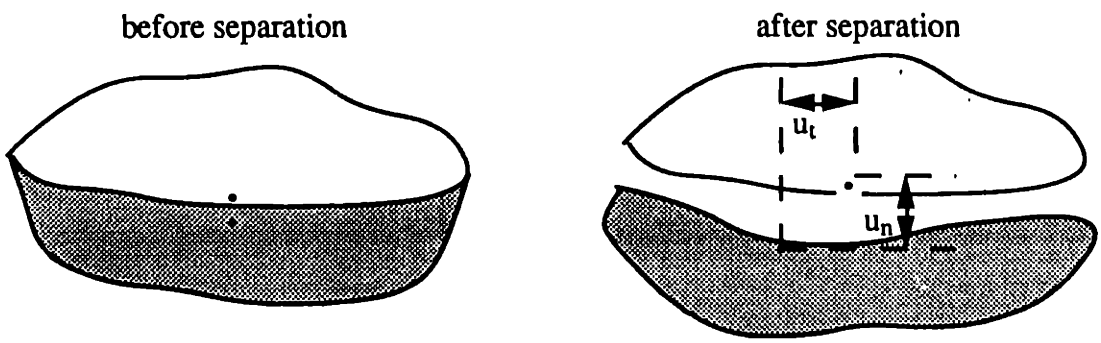

figure 3-2: schematic of definition of relative normal(u_n) and tangential(u_t) interface displacements.

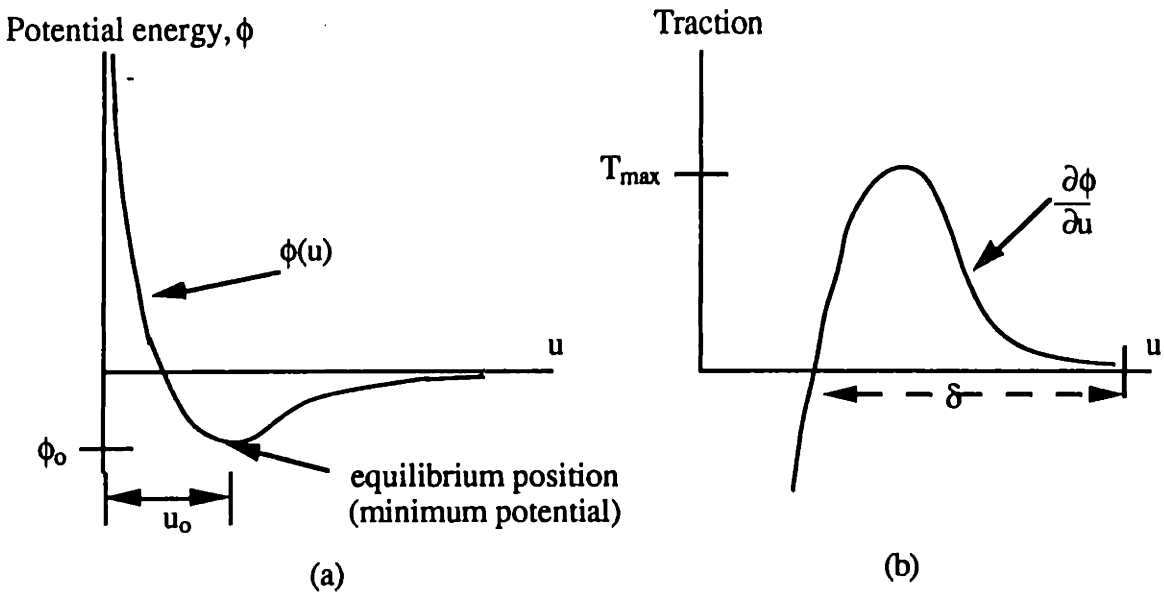

figure 3-3: (a) schematic of the Lennard-Jones potential. (b) corresponding traction-displacement curve

Chapter 4: Obtaining Criteria from Experimental Observations

Although the different methods described in chapter 3 are well suited towards modeling various aspects of the interface behavior, the objective of developing a tool which can be used to reasonably represent the failure behavior of the interface requires careful employment of a physically accurate and quantitatively consistent failure criteria. In principle, a proper criteria is obtainable through a combination of inference and direct observation of experiments. However, as will be discussed below, such criteria are actually quite difficult to obtain and/or quantify.

Background on Interface Experiments

The majority of current experimental work focuses on obtaining the interface work of adhesion/energy, a quantity which encompasses enough information about the interface in order to characterize it. The difficulty in the current experiments is the formidable task of distinguishing between the inherent and apparent energy of the interface. The former characterizes the inherent strength of the material bonding while the latter contains information about the specimen geometry, topology, and other experiment dependent factors. The experiments currently used to study interfaces can be broadly grouped into two categories. One category attempts to deduce the interface work of adhesion through the observed propagation of a pre-existing flaw. The second category attempts to deduce initiation phenomena by employing experimental configurations which do not contain pre-existing flaws. The following is a brief description of some of the experiments in both categories:

experiments which exploit the behavior of pre-existing flaws

There are numerous experiments which attempt to exploit the behavior of pre-existing flaws. Among these are the peel, blister, constrained blister, mixed mode flexure, Brasil, composite cylinder, and double cantelever beam tests. These experiments have much in common in that they all attempt to deduce the interface work of adhesion through an energy balance argument(i.e. during flaw propagation the change in strain energy minus the external work rate should equal the interface work of adhesion) and are hence most effective when applied to inherently elastic systems.

The peel test is widely used to characterize the interface strength of adhesives(fig.4-1)[49]. The end of the sample is pulled until the film "peels" off of the substrate. The test is

appealing in that it is simple to perform. The toughness or characteristic energy release rate of the interface is inferred by computing the amount of work performed by the external load. Unfortunately, for most polymer systems, the majority of the work which is performed by the external load is absorbed by the polymer film in the form of plastic and/or viscoelastic dissipation, thus making it difficult to determine the portion of the work spent on creating the new surfaces[5].

The blister and constrained blister tests induce flaw propagation through pressure loading of thin films(fig.4-2) and facilitate the computation of the interface work of adhesion by observing the change in compliance of the film during the process. The experiment has difficulty because perturbations in the diameter of the flaw are unstable, leading to bifurcations in the outer crack shape(fig.4-3)[50] and the inevitable plastic deformation of the film complicates energy calculations.

The mixed mode flexure, Brasil, composite cylinder, and double cantelever tests(fig 4-4) are all variations of the same test. They all attempt to deduce the interface work of adhesion by observing changes in compliance[51]. Unfortunately, they all suffer from the drawback that their complex geometries are not conducive for rigorous analysis(i.e. closed form solutions for the stress/strain fields are difficult to obtain) due to the stress concentrations created by their geometry. The complex stress fields which arise from these geometries usually induce plastic deformation further making it difficult to distinguish between energy dissipation and energy absorption mechanisms[5].

experiments which are "initially flawless"

The second category of experiments employ interfaces which are initially "perfect"(i.e.they are assumed to have no initial macroscopic flaws). These experiments are similar in that they all attempt to determine a critical stress which corresponds to flaw initiation. Among these are the direct pull-off, lap shear, scratch, and indentation tests.

The direct pull-off is a conceptually simple test which basically attempts to directly measure the tensile stress applied to the interface(fig.4-5). The test suffers due to the complex stress fields which form because of the general film/substrate elastic mismatches and constraint as well as specimen edge effects[52], making interpretation of the behavior difficult. A closely related test to the direct pull-off test is the lap-shear test(fig.4-6). The test attempts to measure the critical shear stress applied to the interface required for flaw initiation. This test too suffers from the complex stress field developing from the elastic mismatch of the film and substrate and from the stress concentrations due to end effects[53].

The indentation test is similar to the lap-shear test because it also attempts to determine the shear stress required to initiate an interface flaw(fig.4-7). It has the advantage over the lap-

shear test of not having any geometrically imposed singularities such as edge effects or sharp shape changes. The test has the disadvantage of generally causing the system to undergo significant plastic deformation during loading, making analysis of the whole process difficult[54]. Also, the high compressive stresses imposed on the interface make the contributions of interface topology to the apparent strength of the interface more prominent(i.e. the surface roughness may act to suppress flaw initiation)[5]. More will be said about this test during presentation of a numerical simulation of the indentation process in the next chapter.

The scratch test differs from the previous tests in that it attempts to determine the critical compressive film stress which causes the initiation of film delamimation. Compressive surface stresses are applied to the film by systematically dragging an indenter across the film(fig.4-8). The many disadvantages of this type experiment include the complex nature of the loading and the inherent difficulties in performing an accurate stress analysis which come with significant plastic deformation of the substrate[55].

4.1 Description of Present Experiments and Observations

The experimental portion of this work was performed by Dr. Andrew Zhuk under the supervision of Professor Robert Cohen at MIT with the monolayer interface construction performed by Dr. Zhuk at the department of chemistry at Harvard University with the cooperation of Professor Whiteside and the remaining sample preparation performed by Dr. Zhuk at MIT. The work described below is a summary of Dr. Zhuk's results.

The ideal experiment chosen for analysis is the tensile loading of an epoxy matrix filled with coated glass beads(fig.4-9). Aspects of the basic test procedure are given in [56] albeit for different systems than those discussed in this thesis. The initiation and evolution of the interface failure process is observed through an optical microscope and the corresponding specimen load-displacement information recorded by a data acquisition system. The matrix is composed of a standard thermoset epoxy and the glass beads have a uniform diameter of approximately 50 microns. Each bead is coated with a thin film in order to specifically tailor the behavior of the interface.

The film is created by evaporating a 10 Angstrom thick chromium film onto the beads, forming a high strength chemical bond. Next, a 70 Angstrom thick layer of gold is evaporated onto the chromium, also forming a chemical bond. Finally, a polymer monolayer of $(CH_2)_{15}$ is bonded to the gold. By varying the composition of the monolayer terminal groups and thus altering the resulting surface free energies, the strength of the interface is systematically increased

or decreased; both high surface free energy systems corresponding to a high strength interface and low surface free energy systems corresponding to a low strength interface were examined. The two terminal groups investigated are CH_3 , a low surface free energy group, and COOH, a relatively high surface free energy group(fig.4-10).

The beads are mixed with the pre-cured epoxy and poured into a mold in the shape of a thin strip with cross sectional dimensions of 4000 by 1000 microns. The specimens contain a .5% volume of glass beads. The mold is rotated to ensure uniform bead distribution and allowed to cure.

The interface is created such that the strength of the bond between the epoxy matrix and the monolayer terminal groups is based solely on secondary forces or surface and interface energy compatibility. The theoretical strength of the interface between the terminal group and epoxy is the sum of the surface free energies minus the interfacial free energy. CH_3 and COOH are selected as ideal terminal groups since their energies are low enough to allow for interface failure before large scale or even any microscopically noticeable local plastic deformation of the constituent materials occurs.

By pulling the specimen in tension and observing the behavior of the beads and the surrounding material through the optical microscope, the moment of interface failure initiation with respect to the applied far-field displacement is recorded. The subsequent propagation of the initial flaw is also noted until fast fracture of the specimen occurs.

The qualitative evolution of all of the interface failures is similar. An initial flaw nucleates at the top or bottom pole of a bead and proceeds to propagate along that hemisphere until a critical angle is reached. After further far-field displacement, another flaw initiates at the opposite pole and proceeds to propagate along the surface until it reaches an angle which is approximately the same as the final angle observed on the opposite hemisphere(fig.4-11).

The irregularities which inevitably appear throughout the experimental preparations and procedures (irregularity of bead shapes, tolerance of bead diameters, spatial distribution of beads, imperfect monolayer formation, etc.) manifest themselves in the statistical distribution of the timing and final angle of debonding for many beads and also account for the observed pattern of failure occurring on only one pole at a time on individual beads. The information obtained during this procedure includes the displacement and corresponding load applied to the specimen, the distribution of debonding occurrences and corresponding far-field loads, as well as the distribution of final debonding angles. Specimens with the CH_3 terminal group interfaces and COOH terminal group interfaces were individually tested with the corresponding failures shown in figure 4-12.

By utilizing this information, different assumptions about the interface can lead to the formulation of different interface failure criteria. Several assumptions are made in order to

simplify the analysis. The volume fraction of beads is such that in the case of perfectly homogeneous bead distribution, the effect of particle interaction is negligible(i.e. each bead is viewed as existing alone in an infinite media). In the actual specimen, beads intermittently group together. This grouping, which introduces various local constraint conditions to the beads, along with the inevitable nonuniformity of interface strengths, probably accounts to some extent for the statistical variation of failures[43]. As a first approximation, the effects of bead interaction as well as the residual stresses induced from contraction of the matrix during cooling(after the curing process) are neglected. These residual stresses are estimated to be on the order of 5-10MPa and can be approximately computed by assuming the particle is rigid and that the matrix is an infinite medium initially at a uniform temperature(i.e. the curing temperature). By also assuming that the thermal coefficient of expansion is invariant and of a typical value for epoxy (2.5×10^{-5}/K), the contraction stress on the particle can be calculated from elasticity using the equation[56]:

$$\sigma_{rr}(R) = \frac{2E}{(1+\nu)} \alpha \Delta T$$

where

R = radius of particle

E = Young's modulus(3GPa)

ν = Poisson's ratio(.35)

α = thermal coefficient of expansion

ΔT = temperature difference($\approx$75K)

With these assumptions, the entire system is modeled as a single glass bead in an epoxy matrix with interface properties which are the average of the distributions recorded from the experiments. The epoxy is modeled as having a Young's modulus of 3GPa and a Poisson ratio of .35. Also, debondings are observed to initiate well before the onset of plastic deformation in the matrix where the yield strength is taken to be 140 MPa as measured in a compression test of the matrix material. Hence the stress distribution around the particle before debonding is approximated through the elastic solution proposed by Goodier(see appendix). It should be noted that the volume fraction of beads is small enough that the farfield stress-strain response of the filled specimen differs negligibly from the stress-strain response obtained for the homogenous matrix material(fig.4-13a).

The normal interfacial stress at the top and bottom of the bead is defined as the pole stress and the pole stress(fig.4-13b) at the onset of interface failure is termed the debonding stress. For the specimen with the CH_3 terminal group interfaces, the average debonding stress is

calculated with the elastic solution as 30 MPa(corresponding to a farfield tensile stress of 15.5MPa) with an average debonding angle of 90° while for the COOH terminal group interfaces, the average debonding stress is calculated as 85 MPa(corresponding to a farfield tensile stress of 44MPa) with an average debonding angle of approximately 68°.

The results of the experiments of Dr. Zhuk allow for the deduction of several possible failure criteria. This is due to the fact that once debonding at the pole occurs, the crack propagates in the presence of both interface normal and tangential tractions. The goal of the remainder of this chapter is to determine which is the most applicable and accurate failure criteria through the use of the models presented in chapter 3.

4.2 Normal Stress Failure Criteria

The simplest criteria possible is the assumption that interface failure occurs when the normal stress at the interface attains some critical value[57], which in this case is the debonding stress calculated through the elastic solutions. The numerical model most readily adaptable to employing this criteria is the method of Lagrange multipliers or the stress-based method of chapter 3. The method imposes a kinematic constraint at the interface which maintains full "bonding" of the interface until the stress at the interface reaches the debonding stress at which point the kinematic constraint is released, allowing the interface to separate and hence simulate interface fracture. By setting up an appropriate finite element mesh to model the system, the validity of this simple criteria(that interface failure is independent of other stress components such as shear) is checked.

From symmetry considerations, proper boundary conditions allow the tensile test to be modeled via a single quadrant axisymmetric mesh of the unit cell system using bi-linear axisymmetric continuum elements. Specifically, the left boundary(x=0) is constrained only to move in the y-direction, the bottom boundary(y=0) is constrained only to move in the x-direction, the y displacement of the top boundary is constrained to follow the y displacement of the node in the upper left hand corner, while the x displacement of the right boundary is constrained to follow the x displacement of the node in the upper right hand corner(fig.4-14). The farfield forces are obtained through the upper left hand node through which the farfield displacement is imposed monotonically. The glass bead is modeled as an isotropic linear elastic solid with a Young's modulus of 100GPa and a Poisson ratio of .33. Compression tests of the matrix material(epoxy) at several strain rates indicate that the material is rate dependent(fig.4-15) with the rate dependency

being most significant during plastic deformation. However, since the beads are observed to debond before the onset of macroscopic plastic deformation of the matrix, modeling the epoxy as a rate independent elasto-plastic material is a reasonable assumption. For cases where significant plastic deformation occurs during flaw initiation and subsequent propagation, the use of a rate dependent plasticity(i.e. visco-plastic) constitutive model for accurate representation of the failure process is necessary. This is due to the notion that interface failure is a direct result of a favorable energy exchange, implying that all energy storing and dissipating mechanisms, which include plastic deformation and viscous damping effects, act together to determine failure[5]. For example, if the matrix is assumed to be rate independent for a large strain problem, its interface will tend to fail sooner than its viscoplastic counterpart since energy that should be released during interface failure as strain energy can only be dissipated through two channels(i.e. surface creation and plastic deformation) as opposed to the three channels available in rate dependent materials: surface creation, plastic deformation, and viscous dissipation(fig.4-16a,b).

results of normal stress criteria simulations

A simulation of the tension test with the CH_3 interface is performed, allowing the interface to debond at an interface normal stress of 30 MPa. The simulation shows that the interface flaw initiates at the pole(as observed in experiments) and proceeds to propagate along the bead(as observed). However, while the experimentally observed debonding angle reaches 90°, the one computed merely reaches 68° (fig.4-17). The corresponding farfield stress-strain response, evolution of the interface stresses, along with samples of the equivalent plastic strain of the system at times varying from prior to flaw initiation to the end of flaw propagation are shown in figures 4-18a through 4-18e. The labels on the figures denote various stages during the simulation with the number ordering corresponding to increasing farfield displacement. As can be seen from the interface stress evolution plot(fig.4-18b), the interface normal stress at the pole increases steadily until reaching the critical stress, 30Mpa, at which time an interface flaw initiates. The flaw quickly propagates until reaching 68° which denotes the angle at which the normal stress changes from tensile to compressive, a direct result of the Poisson contraction of the matrix which makes it "hug" the particle and creates the compressive stress. Hence, the crack does not propagate beyond this point since it is impossible to induce a tensile interfacial stress. It should be noted from the macroscopic stress-strain curve(fig.4-18a) that all of the flaw initiation and propagation occurs well before macroscopic yielding of the specimen. Although the experiment is terminated immediately after the onset of macroscopic yield due to bulk fracture of the specimen, the simulation is continued to determine if further deformation produces an interface stress state such that the crack can propagating beyond 68°(fig.4-18c). The

experimental observation that the CH_3 system continues propagating through the tensile/compressive transition(i.e. 68 ^{o}) and the high interface shear stresses at 68 ^{o} indicates that the shear behavior plays a significant role in interface failure and must be accounted for in the failure criteria either directly or indirectly. By calculating the equivalent plastic strain throughout the analysis, the role and amount of microscopically developing plastic deformation can be assessed. As can be seen from figure 4-18d, the plastic deformation in the specimen during the latter stages of propagation is limited to a very small region near the crack tip. This observation is important in that it provides an indication of how effective energy techniques, which depend on invariance to deformation history, can be in analyzing the interface fracture process. Figure 4-18e shows that significant plastic deformation develops only after onset of macroscopic yield.

Next, the same simulation with a failure stress of 85 MPa is run to approximate the tensile test with the COOH interface(fig.4-18f - 4-18j). As observed from the CH3 interface simulation, the pole stress progressively increases(fig.4-18g) until reaching the critical value, 85Mpa, at which point the flaw initiates and quickly proceeds along the bead until it reaches a debonding angle of 68 ^{o} as observed through the experiments. Again, it should be noted that al crack initiation and propagation occurs well before the onset of macroscopic yield(fig.4-18f). As in the CH3 case, the simulation is continued well beyond the point of bulk fracture from the experiment in order to assess the possibility of crack propagation beyond 68 ^{o} a possibility which is not evident because of the interface failure criteria employed(i.e. the normal stress failure criteria does not allow propagation beyond 68 ^{o} because of the Poisson contraction of the matrix: see fig 4-18h). As done previously, the equivalent plastic strain is computed throughout the simulation and found to be contained in a very small region near the crack tip(fig.4-17i). This limited localized plastic deformation facilitates the use of energy methods to analyze the interface fracture process as will be discussed later. Again, significant local plastic deformation is produced only after the onset of macroscopic yielding(fig.4-17j). It should be noted that by calculating the interface shear stress at the crack tip up to the moment when bulk fracture of the experimental specimen is observed, a lower limit on the interface shear strength($\cong$ 140 MPa) can be obtained since the crack is not observed to propagate beyond 68 ^{o} for the real specimen before bulk fracture. A comparison of the calculated farfield stress-strain curve and the experimental farfield stress-strain curve of the filled matrix is provided in figure 4-19. The figure indicates that there is a negligible difference between the experiment and simulation in the far field response up to macroscopic fracture(denoted in the figure by the X) of the real specimen which occurs shortly after the onset of macroscopic yielding. Also, for both the experiment and

simulation, the effects of particle debonding are not obviously detectable when looking at the far-field stress/strain curve.

The inability of the criteria to properly obtain the correct final debonding angle for the CH_3 system clearly indicates that some phenomena relevant to the interface failure behavior is neglected. The fact that the model correctly predicts the final debonding angle for the COOH system indicates that either the tensile strength of the interface is the dominant parameter governing failure or that compressive normal stresses coupled with a rough interface topology may act to suppress the continuing propagation of the crack in the presence of local shear since 68° is precisely the angle at which the interface normal stress changes from tensile to compressive due to the transverse contraction of the epoxy. Beyond 68°, an interface with a high shear strength and/or great amount of surface roughness may not allow a crack to continue growing[56]. The possibly significant role of shear in interface failure suggests that the use of another method to infer a physically realistic criteria is appropriate.

Although preliminary calculations were performed using the CH_3 interface to probe the applicability of energetic feasibility approaches to deduce interface failure criteria, the remainder of the work focuses on the behavior of the COOH interface system since the COOH interface is better suited for use in thin film indentation samples as will be discussed in the next chapter. The analysis of the CH_3 systems served to ascertain crack increment size effects which helped guide the analysis of the COOH systems.

4.3 Energetic Feasibility

4.3.1 Energetics of Fracture to Deduce Failure Criteria

Another possible criteria can be found by exploiting the energetics of interface failure. Although the direct application of the tools of fracture mechanics may not always be appropriate, since we are interested in crack **initiation** as well as propagation, Griffith's notion of the energetics of fracture is still applicable. In essence, his concept states that failure occurs when it is energetically feasible to do so. In the context of interface failure, an appropriate criteria allows the formation or propagation of flaws when the material system releases more energy by creating the new surfaces than it can continue to store and/or dissipate through other means. In most cases the direct application of this principle is nearly impossible as noted earlier, but its indirect use can be very helpful in characterizing the interface.

The basic quantity that is required before any interface modeling can be performed is some estimate of the interface work of adhesion or interface energy, Γ. Following the assumptions made in chapter 3, the variation of Γ is assumed to be essentially independent of the local mode of loading on the interface(i.e pure normal, normal-shear, or pure shear). Obtaining a reasonably accurate and consistent value is important in characterizing the interface. At this time we do not have an experimentally measured value of the interface. Therefore, a method for inferring the interface energy is described in the following sections.

The General Concept of Energetic Feasibility on the Context of this Work

Before discussing the technique used for deducing the interface energy, a discussion about the basic principles of energetic feasibility in the context of this work is briefly presented. The concepts of this discussion are consistent with the conventional views of energetics in fracture mechanics but are necessarily introduced since fracture mechanics techniques are not applicable to problems which may include flaw initiation; the study of which is an important part of this work.

The concept of energetic feasibility is a simple principle. It states that all events occur to minimize the total energy of a system. Examples of this principle include the application of Hamilton's Principle or the variational formulation of Newton's laws and the strain energy minimization methods of elasticity[58]. Fortunately, this principle can be further generalized and applied to many other situations.

For example, during plastic deformation of a body , there are an infinite number of ways that the body can deform such that equilibrium is maintained. However, the final shape and the intermediate configurations attained during deformation are such that the total energy of the system, which includes elastically stored strain energy, external work, and losses due to dissipative processes, is minimized throughout each infinitesimal increment of deformation. This has interesting implications. It suggests that given some external action on a system, like imposed displacements on a body, the body tends to deform only in the most energetically favorable manner.

For example, given an array of balls connected by springs, with several of the balls subjected to some imposed displacement, the correct resulting configuration is easily and directly found through an energy formulation(Castiglianos', etc.). Alternatively, it is also possible to probe all of the possible combinations of ball displacements and allow only the combination which stores the least amount of energy in the system(fig.4-20). This second approach seems very tedious and laborious at best. It implies that for any system subjected to an external influence,

every possible consequence of that influence must be explored in order to find the consequence which is energetically favorable. Another difficulty arises when time and/or history dependent processes such as plastic deformation, friction, and viscoelastic deformation are present, forcing exploration of every possible consequence in every possible sequence at every possible rate.

For systems other than the most trivial ones, this is clearly impossible. However, for systems in which the events are constrained to follow a particular "path", the method becomes feasible. For example, a purely elastic body containing a crack and subjected to arbitrary far-field loads can be analyzed with this method. It is well known that under certain conditions and while neglecting friction, the J-integral as proposed by Rice[22] determines the moment of initial crack propagation under the assumption that the favorable exchange of stored strain energy to surface free energy of the newly created crack area is the mechanism driving crack growth. However, the approach assumes that the direction of growth is known a priori and thus the J-integral must be calculated by allowing every possible crack growth direction. The correct direction alleviates more strain energy from the system than any other direction.(fig.4-21: The crack follows the direction of the longest arrow which indicates the greatest amount of strain energy released.) Approximately the same result is found by allowing the crack to turn in the direction of the highest strain energy density when friction is neglected[42].

Although the J-integral has been shown to be an effective means of determining the moment of crack propagation for materials modeled using deformation theory and subjected to proportional loading[17], the energetic feasibility approach is more general in that it is applicable to systems with significant frictional dissipation, non-proportional loading, and crack propagation, conditions under which the J-integral interpretation becomes invalid. Again, by maintaining that crack propagation is a result of the exchange of total energy with the surface free energy of the newly created crack area as proposed by Orowan[3], the direction and timing of crack propagation can be found.

Following figure 4-22, each contour represents one instant in time. The arrows indicate the magnitude of total energy released when the crack is incrementally moved in their direction at the time associated with their contour. By probing every direction at several different times, the arrow with the magnitude required to create the new surface at the earliest time indicates when and in which direction the crack grows[41]. All dissipative processes are allowed. Once the crack is allowed to incrementally grow in that direction, the process is repeated to find the next direction and time of incremental crack growth(fig.4-23).

The process becomes much simpler when the crack is constrained to follow only one path. This is frequently the case for systems with weak interfaces where cracks are often observed to grow only along the interface. The analysis for these systems becomes rather straight forward, since only the timing of the propagation events is required(fig.4-24).

4.3.2 The Use of Energetic Feasibility to Deduce the Work of Adhesion

By applying this technique to the epoxy/glass bead system, the work of adhesion is estimated. The information obtained from the experiments on the COOH system includes the debonding stress, calculated to be 85 MPa, and the debonding angle, observed to be 68 ^{o}. The assumption that the majority of the failure process occurs before significant plastic deformation ensues allows the calculation of the energy per unit area associated with the creation of new interface crack surfaces.

By running a finite element analysis of the previously proposed unit cell model and monitoring the pole stress, the strain energy of the region encompassing the bead and the portion of the matrix most affected by the bead's presence is calculated(fig.4-25a,b). The radius of this region corresponds to four times the particle radius which is approximately the distance at which the particle significantly affects the elastic stress/strain fields in the matrix.

By opening a discrete amount of crack area around the pole when the pole stress exceeds the debonding stress, the decrease in the system's strain energy due to the sudden appearance of this discrete crack area is observed(fig.4-26). Since all dissipative processes are assumed to be negligible, the effects of the sudden flaw appearance are thought of as the direct exchange of strain energy for interface energy. Therefore, the energy associated with the interface is simply $\Gamma = \Delta E / A$.

The assertion that there are no dissipative processes present implies that the actual size of the initial flaw can be varied within reasonable bounds with little affect on the resulting interface energy. All initial flaw sizes were found to approximately produce the same amount of interface energy/area. However, the finite element analysis is sensitive to mesh size effects. Large elements near the particle provide extra constraint of the matrix material, thus producing strain energy changes which are smaller that those predicted by a finer mesh for the same size initial flaw(fig.4-27). As the mesh density increases, the computed interface energy should converge to a steady value.

Several calculations are performed to attempt to estimate the interface work of adhesion and its sensitivity to the finite element mesh density. Throughout all of the calculations, it is assumed that the amount of energy dissipated through plastic deformation is negligible compared to the amount stored in the system. As in the analysis using the normal stress failure criteria, the symmetry of the system is used to model only one quadrant of the unit cell. The axisymmetric mesh uses quadratic elements for both the matrix and the particle. Noting that no macroscopic

yielding of the sample occurred before sample fracture, both materials are modeled as elastic with the same elastic constants as used previously(epoxy: E = 3GPa, ν = .35 ; glass: E = 100GPa, ν = .33), hence facilitating the use of energy methods which are most effective when the history dependence of the process is removed.

To ascertain the mesh sensitivity of the calculated work of adhesion, three different calculations are performed to estimate its value. The interface mesh density is progressively increased from 16 to 32 to 48 elements(fig.4-28) circumferentially surrounding one quadrant of the particle and the corresponding work of adhesion for each mesh calculated. By using an initial flaw size of 196 μm(measured from the pole of the particle:fig.4-29) which corresponds to 2,4, and 6 elements for the 16, 32, and 48 element mesh densities respectively, the interface energy for each case is estimated. This initial flaw size is chosen since it is contained along the region of the interface which is still predominantly subjected to pure tension. Any underestimate of the initial flaw size does not affect the calculations since in reality the crack would grow to that length anyway under essentially normal tensile failure conditions and hence, the proper behavior is captured within the calculation. However, if too large an initial flaw size is selected, then an overestimate of the crack length which would actually appear is made, leading to an underestimate of the interface energy. The results are shown below:

interface mesh density	16 elements	32 elements	48 elements
interface energy, Γ	.15597 J/m^2	.16008 J/m^2	.16310 J/m^2

These values seem to indicate that as the mesh density increases, the calculated interface energy increases and seems to converge to a value of the order of .16310J/ m^2 which compares to values on the order of .09 J/m^2 found for epoxy/aluminum interfaces[59]. The increase in the interface energy(work of adhesion) with increasing mesh density is simply explained as a result of crack tip constraint. That is, the coarse mesh, which has less degrees of freedom for a given area, is more constrained near the crack tip than finer meshes. In the absence of a singularity like a crack tip, the strain energy storage characteristics of all three meshes is nearly indistinguishable. However, in the presence of a crack tip, the increased constraint of the coarse mesh causes the system to store considerably more strain energy near the crack tip than the finer meshes. Thus, when the strain energy differences(which are a direct measurement of the interface energy) between the initially perfect interface and the interface with a finite sized flaw are calculated, they appear to be smaller for the coarse mesh than for the finer meshes. It should also be noted that for the same crack length, the different meshes predict failure at farfield stress values which are within 1.5% of one another.

4.4 Applying the Stress-Energy Model

4.4.1 Incorporation of the Interface Energy into a Stress-Energy Model

After obtaining an estimate of the interface energy, Γ, this value is directly used as the governing failure parameter in the stress-energy model presented in chapter 3. The model allows for permanent separation of the interface when the work of the tractions on the interface attains a critical value, the interface energy. Along with the interface energy, other information required to complete the model include the form of the interface potential, the peak normal and shear stresses allowed, and the characteristic lengths of the interface(.i.e. the effective distance over which the potential acts). The simplest form of this type of model uncouples the relative contributions of normal displacement and tangential displacement to the interface potential. The detailed steps required for the finite element formulation for the model are presented in the appendix and follow along the same lines first presented by Needleman[46].

The model basically describes the interface as having some energy state which is at a minimum(i.e. equilibrium) when the interface is fully bonded. Any disturbance of the interface(i.e. separation) from the equilibrium position induces tractions which try to force the interface back to equilibrium. Failure occurs when the externally applied stresses separate the two surfaces of the interface beyond the point from which the internally induced tractions can restore equilibrium. Quantitatively, this type of failure is described as occurring when the work performed by the interface tractions exceeds a critical value.

For simplicity, the potentials used in this work contain uncoupled contributions of normal and tangential tractions for simplicity. Also, the basic forms of the potential corresponding to shear and normal tractions are the same. It should be noted however, that any general form of potential is easily incorporated within the finite element framework.

The model basically assumes that any separation of the interface before failure occurs is elastic(reversible). In order to accommodate failures occurring under conditions of pure shear, the forms of the potential and the values of the required parameters are selected in a way such that interface failure is possible under conditions of pure tension, pure shear, or a combination of both. The three relevant sets of parameters incorporated in the model are the form of the potential, the characteristic lengths, and the peak tractions allowed. Failure occurs when the interface performs a critical amount of work(i.e. area under traction-displacement curve). From figure 4-30, it can be seen that under pure loading conditions(i.e. pure tension or pure shear), interface failure occurs when the area under the traction-displacement reaches the interface energy value. For the case of mixed loading(i.e. some combination of tension and shear), interface failure occurs when the

additive contributions of the tensile potential and shear potential reach the interface energy value(fig.4-31).

Since the forms of the tensile and shear potential are uncoupled, merely integrating the desired traction-displacement functions with respect to the corresponding displacements determines the value of the interface work. Four types of traction displacement functions are tested for their applicability towards modeling interface failure. A brief description of these functions along with their apparent advantages, disadvantages, and the results of their incorporation in the finite element framework to model the epoxy matrix/glass bead system is presented:

"Lennard-Jones" type

The first traction-displacement function investigated is one derived from a Lennard-Jones type potential with a truncated effective distance. The specific form of the traction-displacement function is given by:

$$\sigma_i = A \exp(-\alpha u_i) \sin\left(\frac{\pi u_i}{\delta}\right)$$

where

$\sigma_i \equiv$ interface traction

$u_i \equiv$ interface displacement

$\delta \equiv$ characteristic distance of traction-displacement function

$A \equiv$ scaling constant(scales with the maximum traction, σ_{max})

Both the tensile behavior and shear behavior are modeled using the above form which is shown in figure 4-32. Failure is assumed to occur when sum of the work done by the normal and shear tractions reaches the interface energy value which is given as $\Gamma = .1631\ J/m^2$. To simplify the analysis, the interface' behavior in shear is assumed to be the same as in tension so both $\sigma_{n\text{-}max}$(peak normal stress) and $\sigma_{t\text{-}max}$(peak shear stress) are given as 85MPa which corresponds to the value of the debonding stress determined previously for the COOH interface. By setting the form of the potential and the maximum tractions, the characteristics lengths are immediately determined to be .2167 nonometers since the failure in a pure loading case(i.e. pure tension or pure shear) should cause failure at the maximum effective length of the traction-displacement function(the interface should fail when $u = \delta$):

i.e. during interface failure under pure tension,

$$\text{Interface Work} = \int_{0?}^{\delta} A \exp(-\alpha u_i) \sin\left(\frac{\pi u_i}{\delta}\right) = \Gamma \text{ at failure}$$

$$\therefore \delta = .2167 \text{ nm}$$

The advantage of using the above description of the interface is that it allows for a smooth decrease in the interface tractions before failure occurs for cases where the interface is subjected to conditions close to pure shear or pure tension. This gradual decrease promotes numerical stability of the numerical solution by minimizing the sudden changes in global stiffness caused by the abrupt release of interface tractions during failure. The form of the traction-displacement relationship mimics that of the traction displacement laws derived from atomic level empirical potentials and may provide a fairly realistic representation of the true interface traction-displacement behavior at the micro scale. Also, the use of a potential should act to reduce the sensitivity of the solution to mesh effects by relieving the excessive constraints found in Lagrange multiplier techniques by allowing other regions of the interface to "share" the near crack tip tractions. However, it should be noted that the behavior of the model is not meant to represent events occurring at the atomic level but is meant only to describe the average behavior at the continuum level which may or may not be determined by the characteristic microscopic lengths(ex: chain diffusion length, asperity height, etc).

However, there are many disadvantages in applying the above forms to the epoxy/glass system. The most relevant of these is the initially large difference in relative stiffness that it creates between the interface and the epoxy matrix. By imposing a small characteristic length on the interface, the linearized stiffness of the interface, or Jacobian, which is given by

$$J = \frac{\partial \sigma_i}{\partial u_i} \text{ evaluated at current displacement}$$

is many orders of magnitude higher(especially initially) than that of the surrounding epoxy which is characterized by the Young's modulus. As mentioned previously, the ratio of interface to matrix effective stiffness can be on the order of 10000 to 1. This difference creates great discrepancies in the components of the global stiffness matrix. The effect of these large discrepancies in linearized stiffness are quantified by the condition number[60]. Essentially, the large range of stiffness components produces a wide range of eigenvalues in the global stiffness matrix. The condition number, which scales with the ratio of the largest to smallest eigenvalue of

the stiffness matrix, gives a measure of the sensitivity of the solution to small perturbations, including roundoff errors. The increased sensitivity of the global stiffness to roundoff errors can create singularities which are numerically difficult to resolve. Finally, the complexity of the initial contact conditions at the interface(there are many contact changes initially) act to enhance the numerical difficulties. These difficulties are attempted to be circumvented by modifying the form of the traction-displacement relation as discussed next.

"Lennard-Jones" mirror image

The next traction-displacement relation investigated has the form

$$\sigma_i = A^* \exp(\alpha u_i) \sin\left(\frac{\pi u_i}{\delta}\right)$$

where

$\sigma_i \equiv$ interface traction

$u_i \equiv$ interface displacement

$\delta \equiv$ characteristic distance of traction-displacement function

$A^* \equiv$ scaling constant(scales with the maximum traction, σ_{max})

which is constructed as a mirror image of the Lennard-Jones type in order to attempt to alleviate some of the numerical difficulties associated with the original form and is pictured in figure 4-33. Although this form is similar in that the tractions are allowed to increase and then decay before failure(under pure loading conditions), there is one major difference. The peak of the function is shifted so that the initial linearized stiffness of the interface is small enough relative to that of the epoxy matrix that the difficulties of the complex contact conditions are fairly easily overcome. Unfortunately, after the initially compliant portion of the relation is passed, the extremely high stiffness near the approach of the peak creates the difficulties brought on by large differences in relative stiffness. Again, the numerical solution becomes difficult because of the near singularity and great sensitivity of the global stiffness matrix to perturbations.

linear type

The main difficulty of the above two presented forms is in their extreme stiffness. In both cases, the stiffness is inversely proportional to the characteristic distance, δ. By introducing a form which eliminates the decaying portion of the traction-displacement relation, the

characteristic distance required is increased, thus decreasing the stiffness of the interface. A simple linear form(fig.4-34)

$$\sigma_i = \frac{\sigma_{max}}{\delta} u_i$$

where σ_i, δ, u_i are defined as before

provides the desired effect. Essentially, the traction-displacement is "stretched" out so that the characteristic length corresponds to the peak traction. This "stretching" has the effect of lowering the effective stiffness of the interface(fig.4-35). The advantage of this form is that the overall stiffness of the interface is reduced significantly. However, by allowing failure to occur when the traction is at a maximum, this introduces problems by creating sudden large changes in the global stiffness matrix. The difficulties induced by these changes are adequately handled by introducing a very small residual stiffness to the interface after failure. This residual stiffness keeps the global stiffness from suddenly becoming singular after failure and has very little effect on the overall accuracy of the solution. However, the simple linear form has the disadvantage of being too stiff initially, so the interface contact problems are still significant.

Truncated "Lennard-Jones" mirror image

With all of the above considerations in mind, another possible shape for a traction-displacement relation is of the form

$$\sigma_i = A^{\#} \exp(\alpha u_i) \sin\left(\frac{\pi u_i}{2\delta}\right)$$

where

σ_i, δ, u_i are defined as before

$A^{\#} \equiv$ scaling constant(scales with the maximum traction, σ_{max})

which is shown in figure 4-36. Again, the sudden large changes in the global stiffness matrix are adequately handled by introducing a very small residual stiffness to the interface after failure which keeps the global stiffness from suddenly becoming singular after failure. The shape is "optimal" in that it has an initially shallow slope which aids in handling the complex interface contact conditions and its truncated form stretches out the potential so that its overall effective stiffness is lower than its non-truncated counterpart for a given characteristic length. The main

disadvantage is that in allowing the initial portion of the curve to be relatively compliant, a high stiffness is induced as the peak is approached, leading to the same difficulties of global stiffness sensitivity as the other presented forms.

4.4.2 Comparison of the Various Potentials

This section briefly describes the differences in performance of the four potentials presented. In order to illustrate their marked differences in relative stiffness, each potential is applied to the axisymmetric bead problem in tension with the properties of the matrix and bead remaining fixed. The peak stresses for all of the potentials are set to 85 MPa and the characteristic length, δ, is gradually increased until the simulation becomes numerically stable(obviously the critical interface energy then changes with δ). By comparing the characteristic lengths required for stability for each potential, an estimate of their relative stiffnesses is possible.

The minimum characteristic lengths required for numerical stability given a matrix Young's modulus of 3 GPa and a bead Young's modulus of 100 GPa are as follows:

	"Lennard-Jones"	"Lennard-Jones"mirror image	linear type	truncated "Lennard-Jones" mirror image
minimum δ	22.0μm	17.0μm	10.0μm	9.0μm
corresponding energy	150000J/m^2	620J/m^2	400J/m^2	100J/m^2

As expected, the truncated "Lennard-Jones" mirror image has the smallest minimum characteristic length because of its initial shallow slope, which combats the initial complex interface contact conditions, and truncated potential which essentially stretches out the effective acting distance of the potential. The largest minimum δ is obtained for the full "Lennard-Jones" type potential because of its steep initial slope and long decay length which tends to compress the whole potential, thus making its effective stiffness much higher than truncated potentials. It should be noted that in extending the characteristic length to allow for numerical stability while maintaining the same peak

traction values, the effective energy required to produce interface failure is significantly increased(i.e. more work is required to separate the interface surfaces).

4.5 Conditions of Applicability of the Approach

The main difficulty with the mixed stress-energy approach presented above is that by explicitly giving the form of the interface traction-displacement relations, peak tractions, and the critical interface energy, the characteristic length is automatically determined. This constraint severely limits the effectiveness of the approach for systems where the surrounding material is relatively compliant as is this case with the epoxy matrix. Other studies using this approach[40] in metal systems are possible since the relative stiffnesses of the interface and the surrounding materials are not as different as those of polymer systems. However, for polymer interfaces where the interface energy is not explicitly known the compliant interface description may be feasible. This is especially true of an interface whose strength is due mainly to electrostatic forces where the characteristic discharge gap can be on the order of 1μm[61], hence facilitating the use of a compliant interface potential model.

The sensitivity of the approach to these factors is investigated through varying the conditions associated with the use of the truncated "Lennard-Jones" mirror image form. Two conditions are altered: the stiffness of the surrounding material and the critical interface energy. By fixing all parameters but the one being considered, the conditions under which this approach is applicable are determined.

Stiffness of surrounding material

Maintaining the parameter values used previously for the initial calculations of the "Lennard-Jones" mirror form(i.e. peak tractions = 85MPa, interface energy = .1631J/m^2, characteristic length = 15nm)the stiffness(Young's modulus) of the epoxy is increased until a numerically stable solution is found. The minimum stiffness required for epoxy is 60 GPa which corresponds to 20 times the experimental value. Unfortunately, altering the material properties also changes the overall response of the epoxy/glass system which is unacceptable. However, this demonstrates the reason for the earlier success of other investigators(Needleman, Tvergaard, etc.) in using this form of criteria where the systems studied typically had interface to matrix stiffness ratios on the order of 1 to 1.

Interface Energy

As noted previously, increasing the interface energy directly decreases the overall stiffness of the interface by increasing the characteristic length. By increasing the interface energy by a factor of 600 from .1631J/m^2 to 100J/m^2, the characteristic length increases by a factor of 650 from 15nm to 9μm and a numerically stable solution is possible. Unfortunately, a length of 9μm is probably physically unrealistic. A wire mesh drawing of the interface at the moment of interface failure is shown in figure 4-37. This simulation suggests that the interface is extremely compliant and that macroscopic scale displacements are present before failure, a result not consistent with experimental observations.

4.6 Indirect Use of the Interface Energy to Deduce a Failure Criteria

In light of the numerical difficulties introduced by the direct application of a potential to model the epoxy/glass interface, a more stable yet reasonably realistic method of modeling the interface is preferable. The most stable of the methods introduced is the local stress based approach. As mentioned previously, the difficulty with using a stress based criteria is that the selected stress criteria should be energetically consistent(i.e. the energy release rate of the system should be the same irrespective of what local stresses are present during interface failure) when the assumption of interface energy invariance is applied. One way of obtaining a stress criteria is to use the same technique applied earlier for determining the interface energy. The use of this technique to deduce a possible stress criteria is briefly described:

By using the determined characteristic interface energy and assuming that it is invariant, the evolution of the flaw is deduced through an energetics argument. The interface crack is assumed to propagate when the amount of strain energy released during a discrete increase(ΔA) in the crack area is sufficient to satisfy the energy requirements for the crack area increase, or more precisely when $\Delta E > \Delta A * \Gamma$. Under these conditions and in a discretized formulation of the problem, the crack theoretically proceeds with discrete drops in strain energy during each crack growth increment(fig.4-38).

In the absence of dissipative processes, this behavior and hence the location of these energy "drops" are determined using stationary crack analysis. Theoretically, by running simulations for each crack length while not allowing the crack to grow, the strain energy curves for each simulation trace over the portions of the theoretical discrete crack propagation strain energy curve which correspond to their respective lengths(fig.4-39).

This illustration provides insight on how the crack evolution process is reconstructed. By performing simulations for all possible crack lengths and computing the resulting strain energy curves, the crack is assumed to propagate from one length to another when the differences in their strain energy curves exceed the product of the interface energy parameter and the difference in the crack areas. For example, if the strain energy curve for a crack length of A1 is described by a function of far-field displacement, $E_{A1}(u)$, and the curve for a crack length of A2 by $E_{A2}(u)$, then the propagation from A1 to A2 occurs when $E_{A1}(u) - E_{A2}(u) = \Gamma^*(A2-A1)$ (fig.4-40).

By solving for the global displacement required to create this critical strain energy difference, the stresses at the tip of the interface crack at the onset of propagation are found by calculating the crack tip tractions at the desired global displacement. For these calculations, the tractions are computed at the node defining the crack tip. Solving for the critical displacements at every crack increment provides the entire interface normal and shear stress history. As mentioned previously, preliminary calculations using this technique were performed using the CH_3 interface using a debonding stress of 30 MPa and an interface energy of .055 J/m^2 as computed using the energy difference technique. The results of this procedure applied to a finite element mesh with 16 interface elements surrounding each quadrant with each element representing a crack increment are shown in figure 4-41a.

As stated earlier, in the absence of dissipative processes, the computed energy associated with the interface is invariant. This implies that increasing the incremental crack length produces similar crack tip stress results since all strain energy changes are supposedly absorbed by creating the new surfaces. Again, the procedure is repeated on the same mesh with an allowed crack increment of two interface elements and the results are shown in figure 4-41b. By superimposing the failure loci for the two sets of calculations, the crack tip stresses during propagation appear to be very similar(fig.4-41c).

The interface crack tip failure locus obtained through this very simple energy argument is directly implemented into the Lagrange multiplier modeling approach. The failure locus is represented by a function of the form:

$$\sqrt{\left(\frac{\sigma}{\sigma_{max}}\right)^2 + \left(\frac{\tau}{\tau_{max}}\right)^2} = 1.$$

σ_{max} = maximum interface normal stress during pure tension
τ_{max} = maximum interface shear stress during pure shear

A fit of this function to the CH_3 failure locus data using σ_{max} = 30 MPa and τ_{max} = 22 MPa is shown in figure 4-42. Physically, the locus makes intuitive sense in that it predicts failure due to

moderate combinations of shear and normal stress while still allowing for failure in the absence of one or the other. This stress based approach allows for analysis of systems with or without an initial flaw. However, it is not inherently clear whether the locus is applicable to other geometries since it is generated under certain conditions with a specific geometry and loading configuration. Also, it should be noted that the interface energy used for the failure locus calculation is found from preliminary calculations using the 16 element mesh only(i.e. the CH3 interface energy is not computed to a convergent value), hence producing an interface energy which is lower than the convergent value. A consequence of this lower energy is that the interface is predicted to fail sooner than would be found for the correct energy.

The difficulty of all of this is in the definition of the crack tip. In the work presented above, the critical tractions are most conveniently calculated at the node which defines the crack tip(fig.4-43). Linear elastic fracture mechanics shows that slight changes in the distance away from the crack tip give great changes in the interface stresses calculated[17] due to the singular nature of the stress field of a crack tip. The use of a calculation exactly at the crack tip is a first approximation and is facilitated by the nature of the stress based method which employs Lagrange multipliers. The Lagrange multipliers are most easily and accurately applied at finite element nodal points where they can be directly read as interface tractions required to enforce the kinematic constraint. The disadvantage in doing so is that since the Lagrange multipliers enforce a kinematic constraint, they can theoretically attain any(in many cases very high) value without regard to what values are physically realistic.* We also note that no special mesh refinement was applied to the crack tip as is done in typical stationary crack analysis in order to accurately compute near crack tip stress and strain fields.

Using the J-Integral

Although the procedure described above is necessary for cases where the interface is initially flawless, the initial presence of a finite size flaw allows for an indirect method of determining the stresses at the interface crack tip during failure. The assumption that failures can only occur along the interface facilitates the direct use of the J-integral as introduced by Rice[22]. The J-integral simply states that given a known crack propagation direction, the amount of energy released by a cracked body during an infinitesimal increase in crack length can be found by evaluating the contour integral(fig.4-44):

* As will be shown later, this length/distance effect implies a mesh effect in the finite element analysis. This is indeed found to be the case as will be discussed later.

$$J = \int_{\Gamma} \left(w\, dy - \tilde{T} \cdot \frac{\partial \tilde{u}}{\partial x} ds \right)$$

where

w = strain energy density

$\tilde{T}$ = traction vector along the contour path, C

ds = differential contour element

$\tilde{u}$ = displacement vector

The advantage of applying the integral is that it is theoretically path independent and can be applied to nonlinear elastic as well as deformation theory elasto-plastic bodies with finite sized cracks subjected to proportional loading. Its main disadvantages include being limited to proportional loading cases and/or elastic systems(as is the case assumed here) and the direction of crack growth must be known a priori(also the case assumed here).

It can be shown that the technique introduced above(i.e. energetic feasibility), which is applicable either initially flawed or flaw free interfaces in elastic systems, reduces to the J-integral[17] in the presence of an initially finite sized crack(see appendix). Computationally speaking however, the application of the J-integral has other limitations. Although the approach is theoretically path independent, it has been shown that for finite element calculations, the J-integral typically approaches a steady state value as the contour is moved away from the crack tip(fig.4-45)**[ref]**. In order to account for this discrepancy, all following J-integral calculations involve contours which are at least three elements away from the crack tip. Under these restrictions, in order to obtain a reasonably accurate J-integral evaluation, the initial crack length should be at least three elements long. For crack lengths of less than three elements, the indirect energetic feasibility approach as discussed earlier is used.

The stresses at the crack tip can be deduced with the J-integral by calculating the crack tip tractions when the J-integral obtains the value of the interface energy. Since the system is assumed to be elastic, by evaluating the J-integral at different crack lengths, the crack tip stresses corresponding to failure are easily found. Again, the locus of these stresses can be plotted(fig.4-46).

As mentioned previously, one of the major difficulties in using a stress based criteria which is applied by using a kinematic constraint is in determining the location at which the crack "tip" tractions should be measured. Again, the first approximation is made that the crack tip tractions are measured at the node defining the crack tip. The equivalence of the stress criteria

derived by the J-integral and the stress criteria derived by the use of energetic feasibility is now briefly discussed. The validity of using crack "tip" node tractions is addressed later.

4.7 Equivalence of the Stress Criteria Deduced from both Methods

Several calculations are performed on the COOH interface systems to determine the equivalence of the stress criteria derived from the energetic feasibility(strain energy difference) method and the J-integral method. The locus of interface stresses determined from the energy difference calculations for an interface with a mesh density of 16 elements are combined and fit to the previously introduced failure locus function. The J-integral calculations use a contour which extends to enclose the three elements in front of the crack tip(fig.4-47). Hence the results for the cracks of length one element and two elements are not included in any of the calculations. The results of both methods(energetic feasibility and J-integral evaluation) are superimposed and found to be very similar(fig.4-48). Using the same interface energy, $\Gamma = .1631$ J/m^2, the sensitivity of both methods to the mesh effects is investigated by increasing the mesh density from 16 elements to 32 and 48. The normal and shear stresses calculated at the crack tip during failure for both methods are shown in figure 4-49. The figure shows that although the results of both methods are nearly identical when using the same mesh, the sensitivity of the results to the mesh density is quite significant. This effect is probably a result of the reduction in crack tip constraint as the mesh density increases. The reduced constraint allows the simulation to proceed further before the critical energy difference is attained(i.e. the near crack tip elements store less strain energy for dense meshes than coarse ones), an effect which dominates the expected reduction in interface stresses from constraint relief. In fact, the values of the stresses calculated are not physically likely since they suggest that in the presence of shear, the normal stress required to induce interface failure is actually much higher than the debonding stress, $\sigma_d = 85$MPa, which is defined as the amount of normal stress required in the absence of shear.

Because of the equivalence of the results of both methods, all subsequent calculations solely use the J-integral method which although limited to cracks of at least 3 elements in length, is much easier to apply.

4.8 Sensitivity to Location of Traction Measurement

Since the main objective of work is to create an applicable interface failure criteria, the criteria should be independent of the geometry as well as mesh effects. The sensitivity of the results to the mesh density suggests that the elastic matrix assumption makes the location of stress measurement very important.

Several calculations are performed to determine the sensitivity of the calculated stresses to this effect. By gradually increasing the distance away from the crack tip at which the stresses are measured, the distance at which the results are no longer affected is hopefully obtained. The hope is that this minimum distance is scaleable by some material characteristic length, thereby making it independent of the specific geometry considered.

Interface stresses calculated at various distances away from the crack tip for a mesh density of 48 elements are plotted in figure 4-50. The figure suggests that the interface stresses drop dramatically at a fairly small distance away from the crack tip. Beyond this small distance, taken to be 16μm for these calculations, the interface stresses change only slightly. This initial dramatic change is probably attributable to the amount of constraint at the crack tip introduced by the Lagrange multipliers and the asymptotic nature of the true solution and is isolated to a region very close to the crack tip.

Calculations with mesh densities of 16, 32, and 48 elements are performed to determine their sensitivities to measurement distance. A quick comparison of all the results shows that at a distance of 98μm away from the tip, the failure loci for all three meshes are identical(fig.4-51). One additional physical aspect which these loci do suggest is that the interfacial shear strength is lower than the normal/tensile strength. Although the exact distance at which the distance sensitivity is negligible is not easily determined by these calculations(98μm is the minimum distance away from the crack tip that can be measured for the 16 element interface), the results qualitatively suggest that relief of the tip constraint is necessary before realistic crack tip behavior is obtainable. Relief of crack tip constraint occurs in real systems through plastic deformation or some sort of blunting mechanism. It is the sensitivity of the results to this constraint which is investigated next.

4.9 Sensitivity to Crack Tip Constraint

The results of the previous section show that the direct and sole use of a Lagrange multiplier method to model the interface produces an over constraint or "pinning" of the crack tip which is not representative of the true behavior of a real interface. To combat these difficulties, it

is possible to combine the stress and stress-energy approaches to produce a more realistic and still applicable model of the interface behavior.

A combined model uses a potential to describe the crack tip behavior and the Lagrange multipliers to describe the remainder of the interface(fig.4-52). The use of a potential at the tip relieves the undesired constraint while the use of Lagrange multipliers isolates the severe differences in relative stiffness between the interface and the epoxy to only one or two nodal points in the system. The reduced number of these "singularities" are more readily circumvented and the number of contact points which must be resolved is also greatly reduced leading to a smoother solution. In this sense, the use of the potential here can be considered more along the lines of a penalty function which enforces the interface constraint in a "weak" sense as opposed to Lagrange multiplier techniques which enforce it exactly.

The interface energy computed for the potential is not explicitly used in the model to determine failure(i.e. the work of the interface tractions is not calculated). Instead, the tip potential is used in conjunction with the J-integral methodology† to derive the crack tip stresses which are measured through the assumed traction-displacement relationships at the node defining the crack "tip".

Because of its computational efficiency as explained previously, the traction-displacement relation selected is the previously discussed truncated "Lennard-Jones" mirror image which takes the form:

$$\sigma_i = A^{\#} \exp(\alpha u_i) \sin\left(\frac{\pi u_i}{\delta}\right)$$

For simplicity, the normal and shear traction-displacement relations are assumed to take the same form and are uncoupled from one another. Since the constraint of the crack tip is essentially determined by the stiffness of the interface(i.e. in the limit as the stiffness becomes infinite, the interface behaves as if it were constrained by Lagrange multipliers), the peak tractions are arbitrarily taken to be 85 MPa with the characteristic lengths being selected independently(i.e. the interface energy is not explicitly used to determine failure). The lengths, which are selected for numerical convenience, are physically plausible values(i.e. they are not inconsistent with experimental observations which have found characteristic lengths on the order of 1μm for interfaces dominated by electrostatic forces[61]) but are not meant to represent any microscopic material or system scale.

At each crack increment, the simulation proceeds until the J-integral attains the critical value, .1631 J/m^2, at which point the traction computed from the potential is noted as the traction

† note: The energy stored in the crack tip potential is not included in the J-integral calculations.

which would be present at or near the crack tip during propagation. In the event that the peak traction of the potential is exceeded before the critical J-integral value is obtained, the potential's peak stress would be increased and its characteristic length adjusted accordingly(since crack tip constraint is only dependent on the stiffness of the interface). However, for the cases tested, this adjustment was unnecessary since the critical J-integral value was always obtained before reaching the peak stress.

By varying the mesh density and the characteristic length, the sensitivity of the failure locus to these parameters is ascertained. The length of the "tip" was taken to be the interface element length. Hence lengths of 98μm, 49μm, and 32.7μm are used for interface element densities of 16, 32, and 48 elements respectively. The results of several of these investigations are shown in figures 4-53. The results show that for a given characteristic length, increasing the mesh density decreases the size of the failure locus(fig.4-54a) and that increasing the characteristic length for a given mesh density also decreases the size of the failure locus(fig.4-54b).

These observations seem to suggest that the failure locus is most sensitive to some normalized measure of the tensile crack tip opening angle(CTOA)[17] which is a measure of the "bluntness" of the crack. The tensile CTOA can be roughly approximated for each mesh by dividing the elements length by the characteristic length(fig.4-55). In order to compare the data for the various cases, an estimate of the effective stiffness of the surrounding material should be incorporated in any calculation. The effective stiffness is required since an effectively high stiffness matrix(epoxy) shields the interface from any loads while an apparently highly compliant matrix more readily sheds its load to the interface. Although all cases employ the same material model, the density of the mesh affects the apparent stiffness of the system for loading cases other than those of pure tension and pure shear. By idealizing the crack loading as some form of bending, the schematic in figure 4-56 illustrates the differences in effective stiffness for a coarse versus dense mesh.

Computationally, the higher effective stiffness of the coarse mesh is due its having less degrees of freedom than the dense mesh since the number of nodes roughly determine the number of degrees of freedom. A global stiffness matrix with few degrees of freedom is much more constrained than one with a large number of degrees of freedom. The number of degrees of freedom of a system is determined by the number of basis functions(shape functions) used for the construction of the approximate solution or by the number of eigenvectors of the global stiffness matrix. Since any general deformation is a linear combination the basis functions[44], a system with very few of these functions cannot accommodate a general deformation pattern easily, Consequently, its finite element solution appears to be much "stiffer" than a system with a larger number of basis functions or eigenvectors(i.e. a denser mesh). Exceptions to these general rules occur during pure tension and pure shear. In these cases, the true deformation pattern is exactly

representable by the basis functions of one element. Hence, any mesh density identically describes the exact behavior. For the complex case of near crack tip deformation, this is not the case and the number of degrees of freedom has a significant effect on the solution.

For the purposes of this work, a measure of the effective stiffness of the surrounding matrix is estimated as the number of degrees of freedom within an arbitrarily chosen region near the crack tip(fig.4-57). The calculations indicate that for a given CTOA, increasing the apparent stiffness of the surrounding matrix leads to a downward shift in the failure locus(fig.4-58), a result consistent with the above discussion. Therefore, in order to obtain a relationship between all three factors(interface element size, characteristic length, and apparent stiffness of surrounding material), the CTOA should be normalized by some measure of the effective stiffness of the surrounding material.

By selecting the failure locus computed for the 32 element interface with $\delta = 2.5\mu m$ as the ideal failure locus, the relationship between this ideal and systems with other parameters can be established. The 32 element-2.5μm system is chosen as the ideal since it seems physically plausible in that it displays a smooth transition from pure tension to mixed crack tip conditions. The table below shows the normalizing of the failure loci of the other systems with respect to the ideal system:

element density	characteristic length, δ (μm)	normalized locus	CTOA (δ*elmnt dens)	#nodes in region near crack tip
48	2.5	0.9	120	133
32	2.5	1.0	80	65
32	4.0	0.6	128	65
32	5.0	0.6	160	65
16	5.0	0.75	80	21
16	6.0	0.65	96	21
16	7.0	0.575	112	21
16	7.5	0.55	120	21

By normalizing the CTOA values by the natural log of the number of degrees of freedom near the crack tip, a consistent relationship between the interface element size, characteristic length, and surrounding mesh density is established(fig.4-59). This relationship approximately determines what parameters are required to produce consistent interface behavior for a given material system.

Unfortunately, this interpretation fails to give an indication of what the true failure locus looks like, a consequence of the sensitive coupling of the parameters(i.e. mesh density,

characteristic length, etc.), and serves only to quantify the relationship between interface failure and tip constraint. In other words, the parameters could not be varied individually to check for convergence of the results to a single failure locus. Also, the normalized CTOA may not be the only parameter which characterizes the crack tip behavior. By varying the "blunting" length for several meshes, there may be another parameter found relating the characteristic distance, interface element density, effective matrix stiffness, and blunting length which may provide a better characterization of the interface crack tip.

There are several other alternatives to the crack tip potential for relieving crack tip constraint. One possibility is to use focused mesh techniques at the crack tip for each increment, hence allowing the crack tip to blunt explicitly. This technique is difficult to implement since a new mesh must be created at each crack increment. Another possibility consists of moving the near crack tip nodes to positions such that the isoparametric mapping produces a singularity of the same form as the analytical solution. Although it may be possible to capture the singular behavior fairly accurately with this technique through calculation of interface stress intensity factors, it fails to produce a stress failure criteria for use in initially flawless systems. Finally, introducing plasticity to the matrix might relieve some of the constraint by increasing the compliance of the near crack tip material. However, since the constraint enforced by the Lagrange multipliers is a kinematic one, the effective stiffness of the surrounding elements(a quantity strongly tied to the local arrangement of the elements) will still be very high.

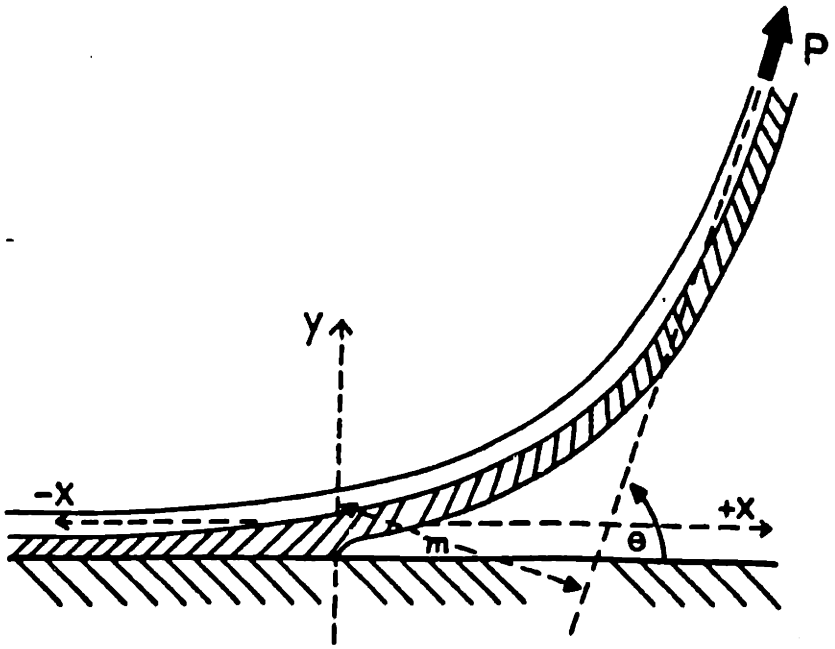

figure 4-1: schematic of peel test

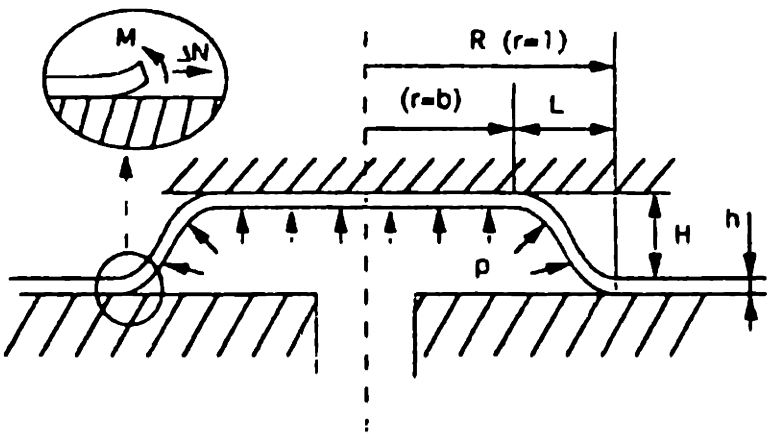

figure 4-2: schematic of blister test

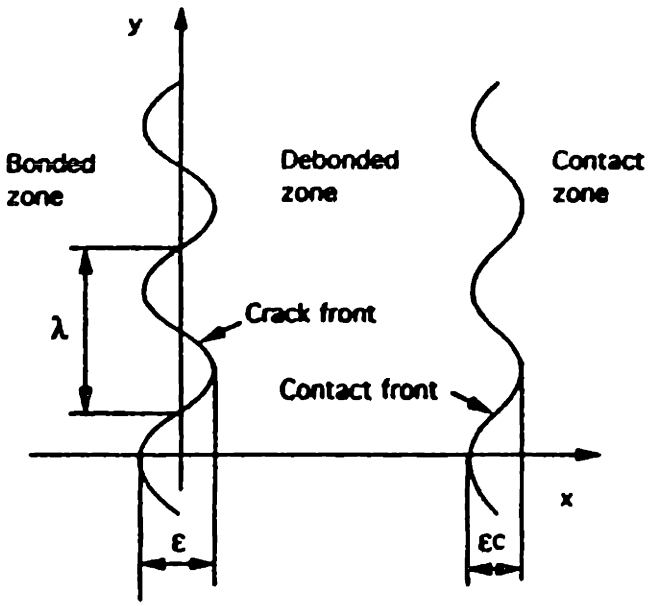

figure 4-3: schematic of perturbed crack front

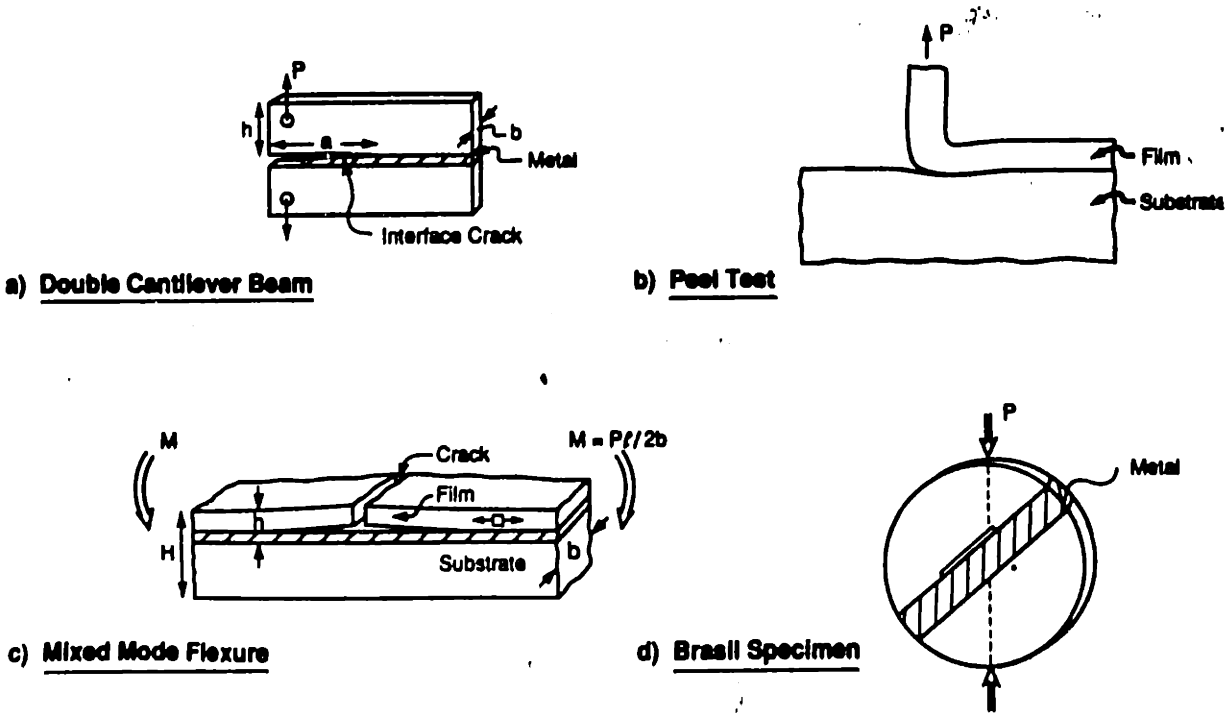

figure 4-4: schematic of mixed mode flexure, Brasil, composite cylinder, and double cantilever tests

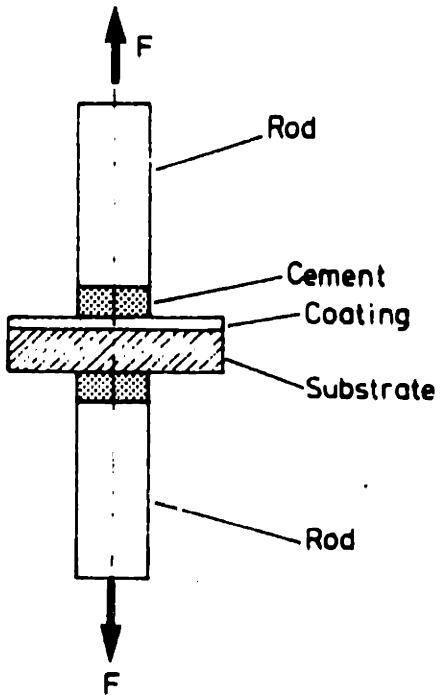

figure 4-5: schematic of direct pull off test

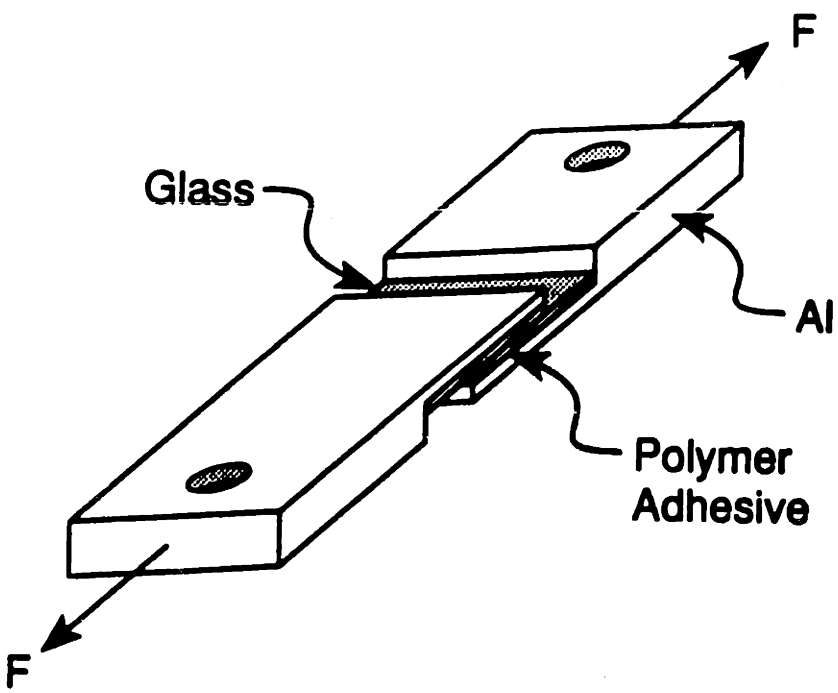

figure 4-6: schematic of lap shear test

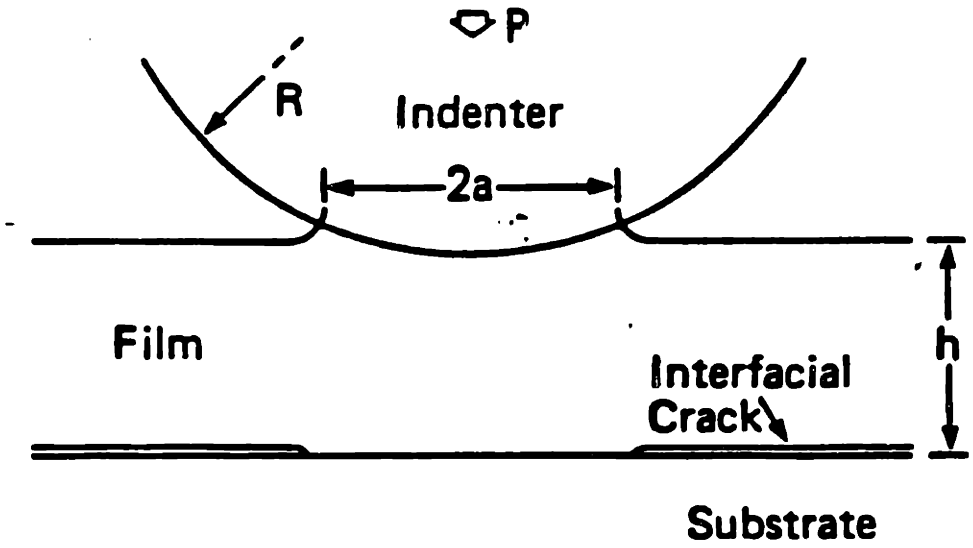

figure 4-7: schematic of indentation test

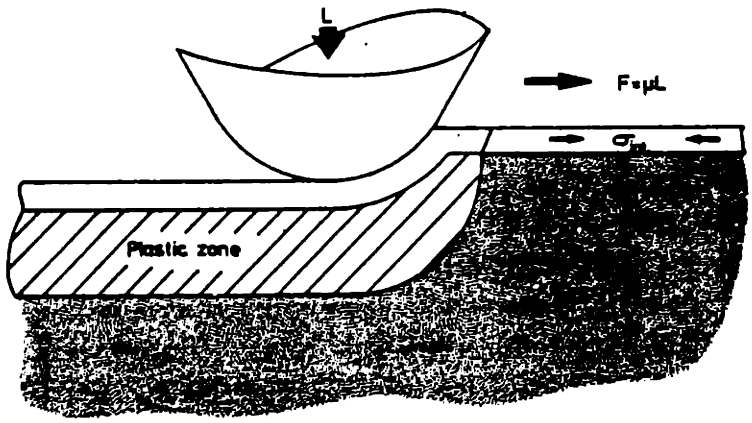

figure 4-8: schematic of scratch test

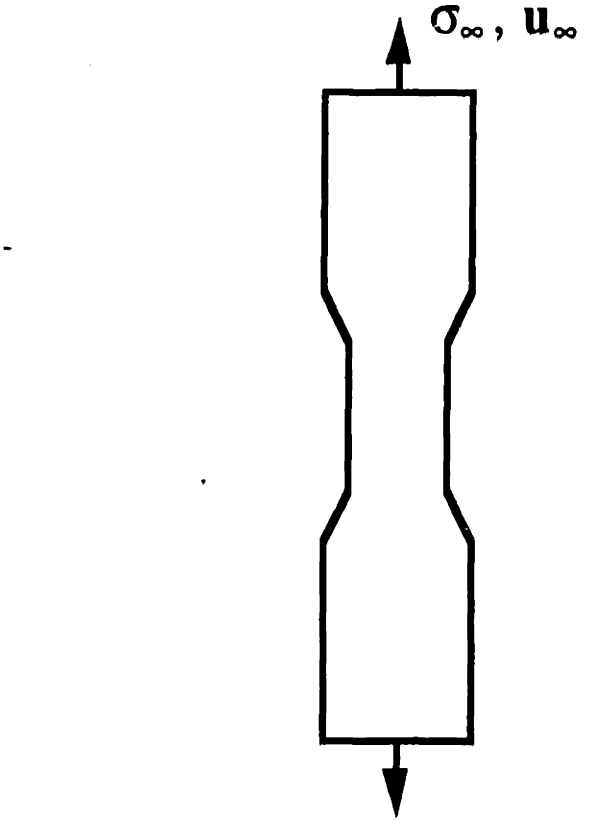

fig. 4-9 Schematic of specimen pulled in tension

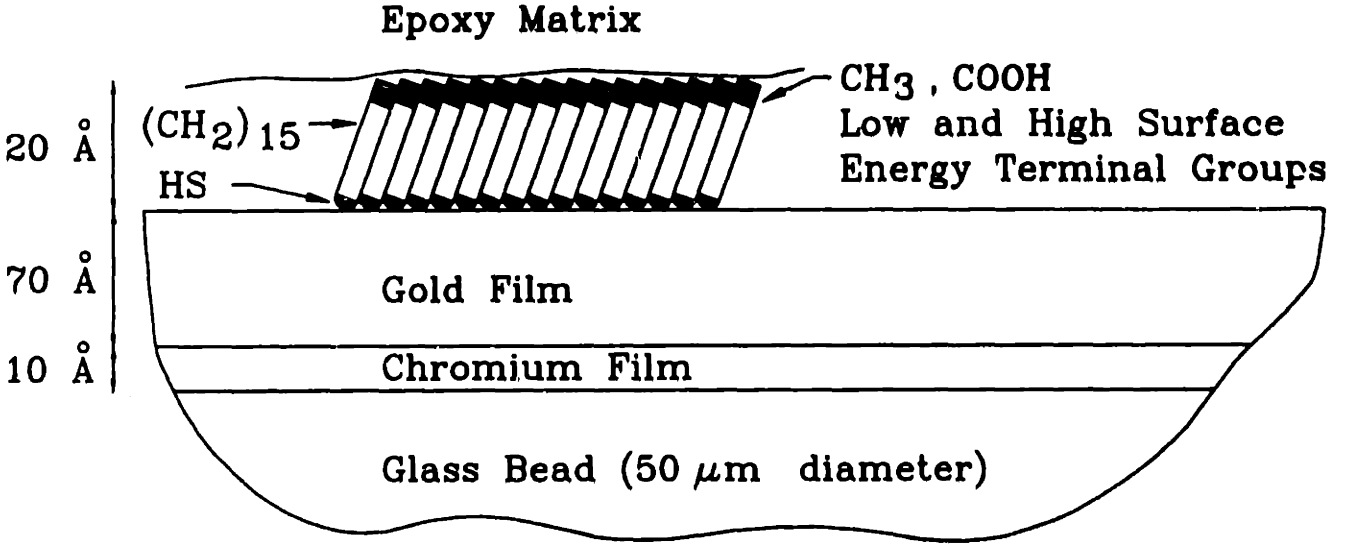

figure 4-10; schematic of interface monolayer

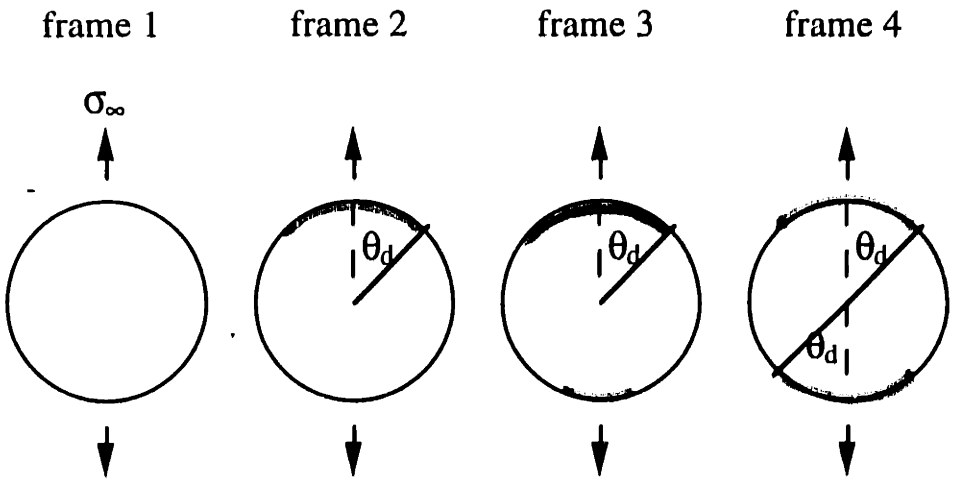

fig. 4-11 Schematic of frame by frame evolution of interface crack on glass bead.

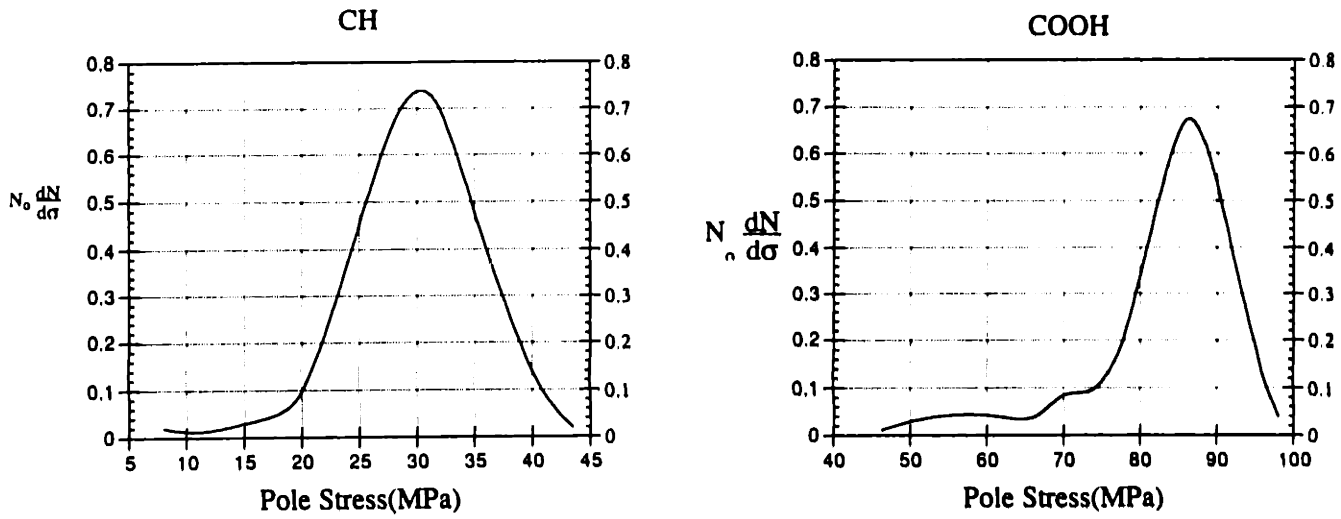

figure 4-12: normalized distribution of number of debondings as a function of pole stress for the CH_3 and COOH interfaces. (note: the total number of failures scales with N_O)

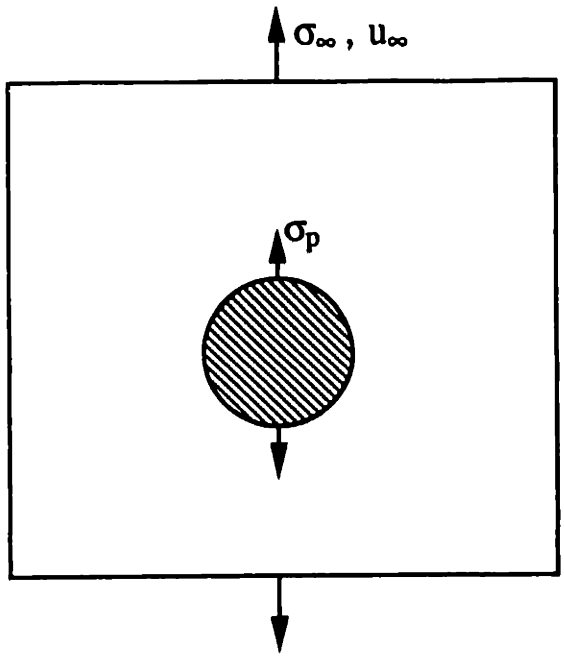

figure 4-13: schematic of location of pole stress

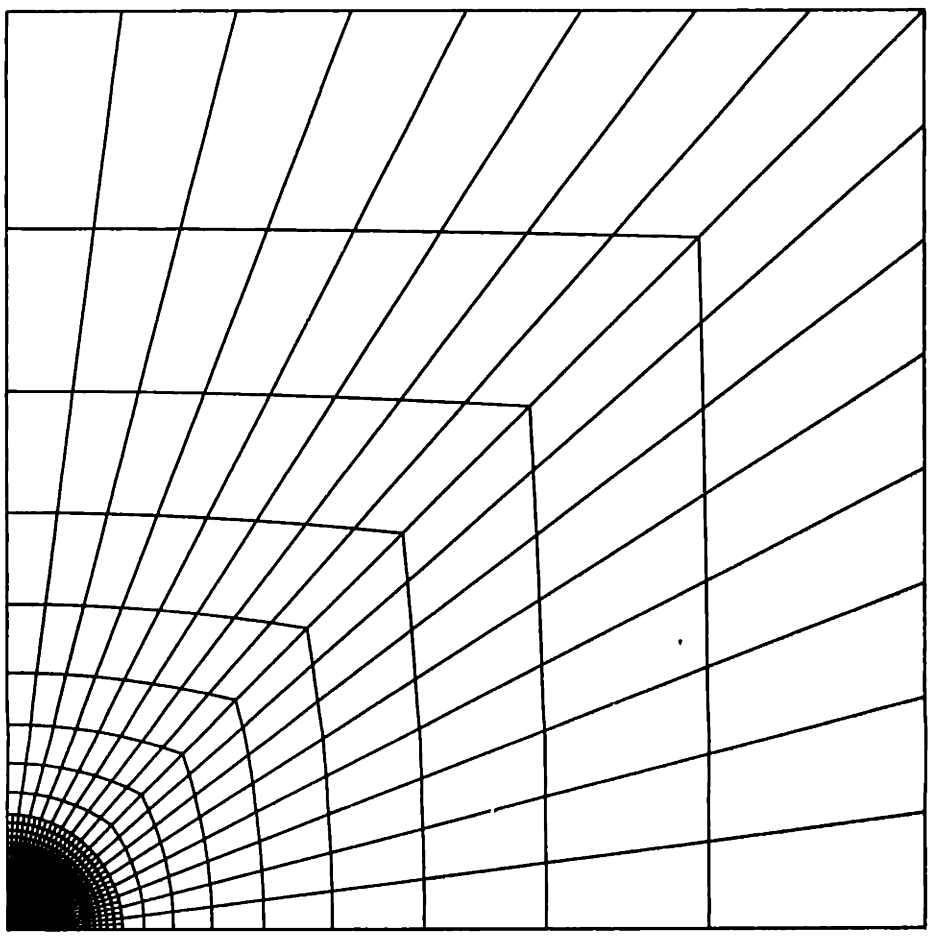

figure 4-14: finite element mesh used for tensile test simulation

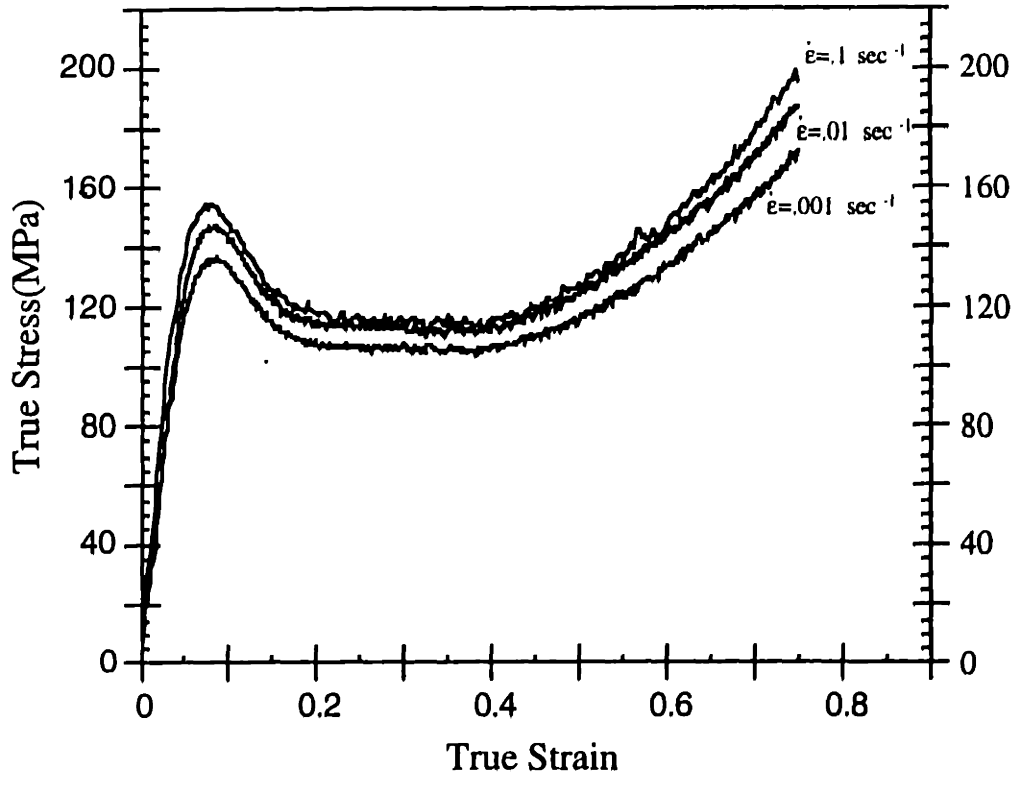

figure 4-15: compression test data of the epoxy matrix for several strain rates

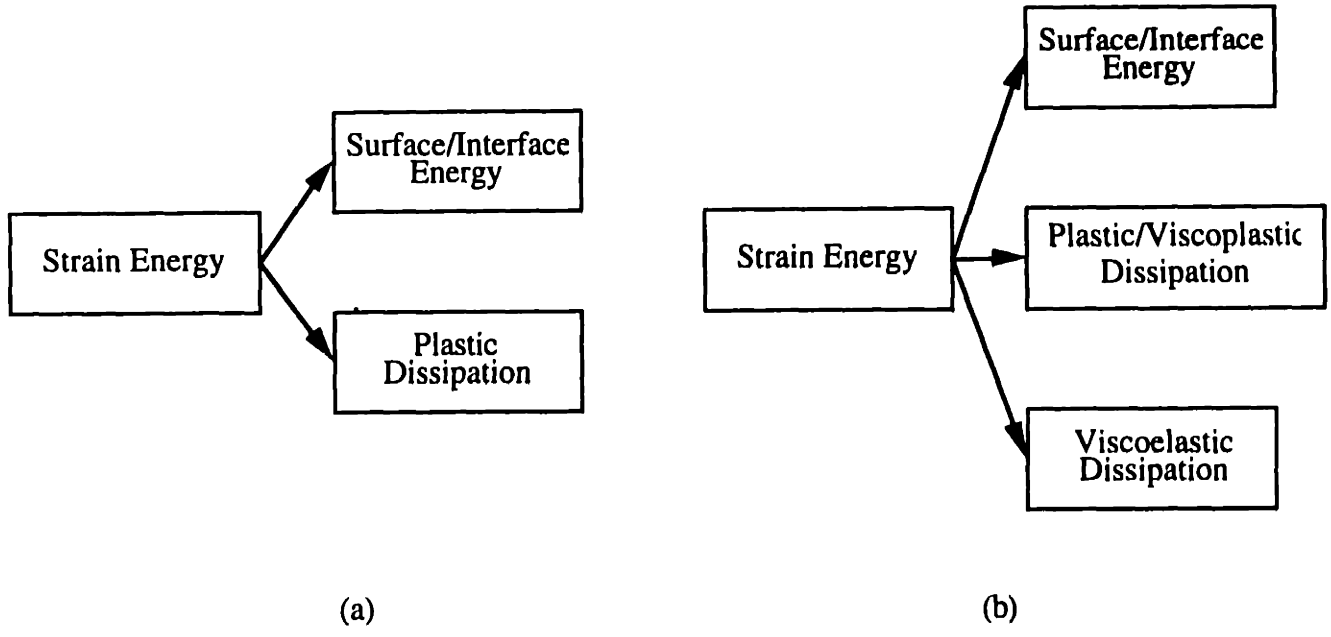

figure 4-16: (a) for a rate independent elasto-plastic system, strain energy which is released during flaw initiation/propagation is channeled through only two paths: surface creation and plastic dissipation. (b) for a rate dependent viscoelastic-viscoplastic system, the strain energy can be channeled to three paths: surface creation, plastic-viscoplastic dissipation, and viscoelastic dissipation. Hence more energy is generally required to cause interface failure in a rate dependent system.

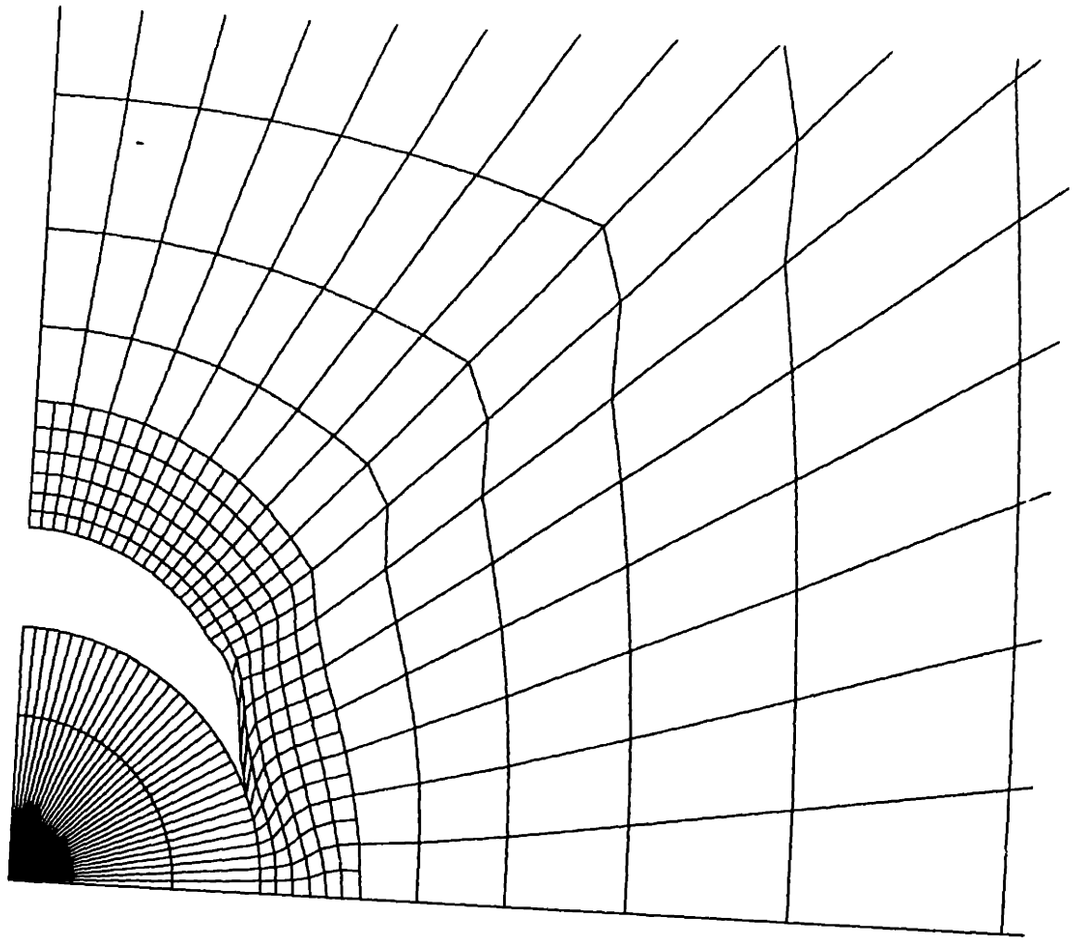

figure 4-17: wire mesh showing the end of crack growth

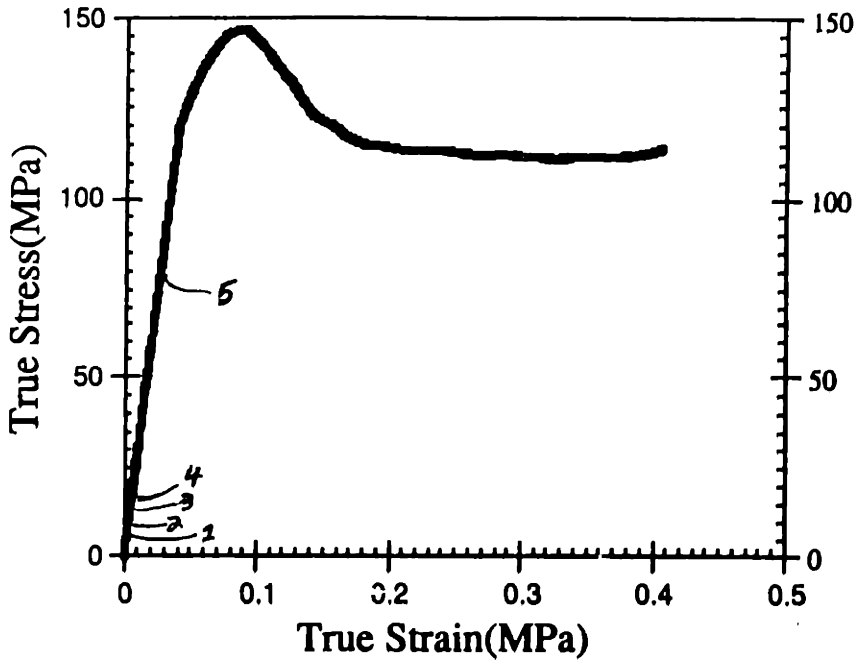

(a)

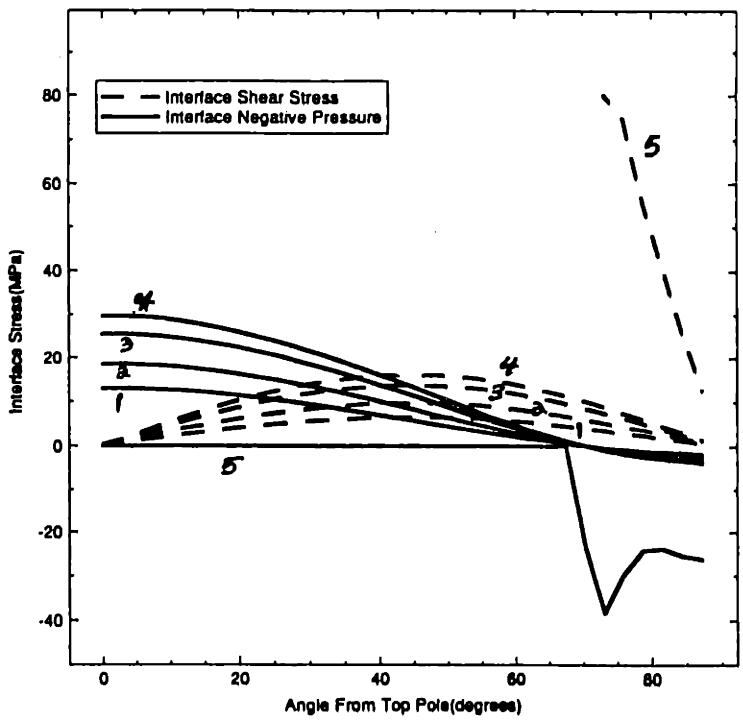

(b)

figure 4-18: CH3 interface simulation - (a) farfield stress-strain curve (b) evolution of interface normal and shear stress(the numbers mark increasing displacement

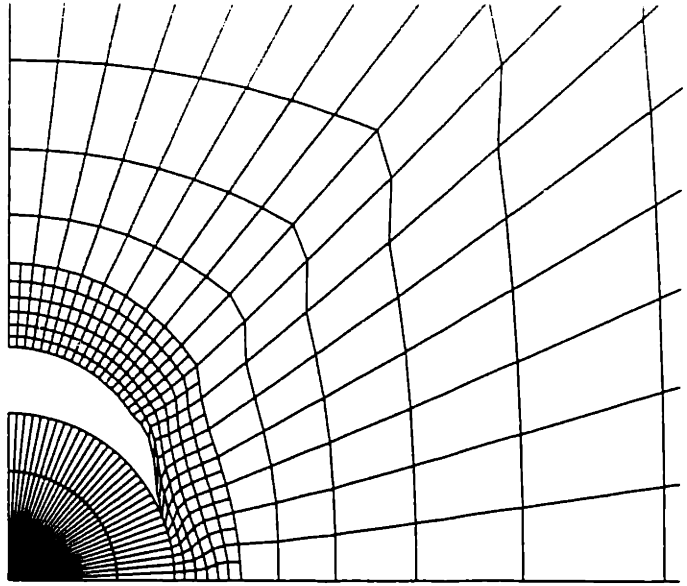

(c)

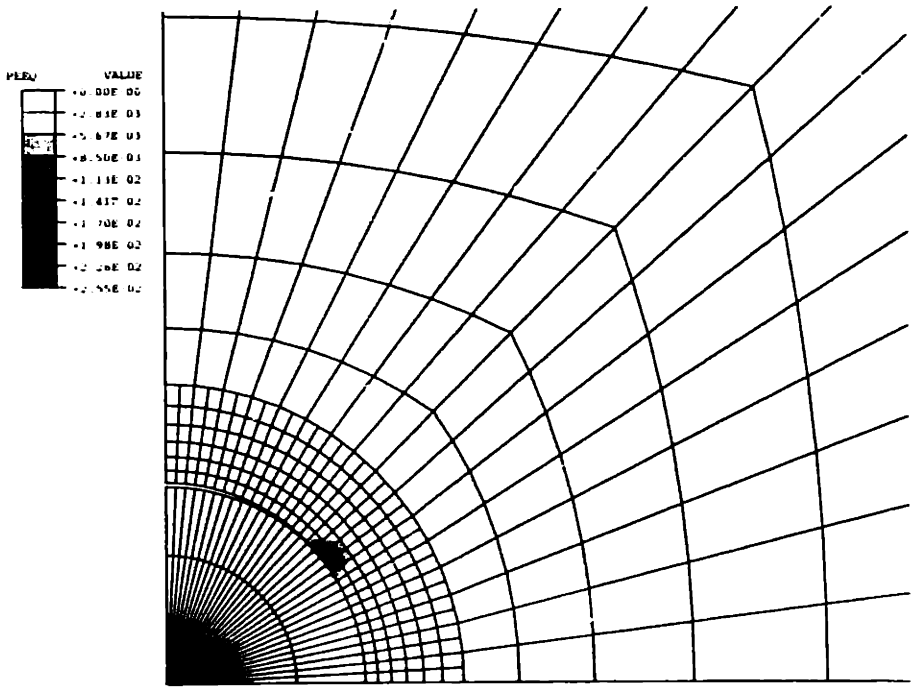

(d)

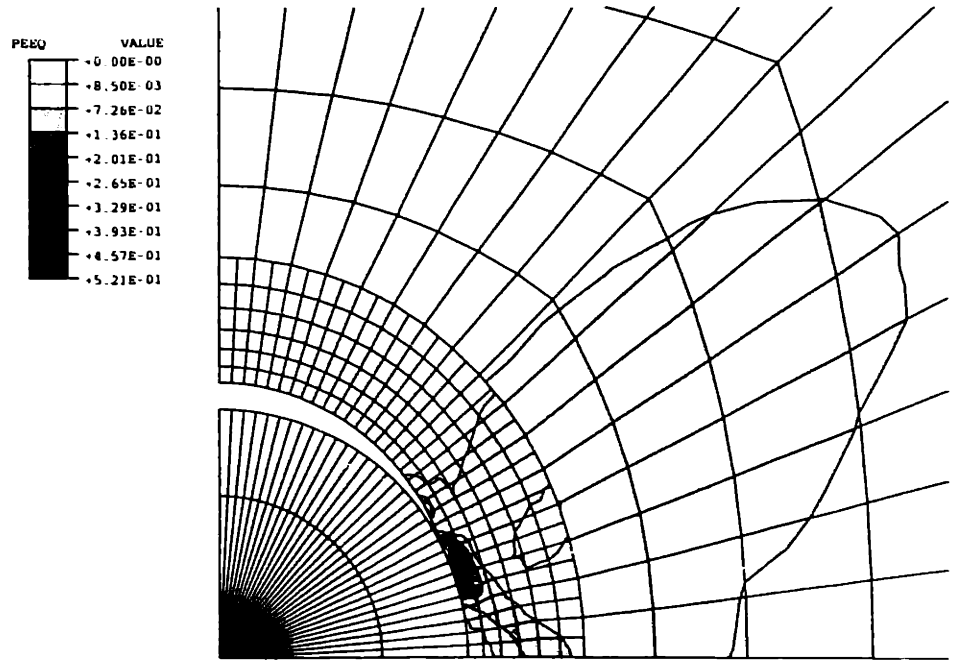

(e)

figure 4-18: CH3 interface simulation - (c) deformed mesh after 30% farfield strain (d) equivalent plastic strain contour during crack propagation - note the very limited plastic deformation(marked green) (e) growth of equivalent plastic strain contour after propagation ends.

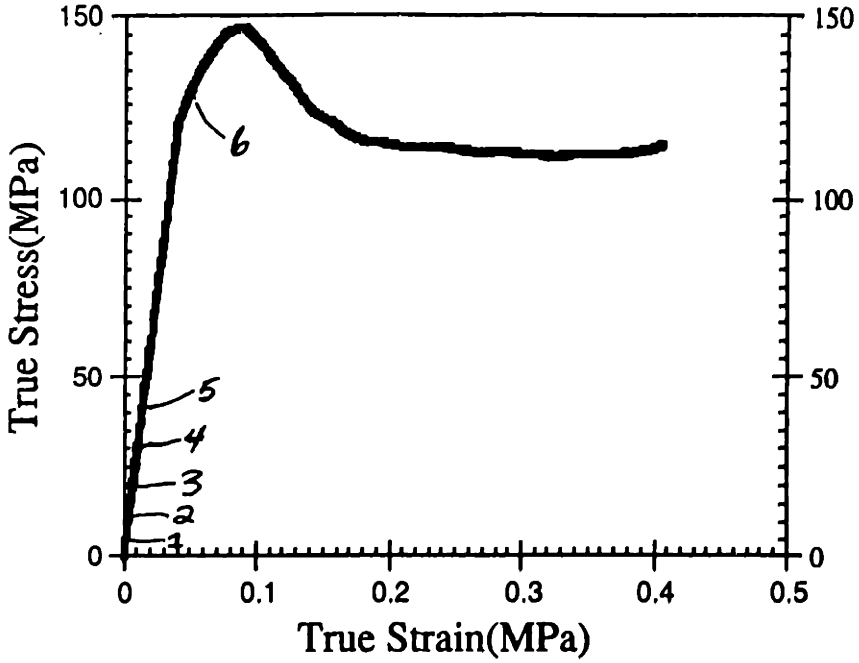

(f)

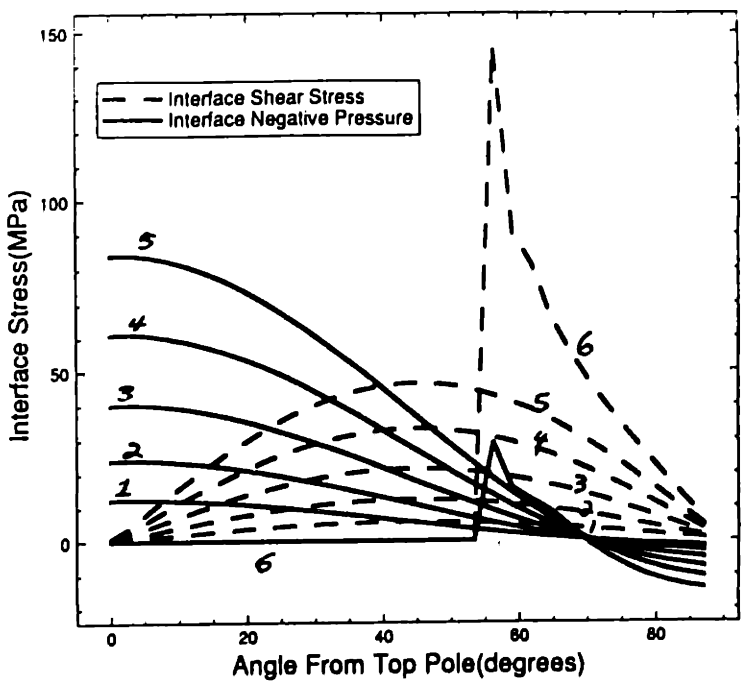

(g)

figure 4-18: COOH interface simulation - (f) farfield stress-strain curve (g) evolution of interface normal and shear stress(the numbers mark increasing displacement

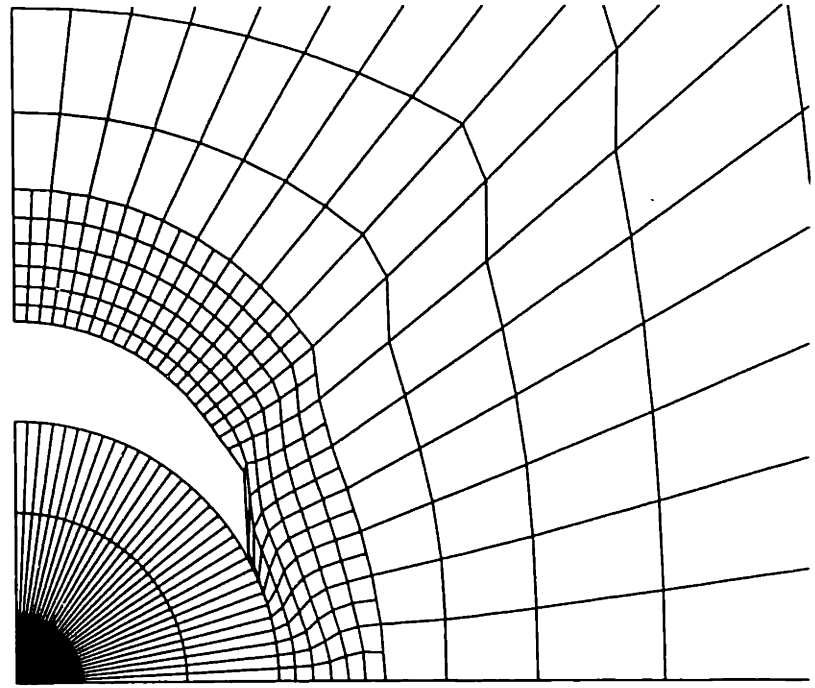

(h)

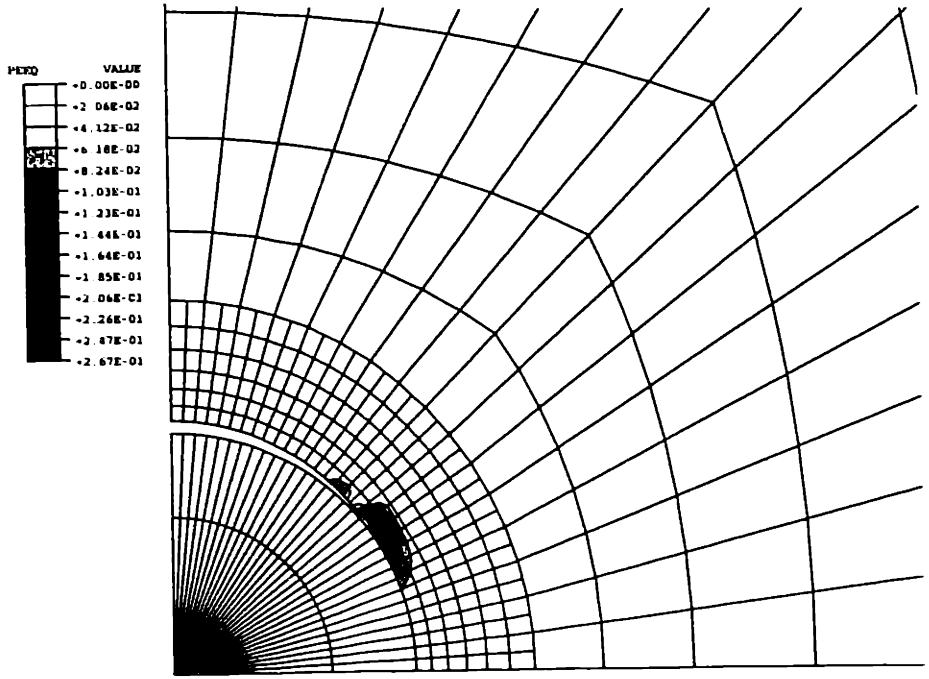

(i)

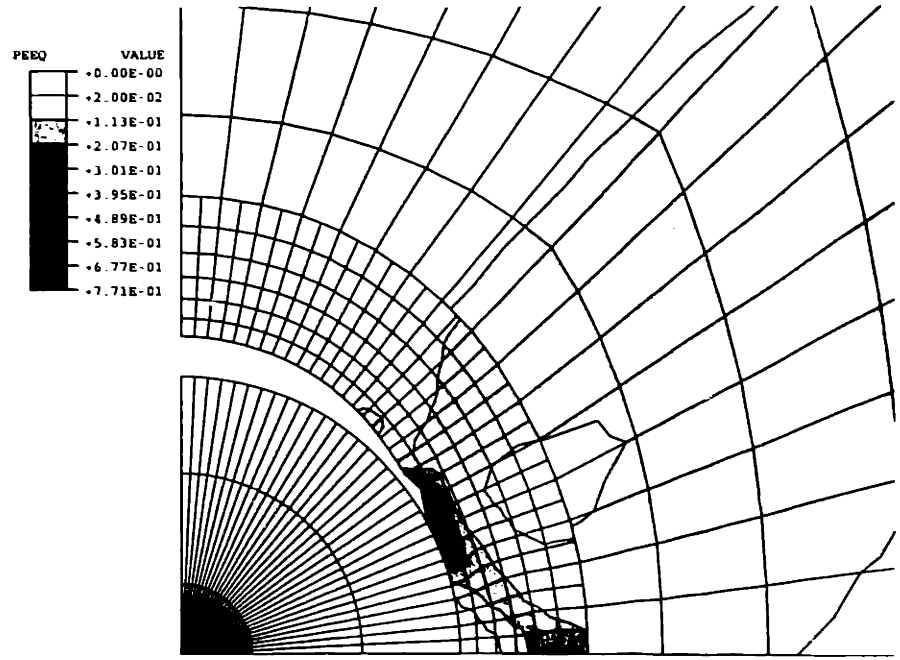

(j)

figure 4-18: COOH interface simulation - (h) deformed mesh after 30% farfield strain (i) equivalent plastic strain contour during crack propagation - note the very limited plastic deformation(marked green) (j) growth of equivalent plastic strain contour after propagation ends.

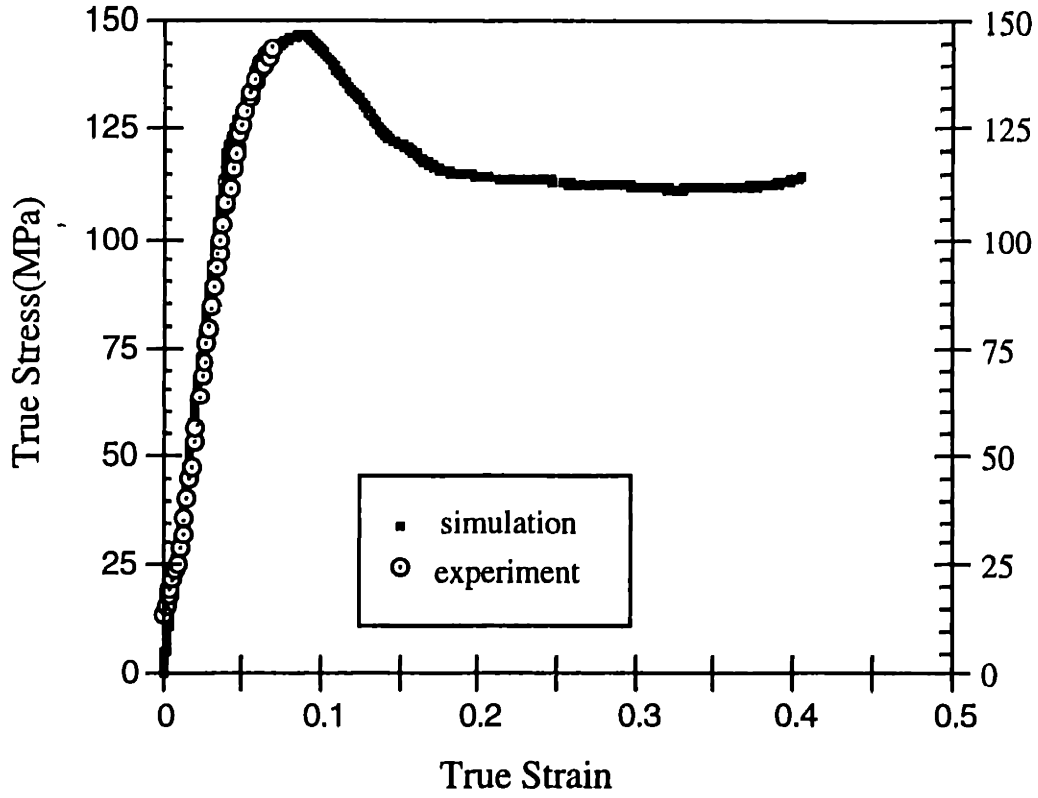

figure 4-19: comparison of farfield stress-strain data for the simulation and the experiment

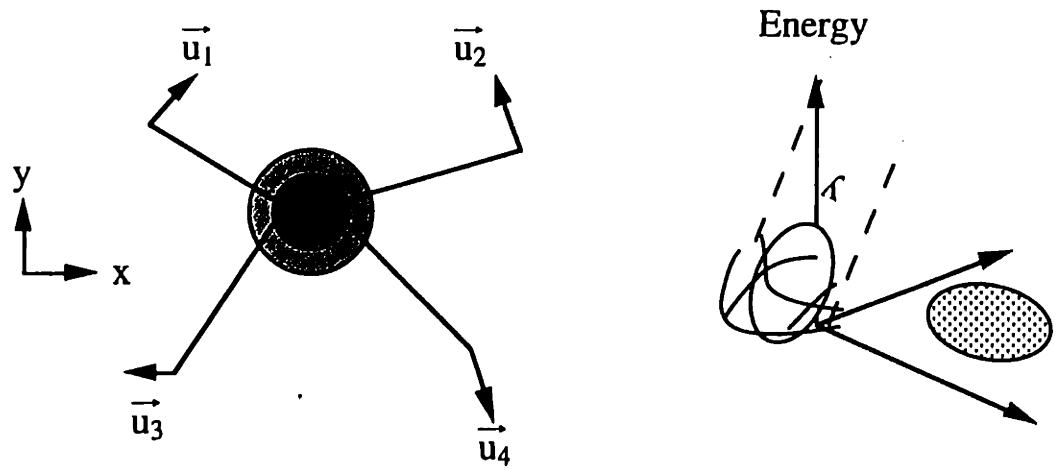

fig. 4-20 (a) Schematic of spring network and ball with imposed displacements, $\vec{u}_i$. The lightly shaded region represents possible positions for the ball. (b) The plot of energy stored in the system w.r.t. the positions within the shaded region. The ball moves in a direction towards the lowest energy.

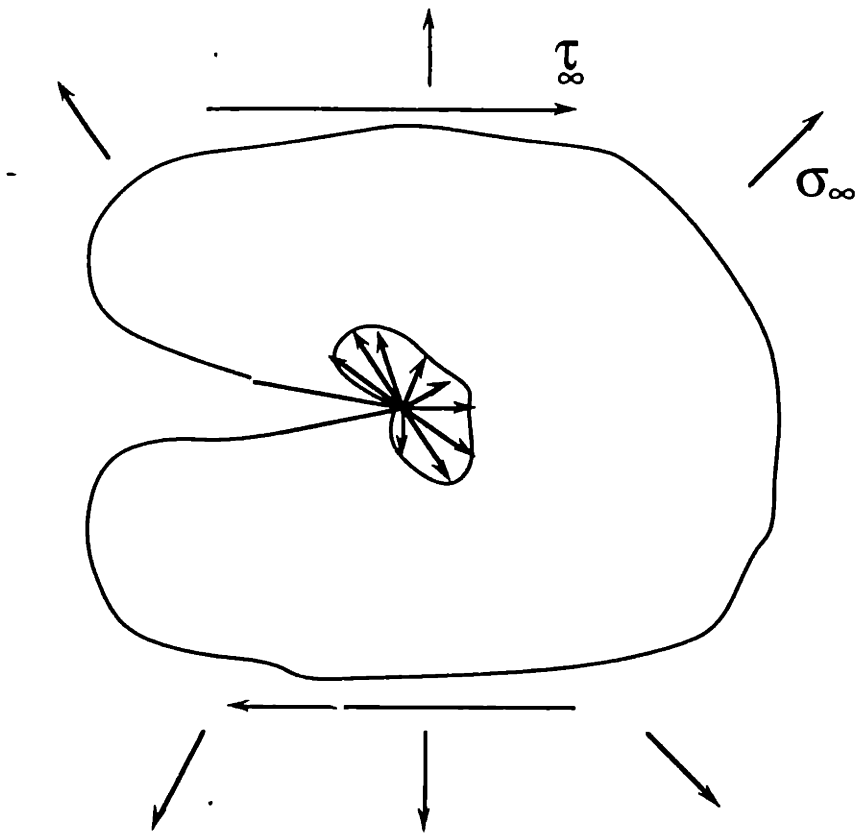

fig. 4-21 Arrows near crack tip indicate magnitude of energy released from the system if the crack is propagated in that direction.

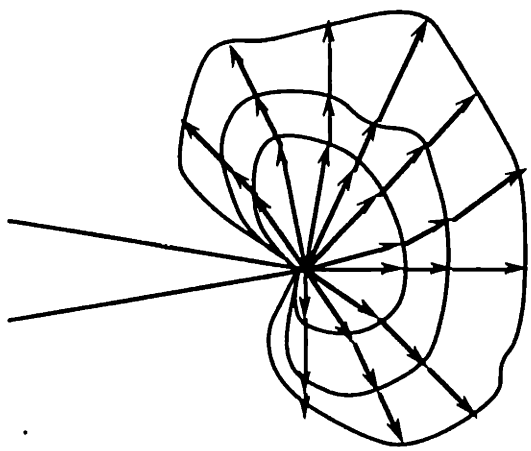

fig. 4-22 Arrows indicate magnitude of energy release in that direction. Each contour represents a different time. The larger radii contours represent later times.

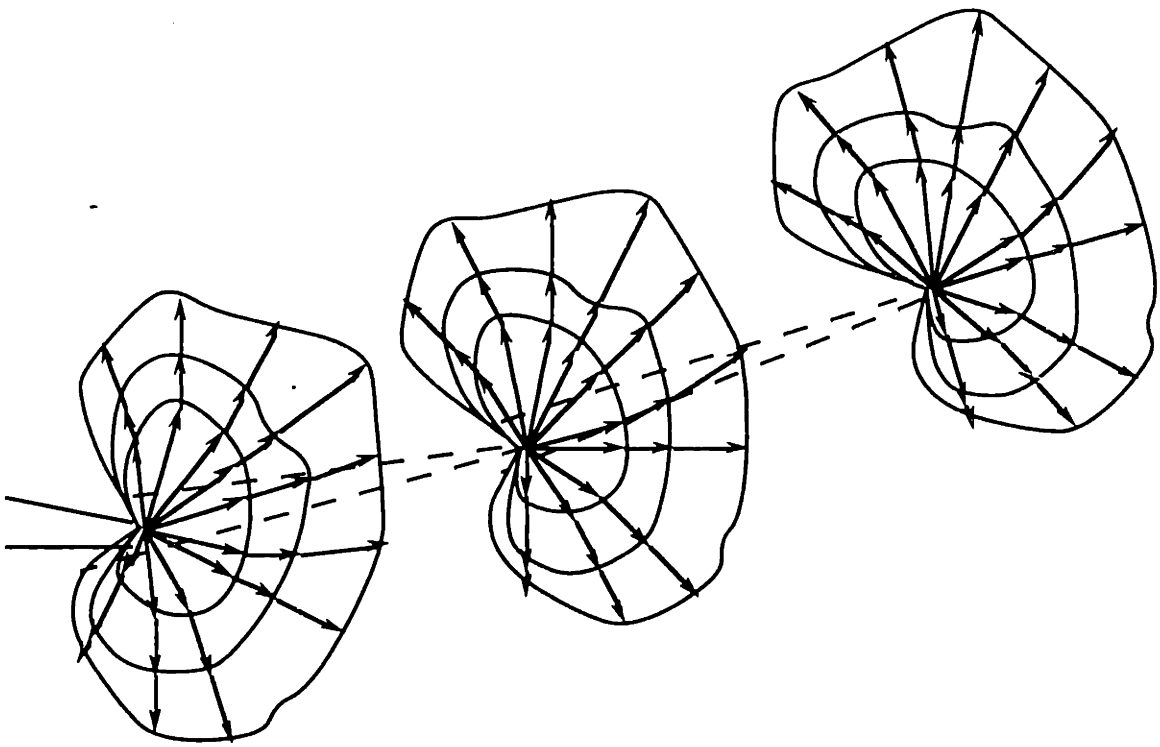

fig. 4-23 As the crack grows from left to right, each set of contours represents the possible energy releases(for various times) at different crack lengths.

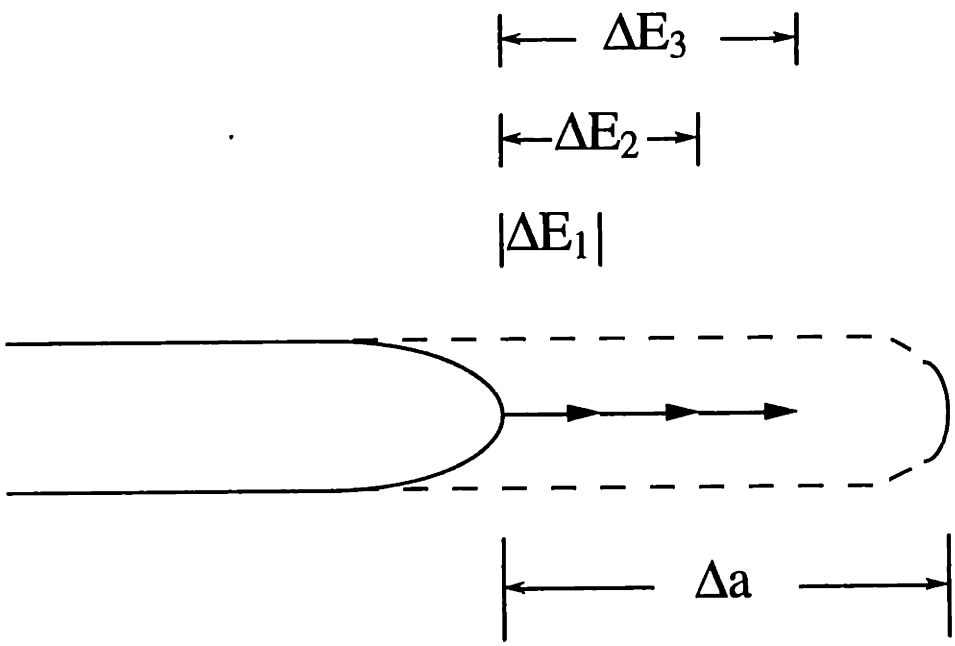

fig. 4-24 The crack is constrained to follow one path. Failure/propagation occurs when $\Delta E_i = \Delta E_{crit}$

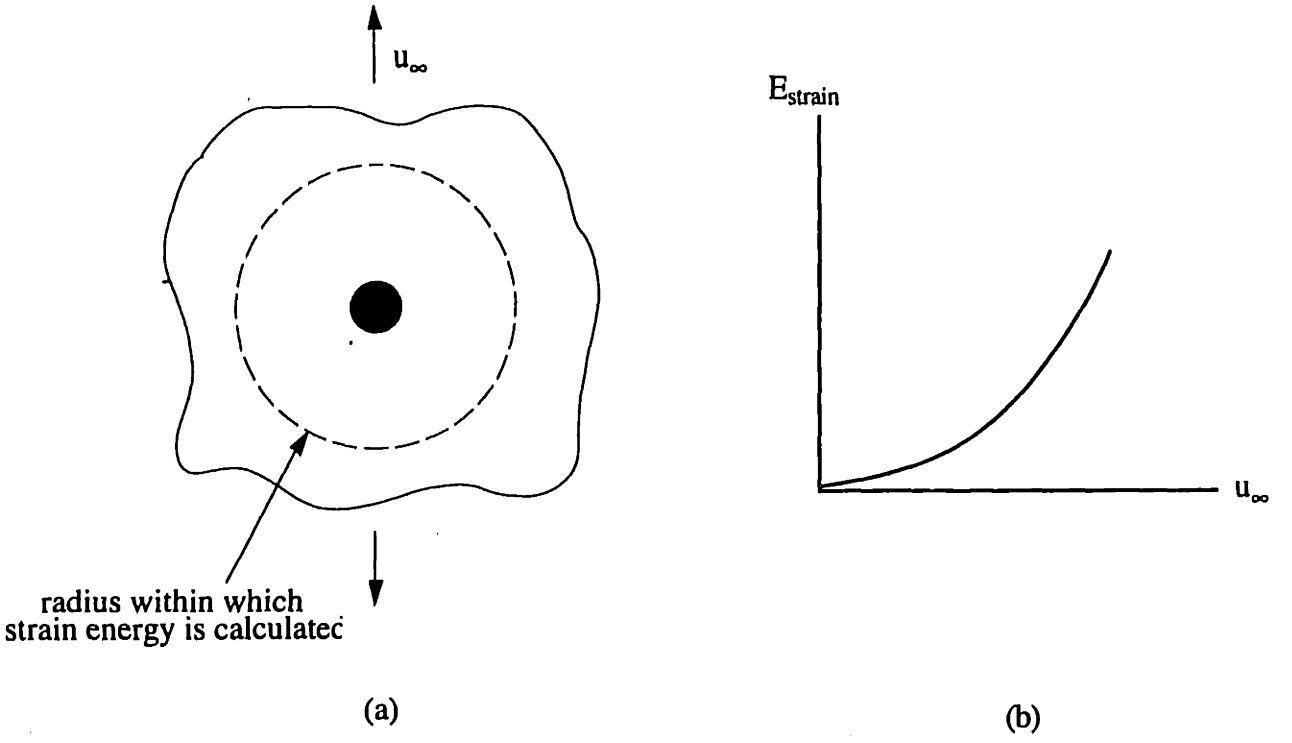

figure 4-25: (a) schematic of region within which the strain energy is computed. (b) schematic of strain energy variation with far-field displacement.

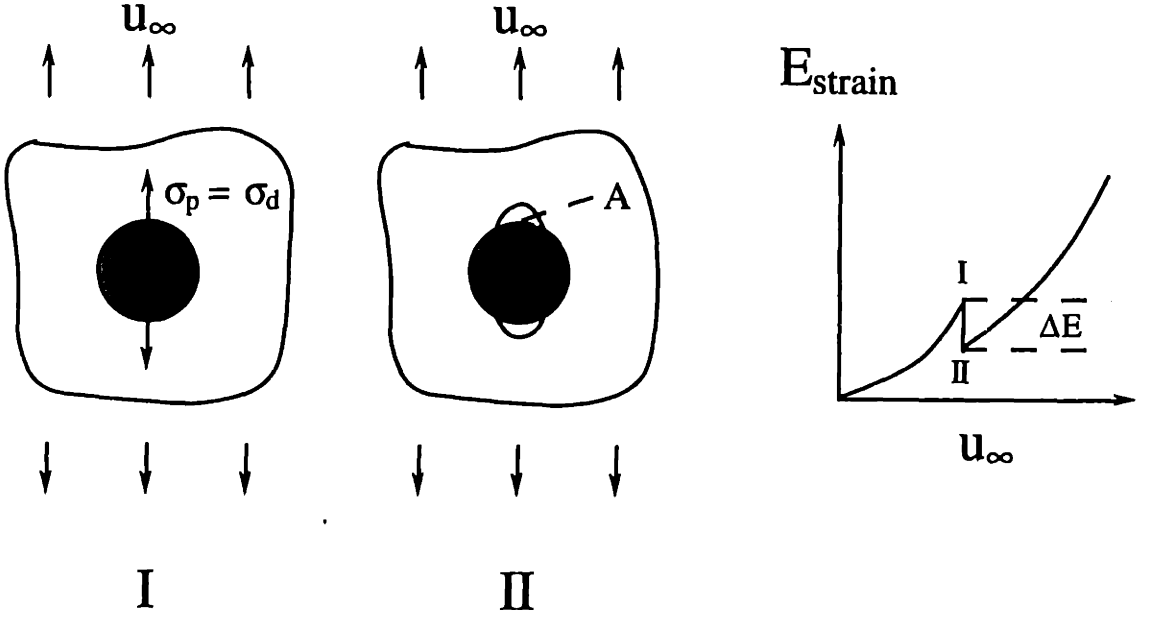

fig. 4-26 (a) At the moment of flaw initiation, the pole stress(σ_p) equals the debonding stress(σ_d). (b) An interface crack of area A is introduced at that moment. (c) The corresponding change in strain energy is recorded.

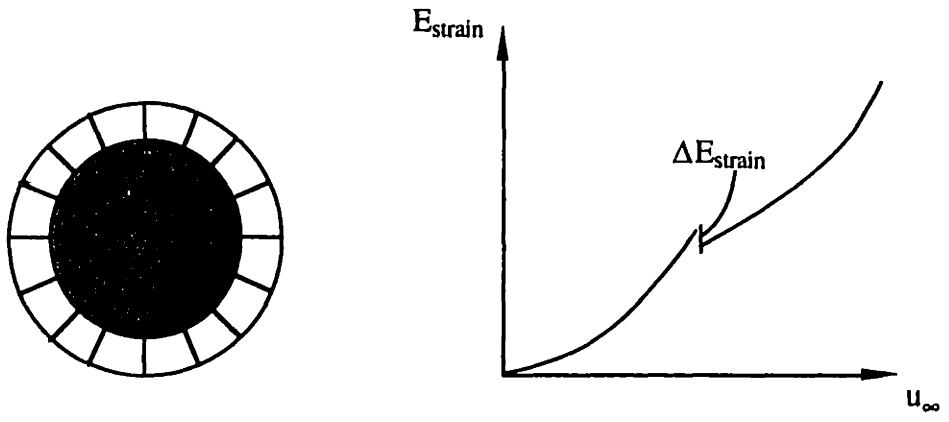

(a)

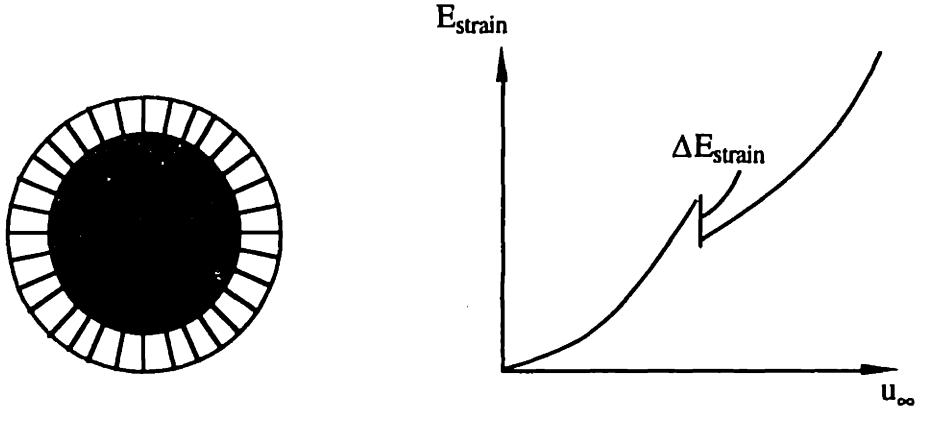

(b)

figure 4-27: A coarse mesh, (a), produces smaller strain energy changes than a fine mesh, (b), for a given crack increment.

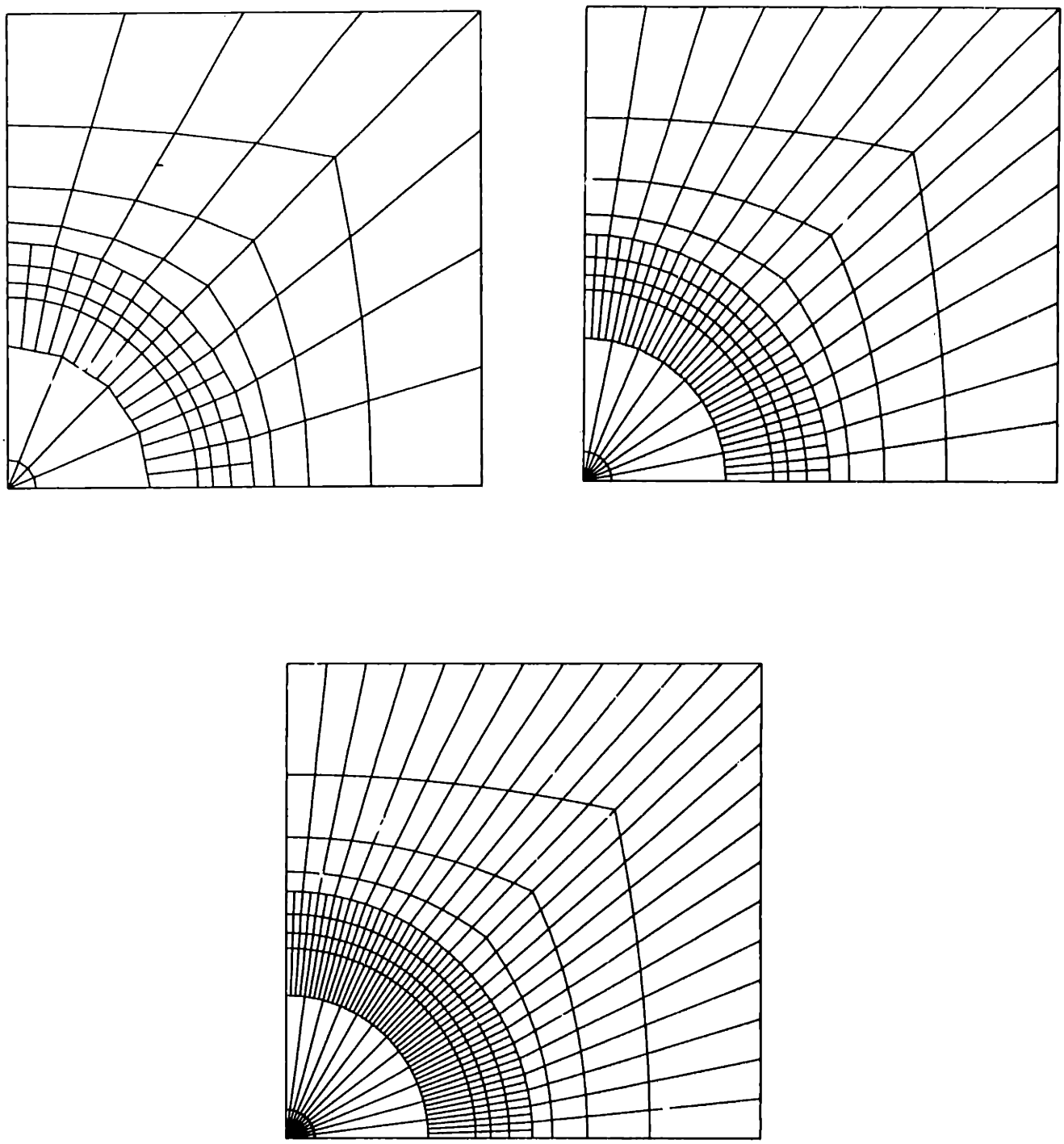

figure 4-28: mesh plots for the (a) 16, (b) 32, (c) 48 element interfaces respectively

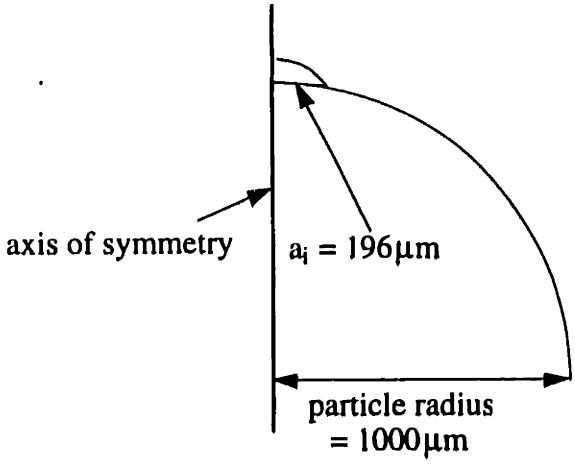

figure 4-29: schematic of initial flaw size used to calculate the interface energy

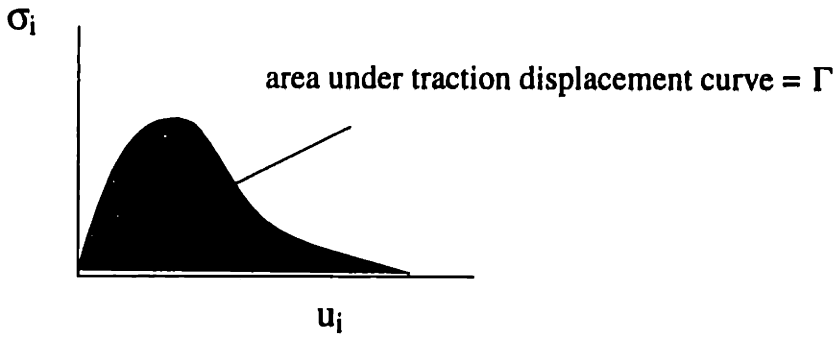

figure 4-30: in pure tension, failure occurs when the entire area under the tensile traction-displacement curve reaches a critical value, Γ.

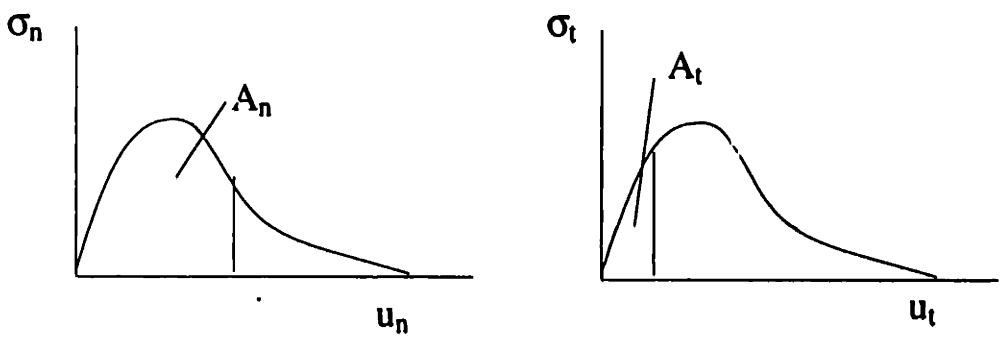

figure 4-31: during mixed mode loading, failure occurs when the total work of the interface ($\sigma_n \equiv$ normal component, $\sigma_t \equiv$ tangential component) reaches a critical value, Γ.

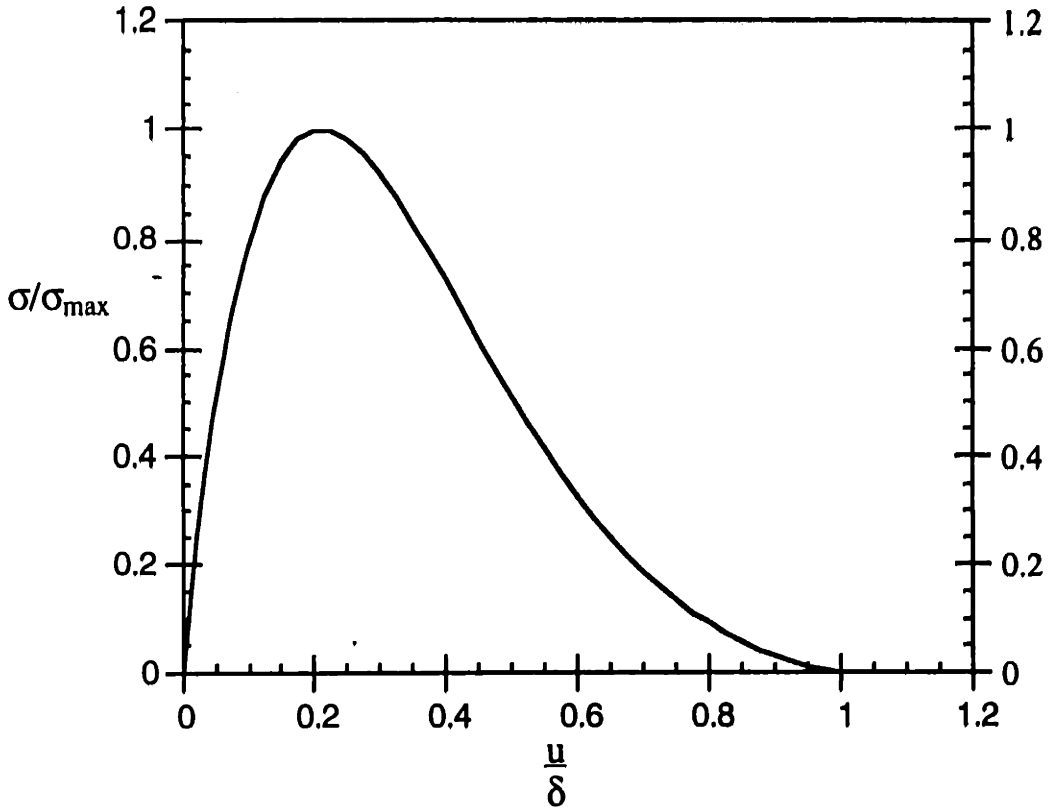

figure 4-32: normalized traction-displacement relation for "Lennard-Jones" type function.

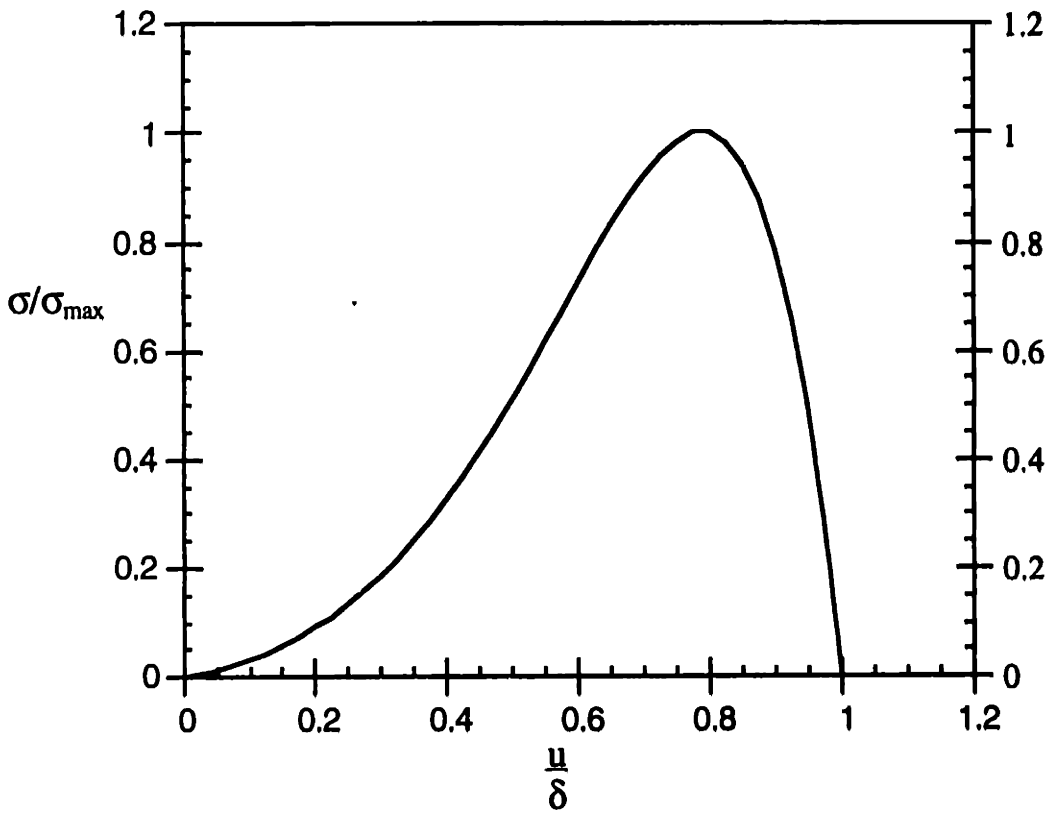

figure 4-33: normalized traction-displacement relation for "Lennard-Jones mirror image" type function.

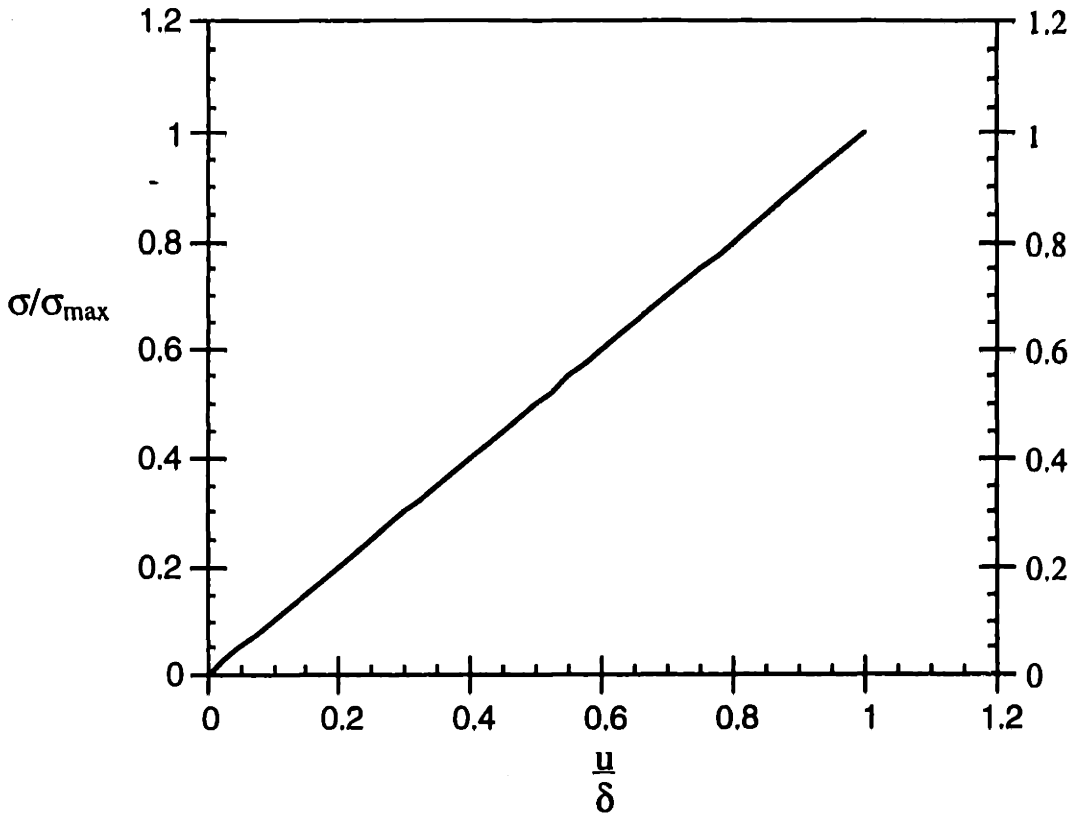

figure 4-34: normalized linear type traction-displacement relation.

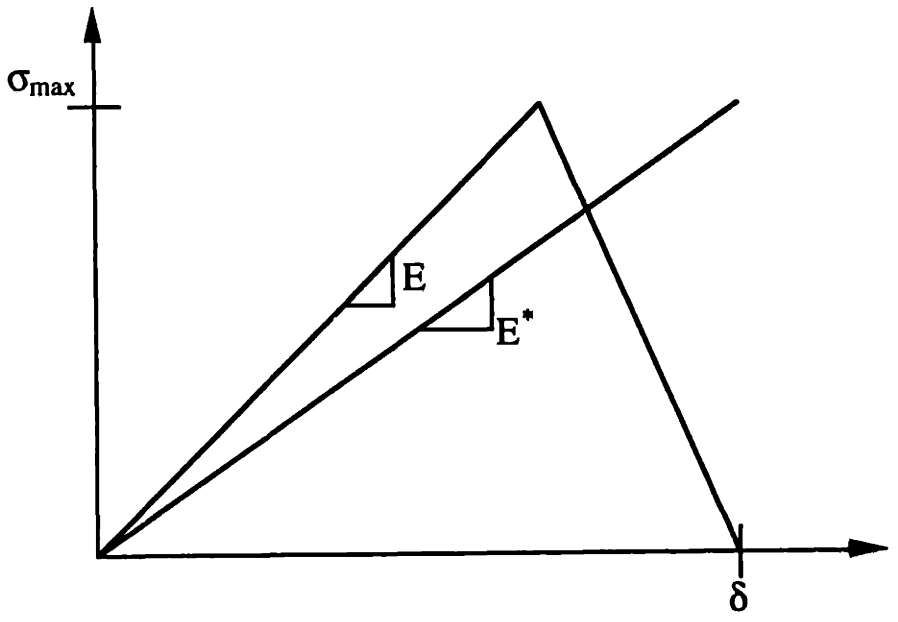

fig. 4-35: By eliminating the descent in the traction-displacement relationship, the effective stiffness of the interface is reduced from E to E^*

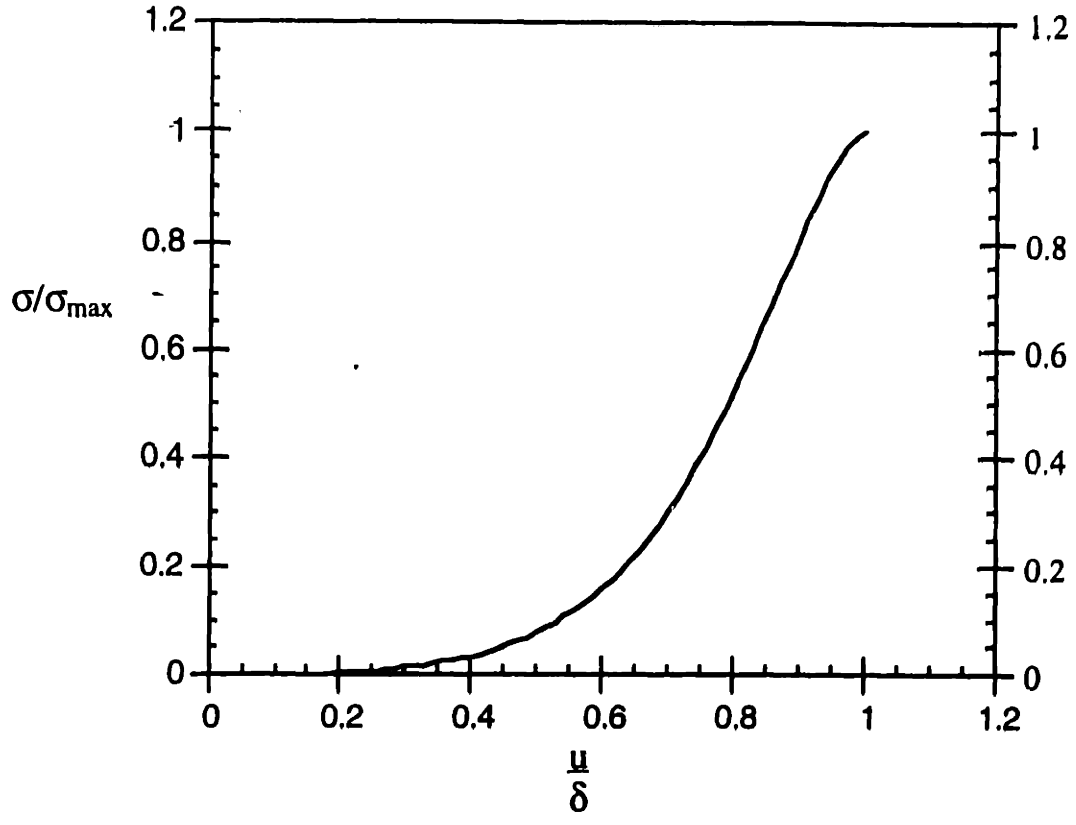

figure 4-36: normalized traction-displacement relation for "truncated Lennard-Jones mirror image" type function.

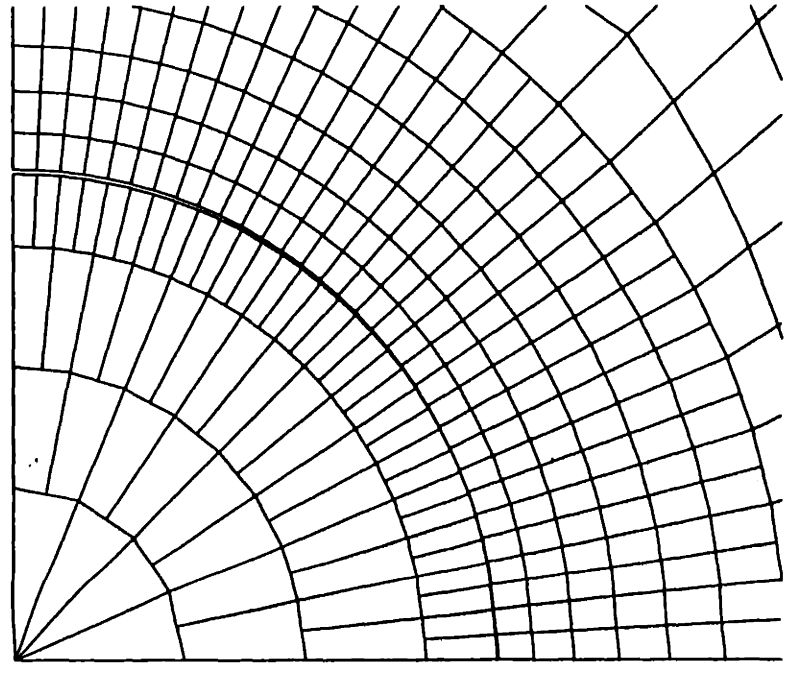

figure 4-37: plot of deformed mesh and spacing of interface during interface failure initiation for the minimum δ possible.

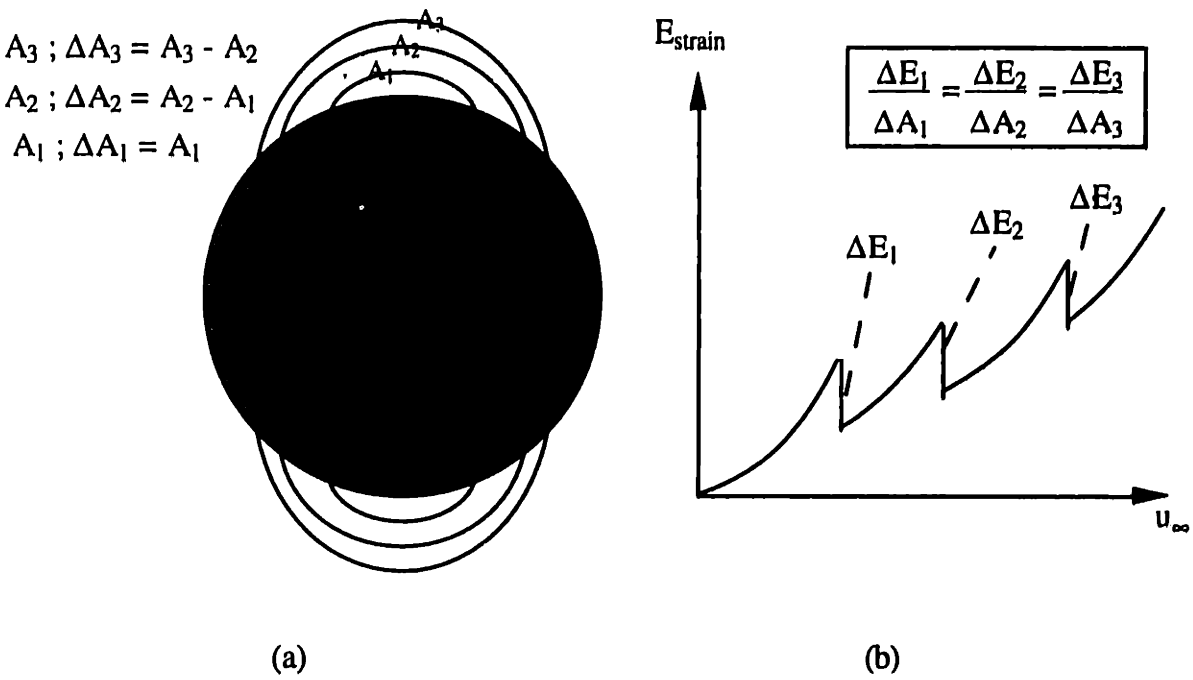

figure 4-38 (a) schematic of incremental changes in crack area as the crack propagates. (b) schematic of corresponding strain energy curve

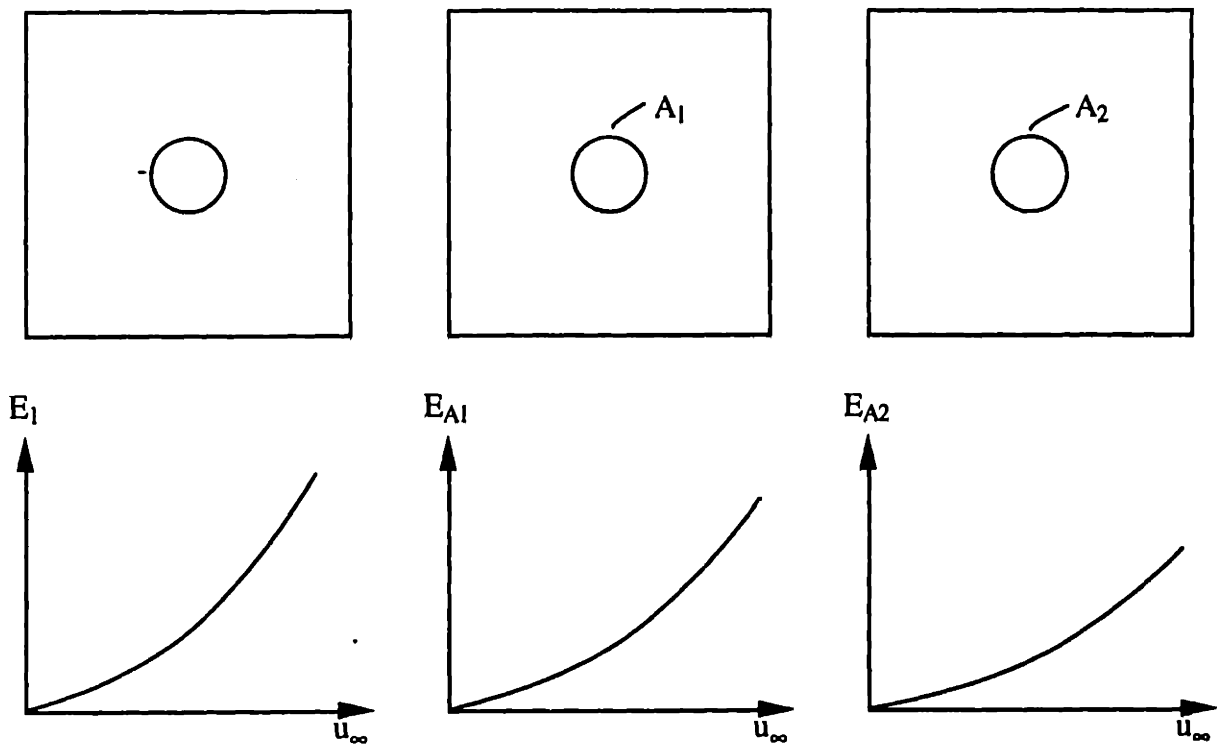

(a)

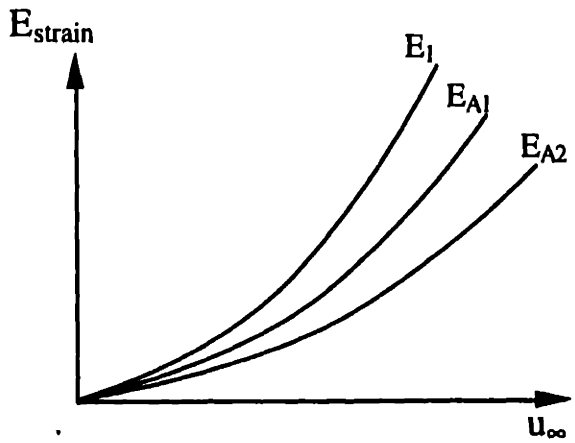

(b)

figure 4-39 (a) schematic of strain energy curves for an interface with fixed crack areas. From left to right: no crack, small crack, larger crack. (b) schematic of strain energy curves for the stationary cracks superposed over the strain energy curve for the incrementally propagating crack.

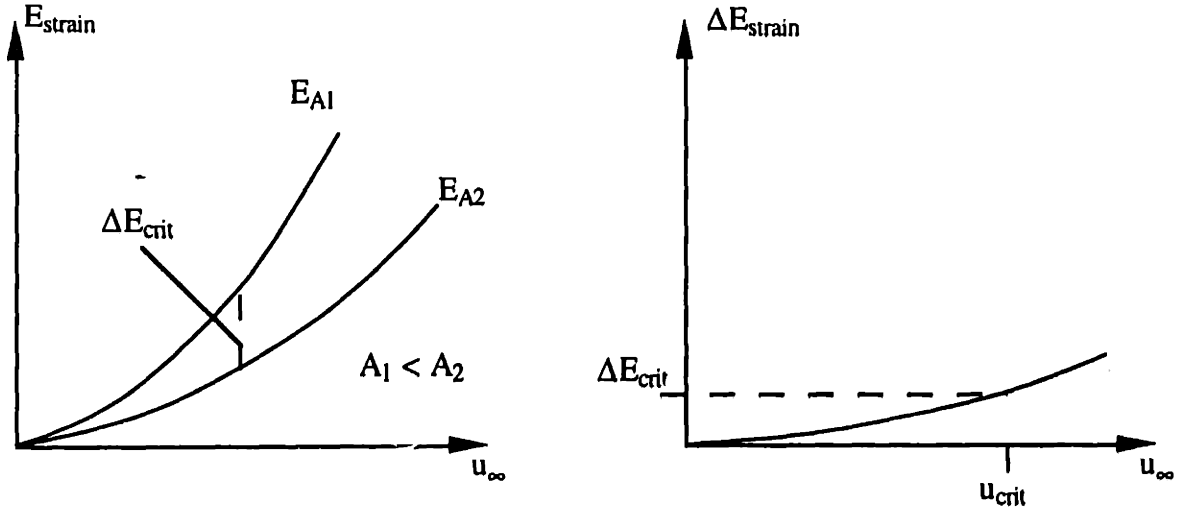

figure 4-40: The flaw propagates when the difference between the strain energy curves for different crack areas reaches a critical value. The farfield displacement at that point is calculated(u_{crit}).

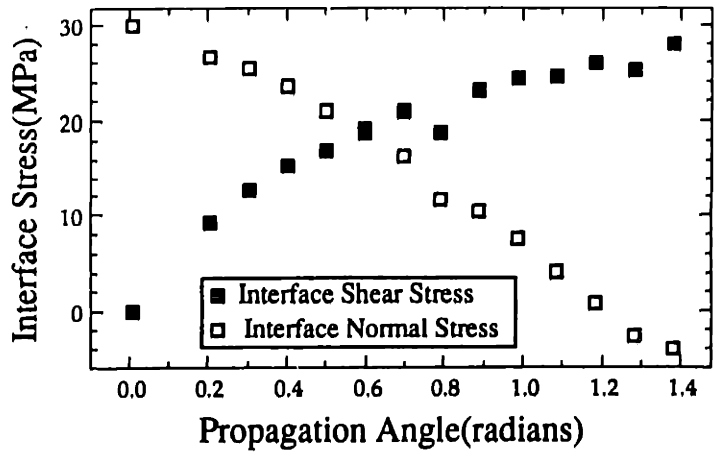

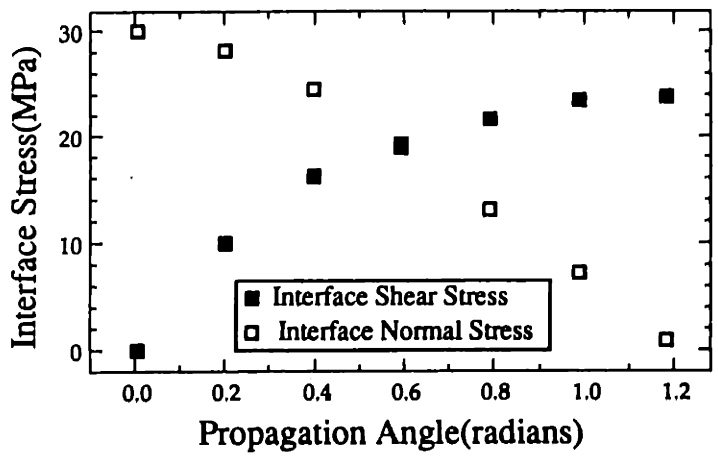

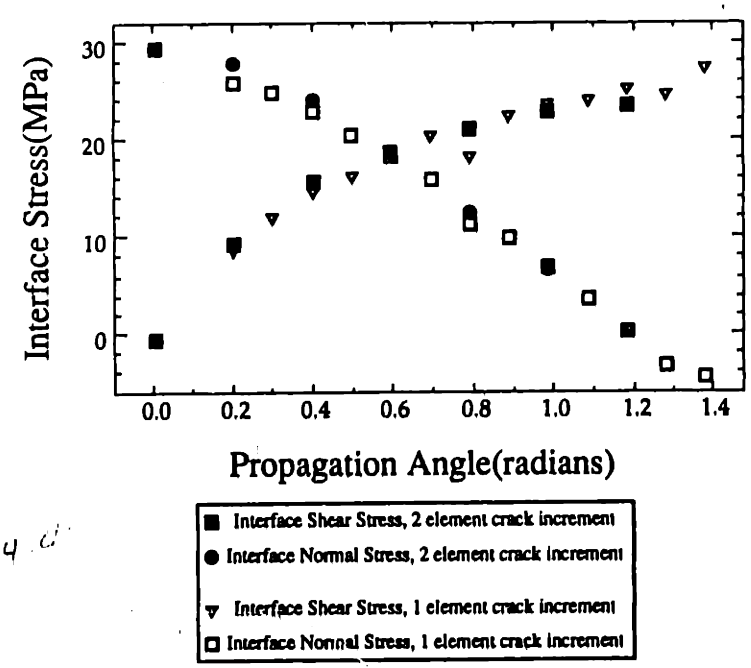

figure 4-41: (a) failure locus calculated using a crack increment of one element (b) failure locus calculated from using a crack increment of two elements (c) superposition of both loci

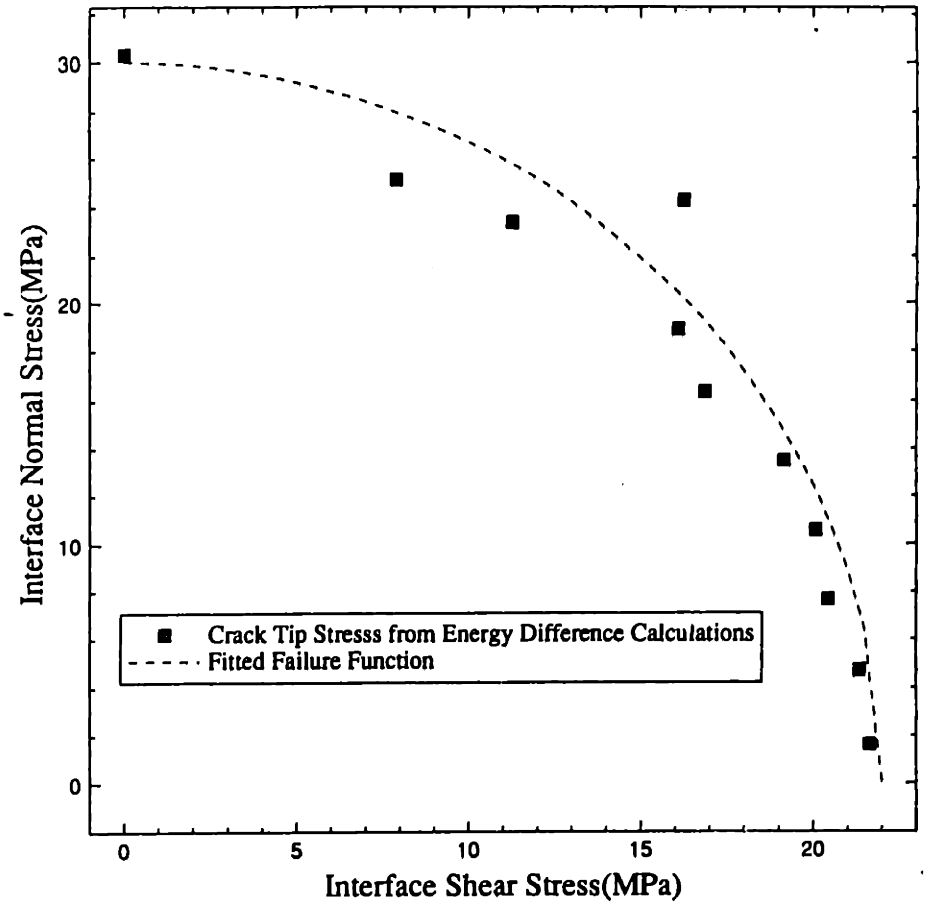

figure 4-42: failure function fit to the computed locus

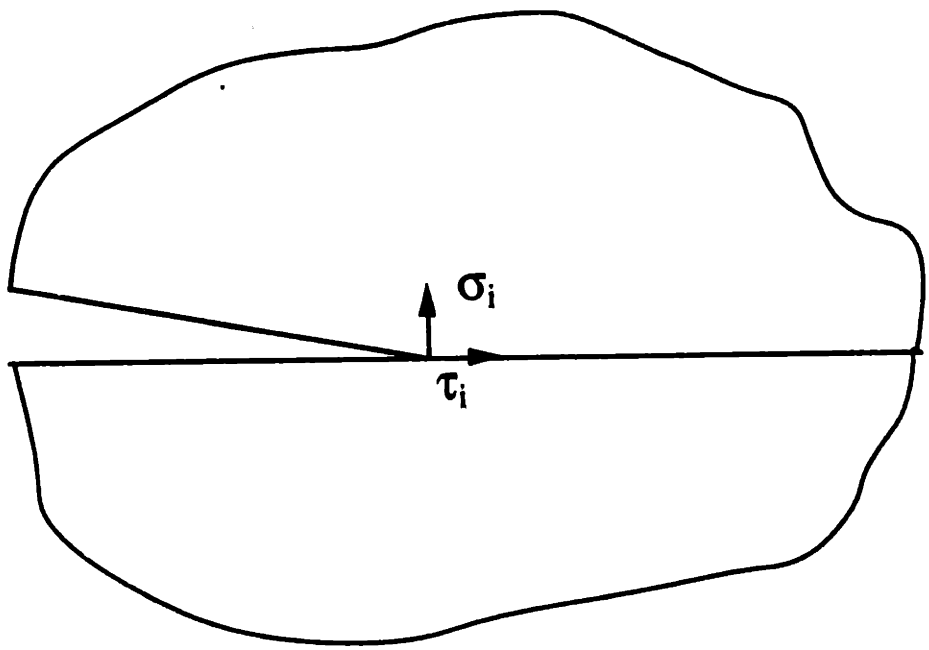

figure 4-43: location at which failure locus stresses are computed.

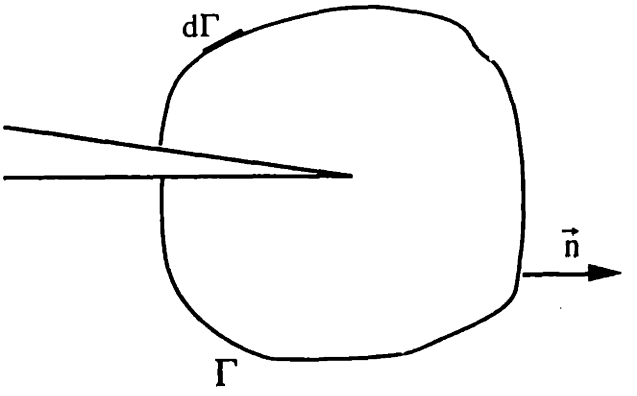

figure 4-44: definition of the J-integral contour.

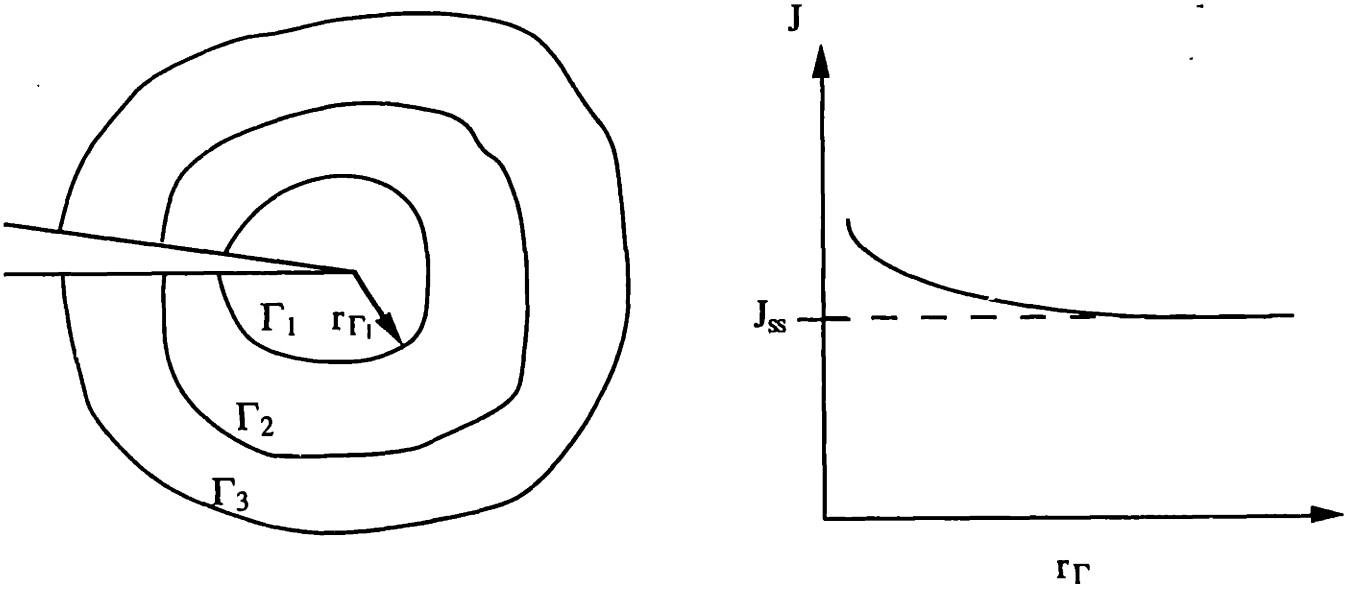

figure 4-45: schematic of J values calculated from successively expanding contours. note: the J value decays to a steady state value.

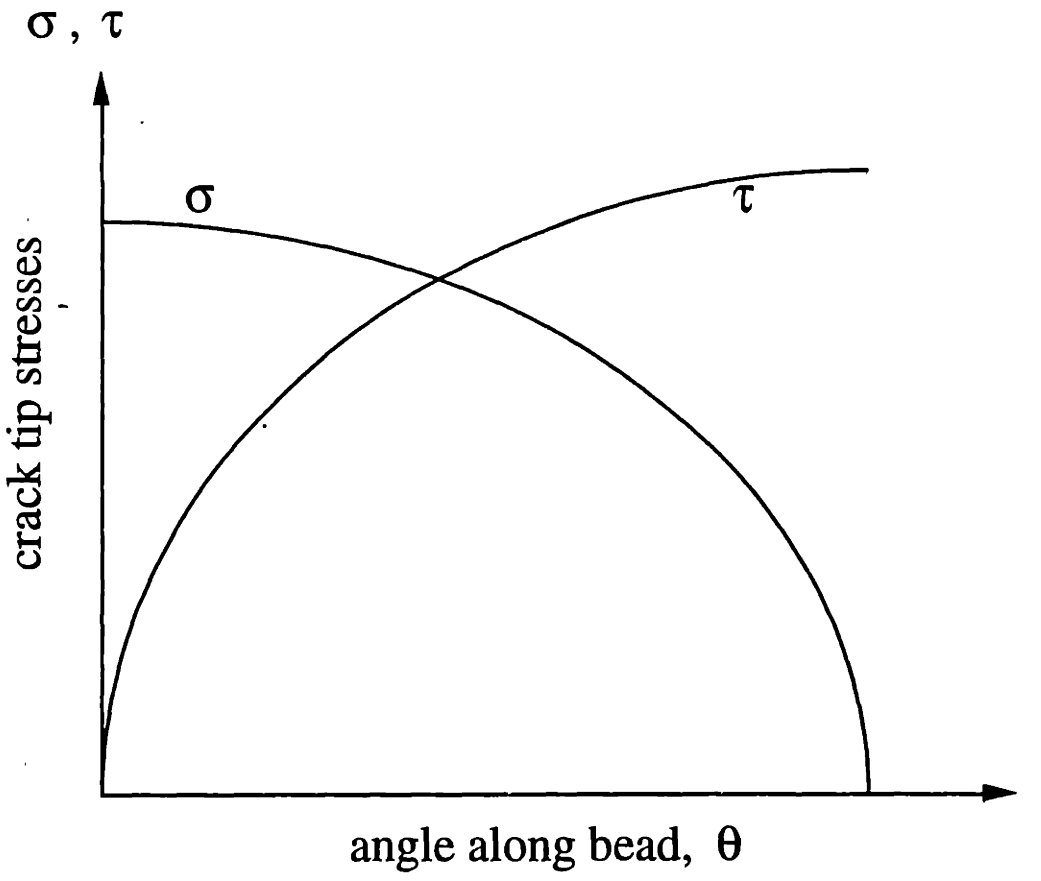

figure 4-46: schematic of crack tip stresses during failure as calculated by the J-integral

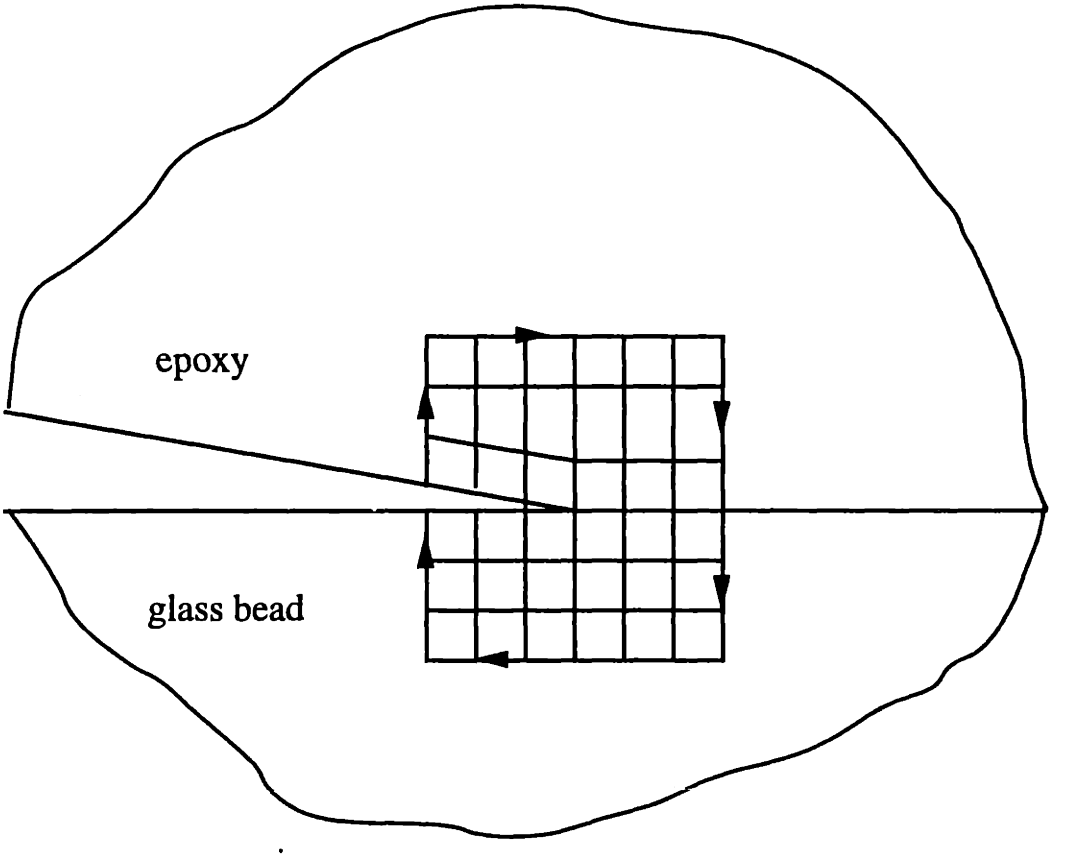

figure 4-47: schematic of J-integral contour used for failure locus calculations.

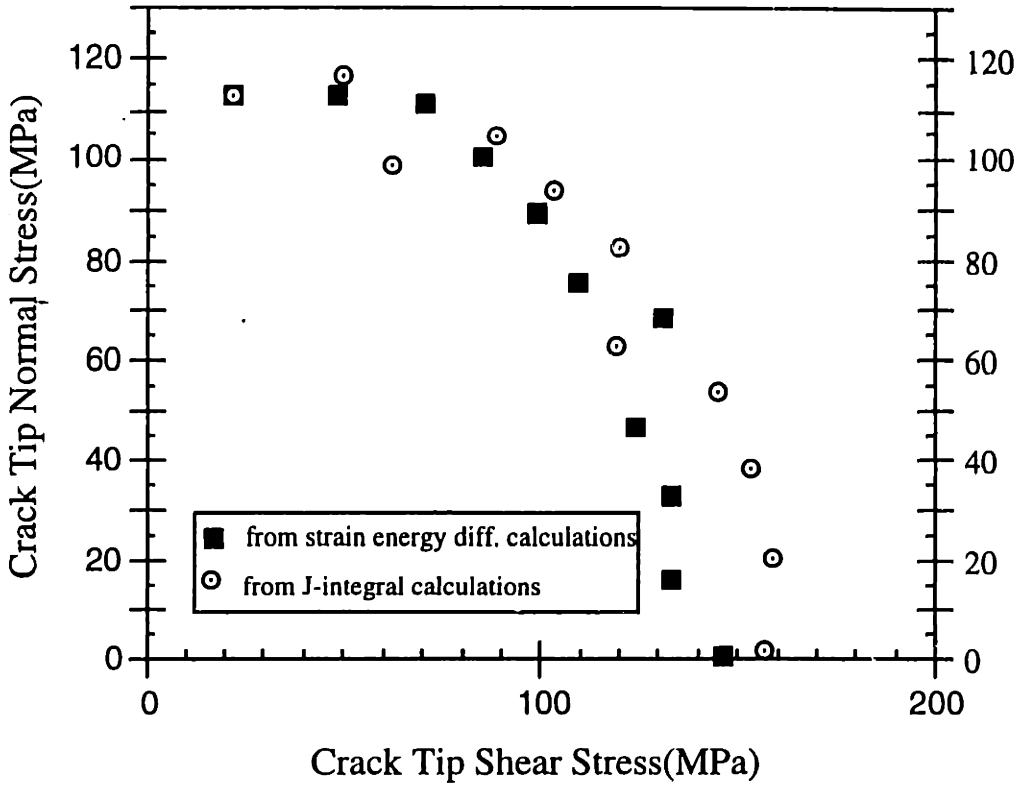

figure 4-48: comparison of failure loci computed for an interface with 16 elements from J-integral and energy difference calculations.

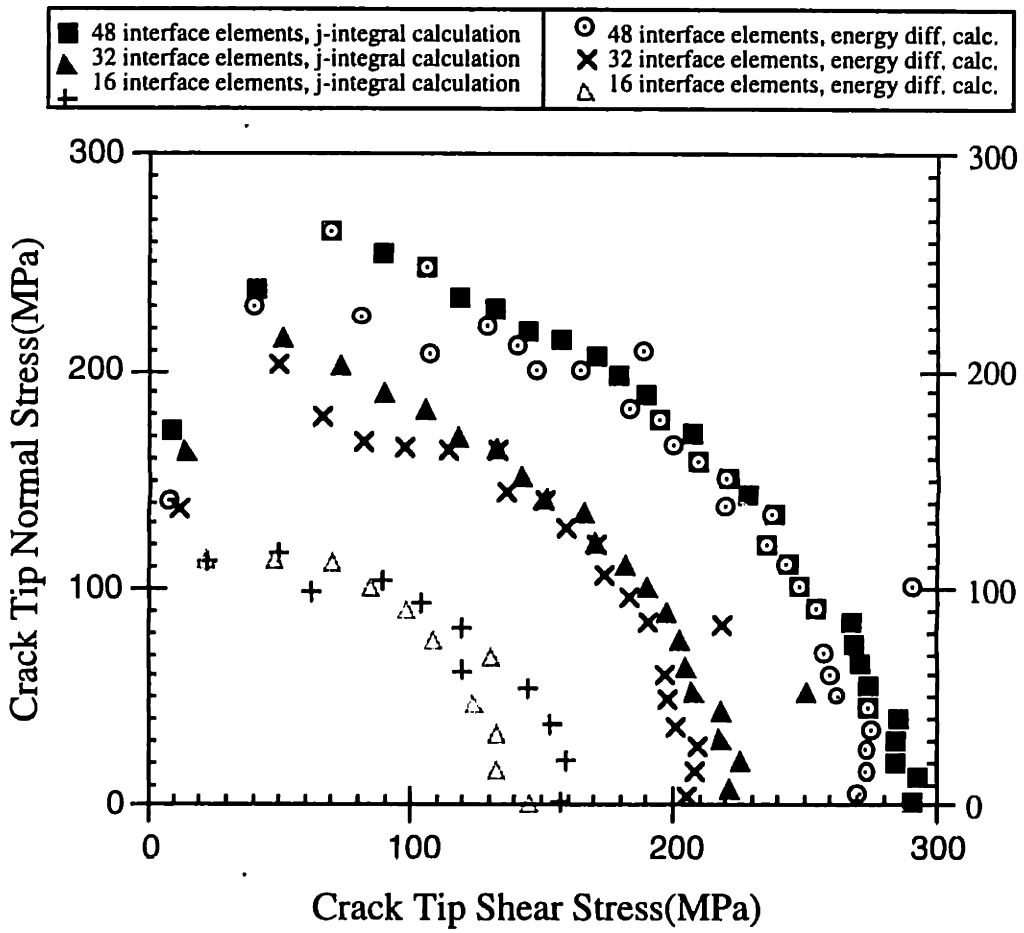

figure 4-49: failure loci for various interface mesh densities using the J-integral and energy difference methods. note: both methods produce nearly identical failure loci.

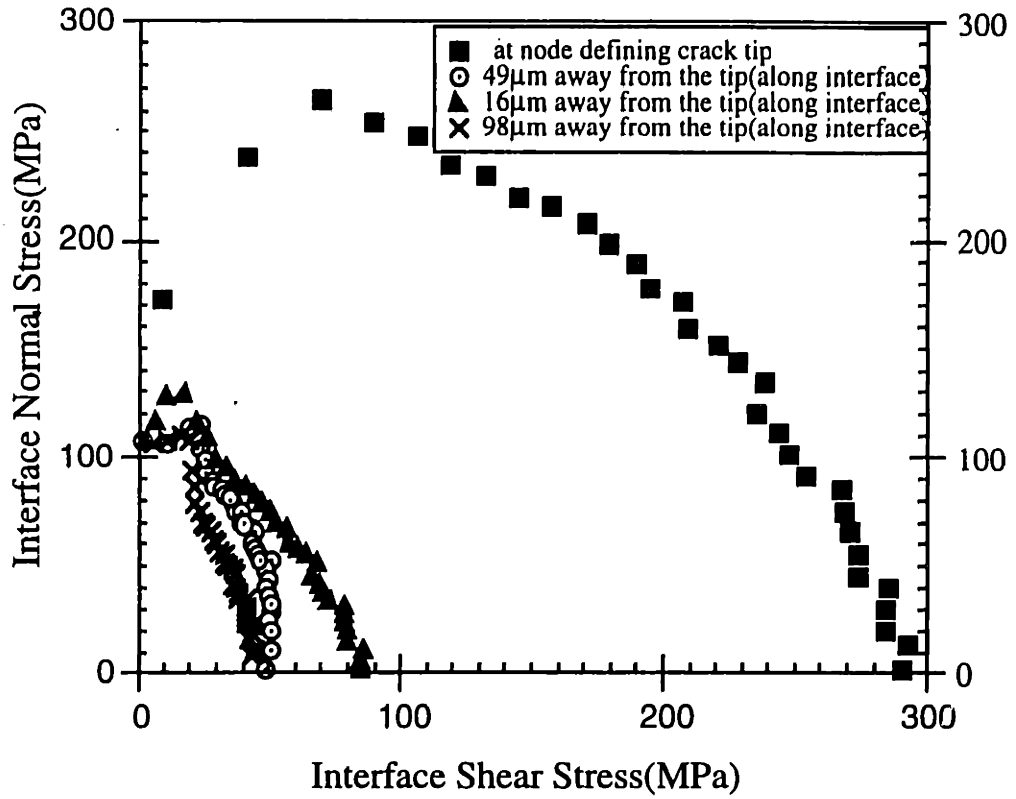

figure 4-50: failure loci as computed from various distances away from the crack tip for an interface density of 48 elements.

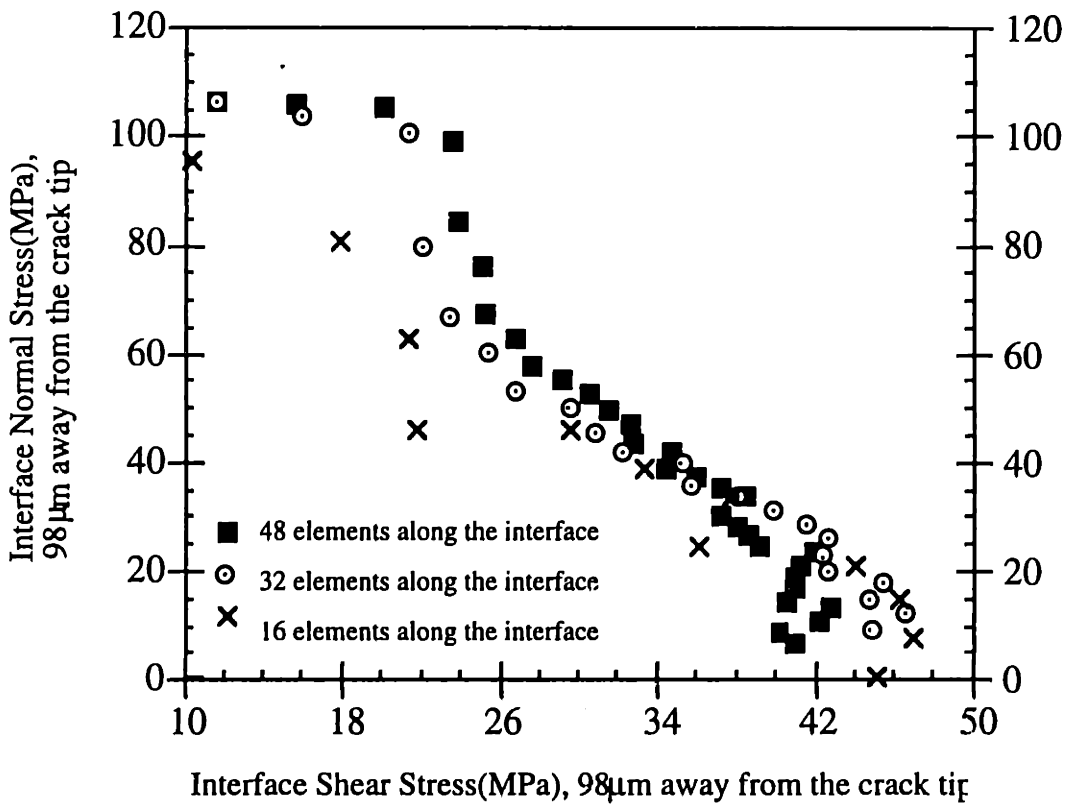

figure 4-51: failure locus as computed from 98 microns behind the crack tip for various interface element densities.

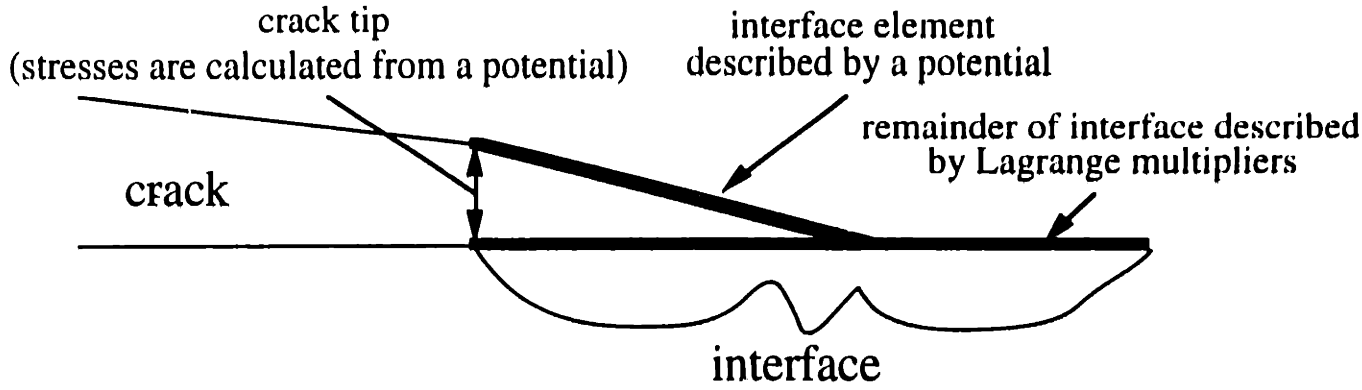

figure 4-52: schematic of modified interface crack model: the tip element is modeled as having a potential relation while the remainder of the interface is constrained by Lagrange multipliers.

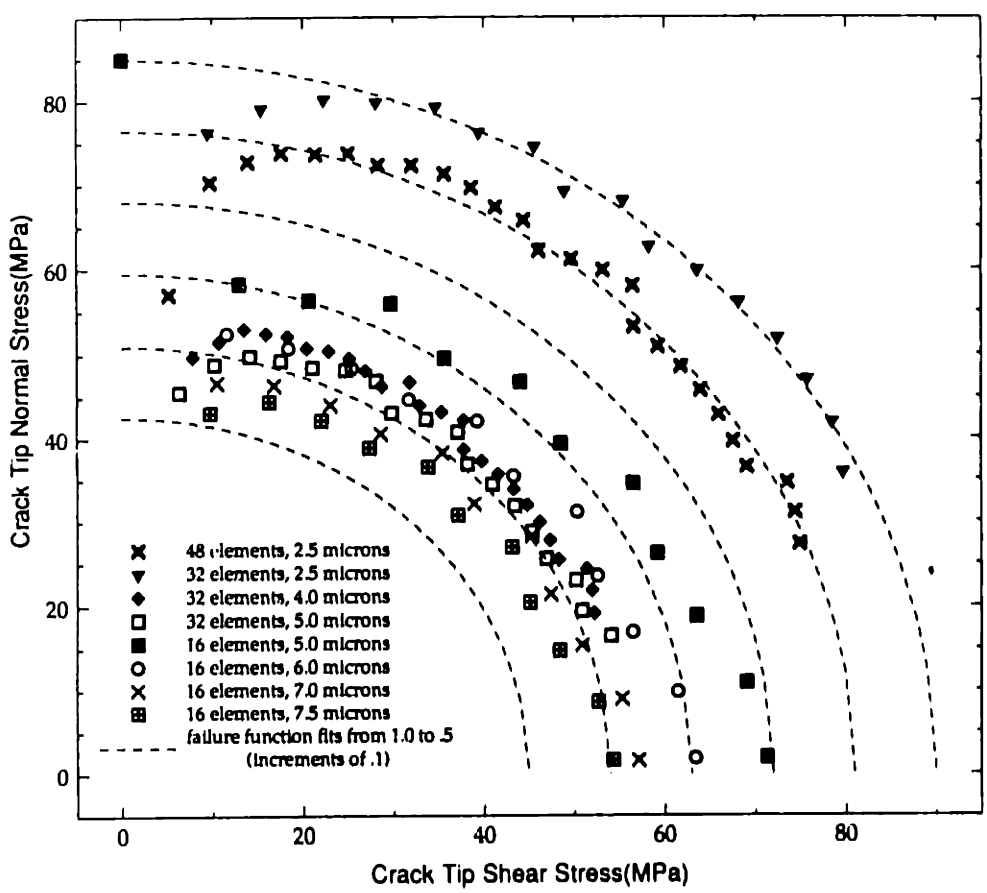

figure 4-53: failure locus calculations with crack tip potentials for various mesh densities and characteristic lengths.

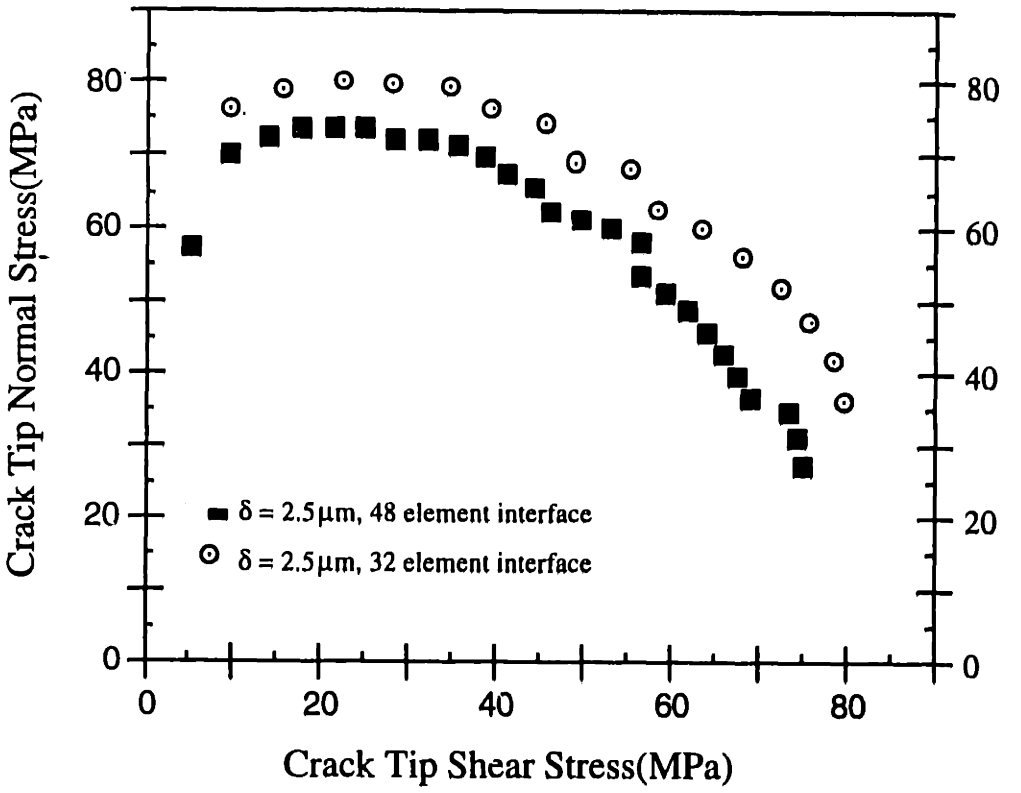

figure 4-54: (a) variation of the failure locus with the interface element density for a given characteristic distance, δ.

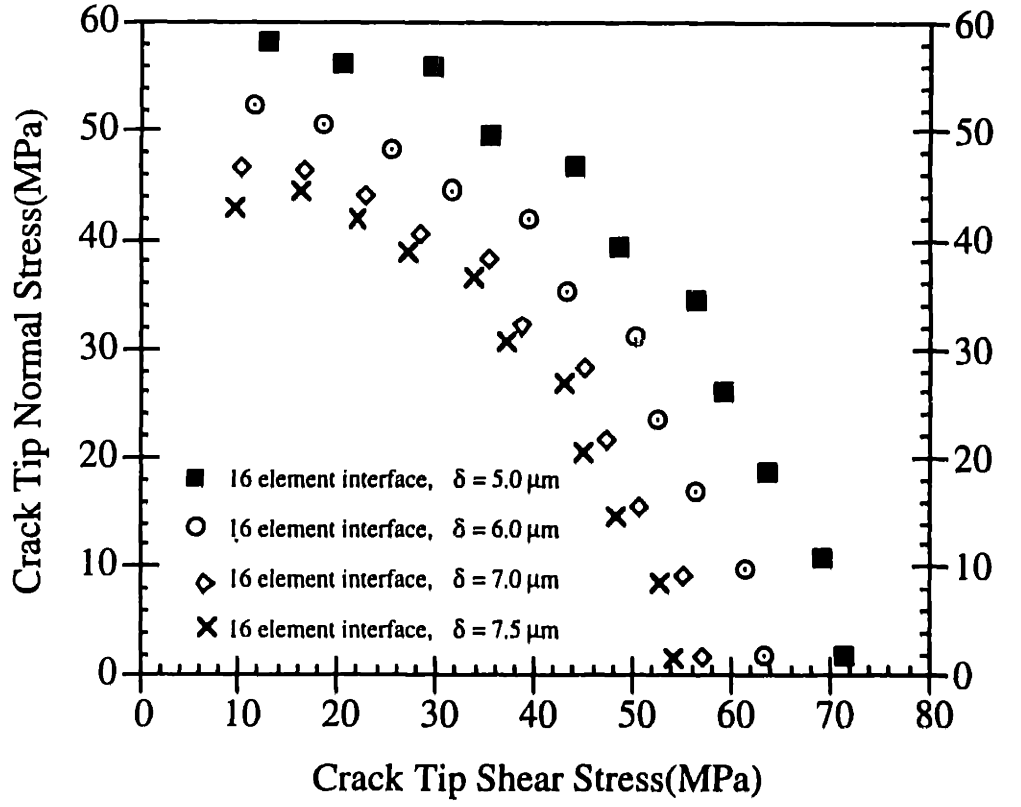

figure 4-54: (b) variation of the failure locus with the characteristic distance, δ, of the interface traction-displacement relation for a given interface element density.

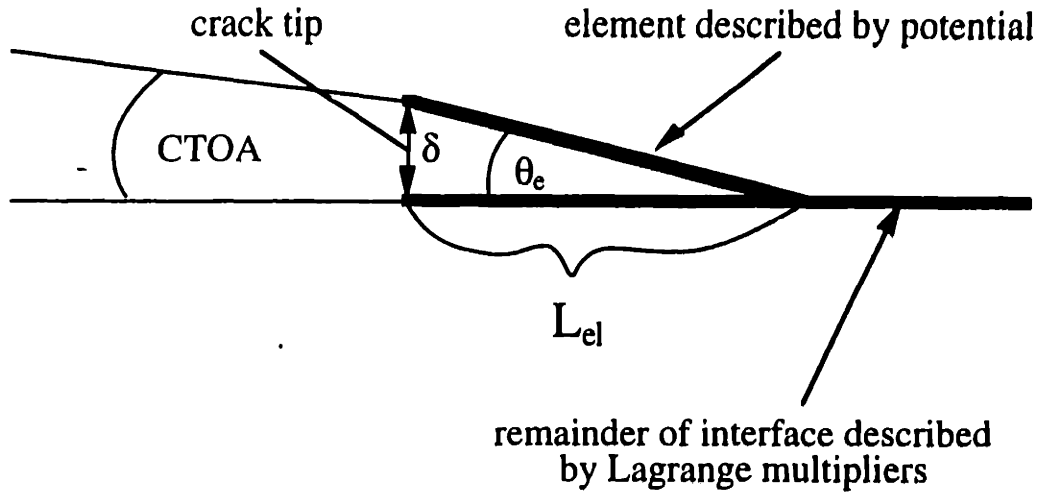

for small deformations,

$$\theta_e \approx \frac{\delta}{L_{el}} \quad , \quad CTOA \approx \theta_e$$

figure 4-55: for infinitesimal deformations, the critical tensile crack tip opening angle(CTOA) can be estimated by the interface element length, l_e, divided by δ, the characteristic distance of the interface traction-displacement relation.

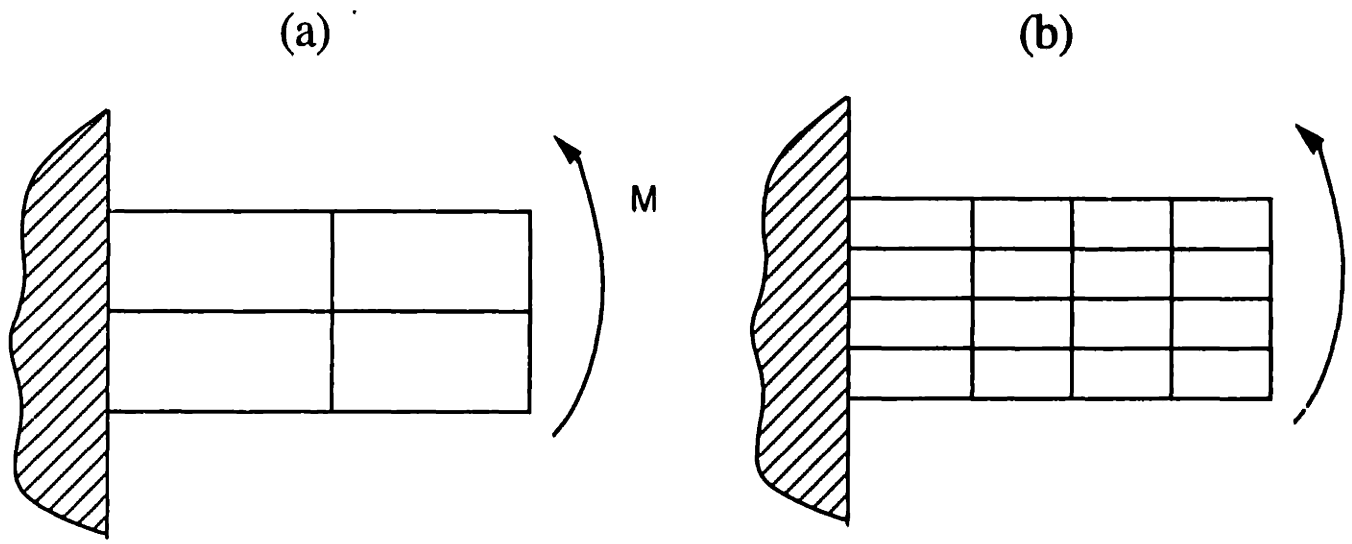

$$K_{eff,(a)} > K_{eff,(b)}$$

figure 4-56: the apparent stiffness, $K_{eff,(a)}$, of a coarse mesh in bending is higher than that of a fine mesh($K_{eff,(b)}$).

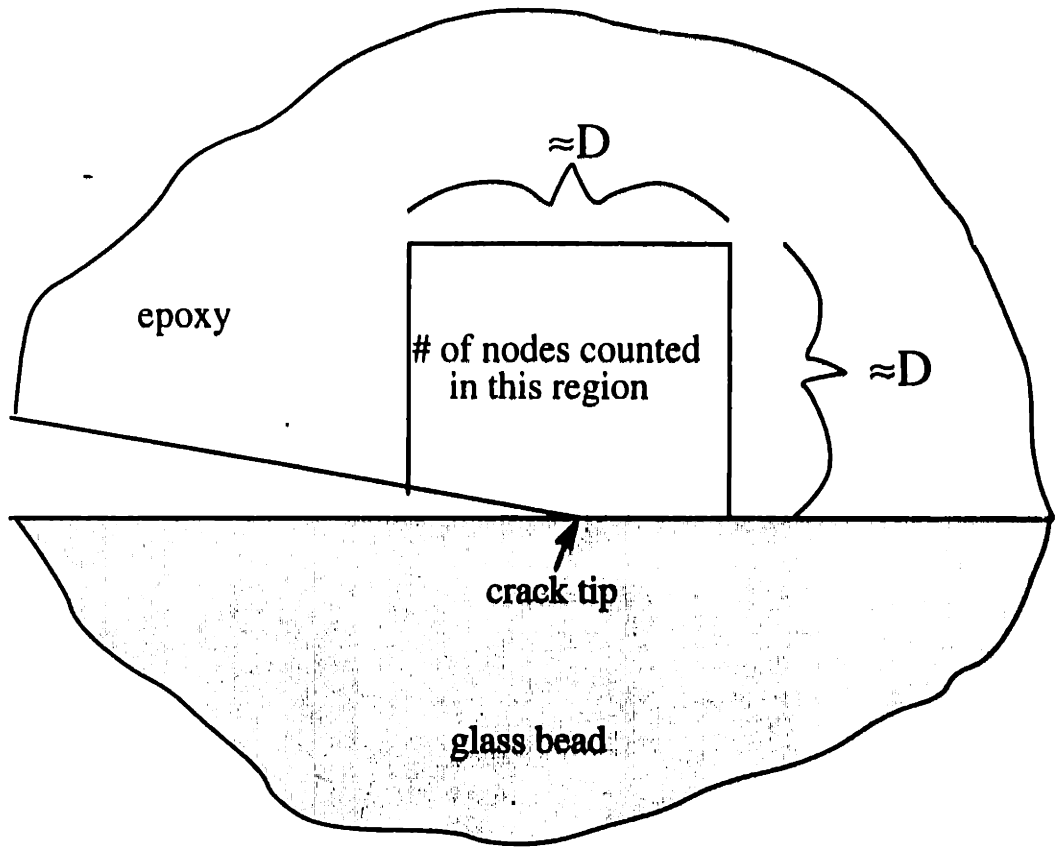

figure 4-57: region near crack tip where the number of degrees of freedom(#dof) are counted. D ≈ 100μm.

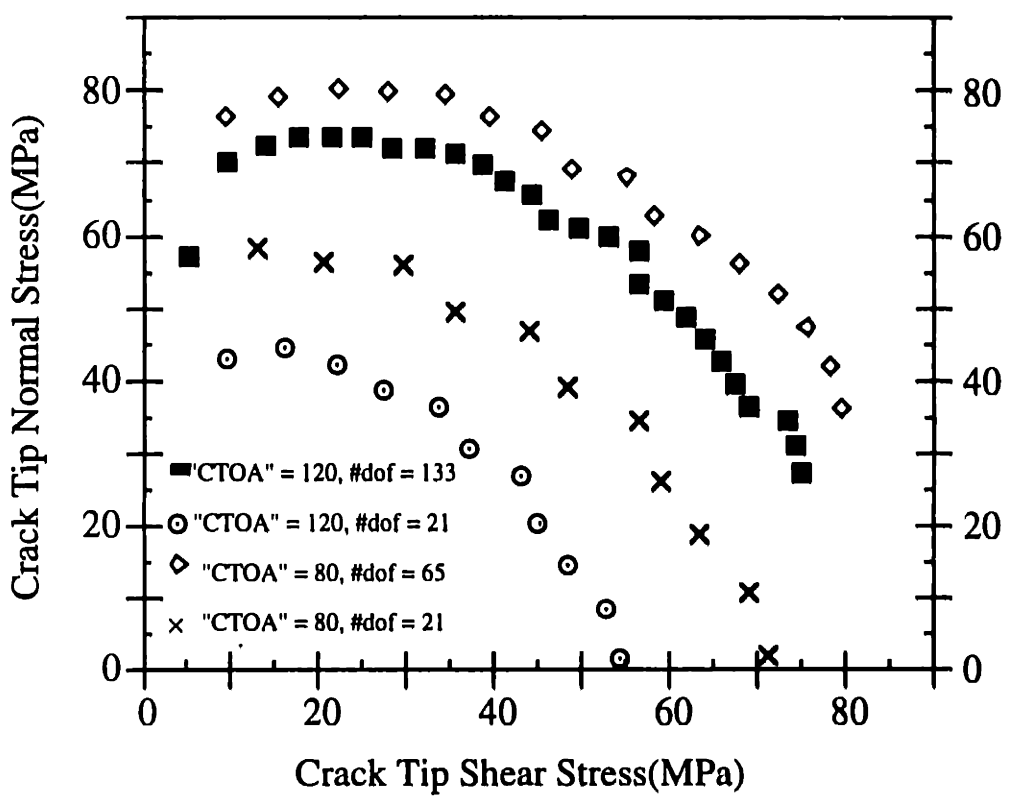

figure 4-58: variation of failure locus with apparent stiffness of surrounding matrix.

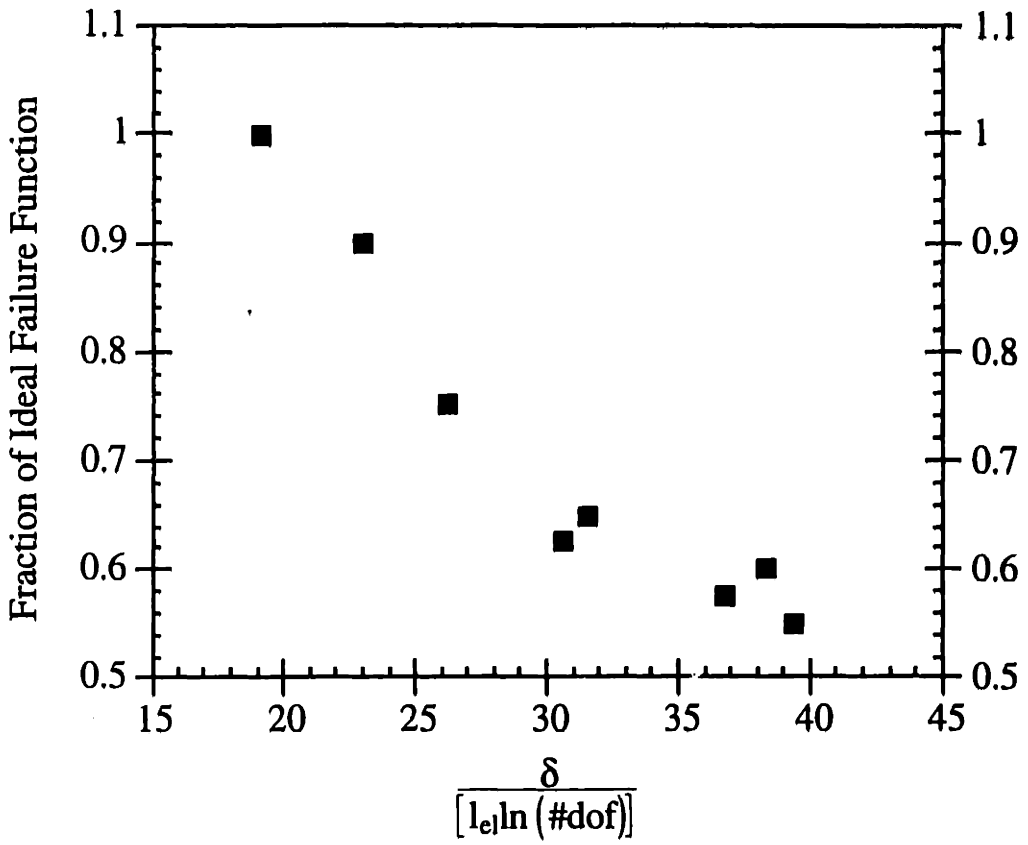

figure 4-59: variation of the normalized failure function with dimensionless interface element size, $\frac{\delta}{(l_e \ln(\#dof))}$

Chapter 5: Preliminary Results and Future Work

5.1 Energetic Consistency of the Failure Locus

The validity and the applicability of the interface stress based failure criteria is discussed in this chapter. The validity of the criteria hinges on one issue: energetic consistency. Simply stated, the locus, when applied to other geometries or loading configurations, should allow the system to release the same amount of total energy as is required to create the new surfaces. In all of the work discussed thus far, the simulations are restricted to the case of far field tension of an epoxy matrix surrounding a glass bead for which the failure locus is assumed to be applicable.

Ideally, the locus should only be a function of the constituent materials and not dependent on the specific geometry. Specifically, the failure criteria should release the correct amount of energy during flaw propagation when the material in the vicinity of the interface is subjected to predetermined combinations of stress which are independent of farfield loading conditions and macroscopic geometry(fig.5-1). A preliminary check of this feature is obtained by testing the locus on a simulation of biaxial loading of a glass fiber in an epoxy matrix. The model is simplified as a plane strain biaxial tension test. By monitoring the amount of strain energy released during flaw initiation and propagation for different ratios of transverse to longitudinal farfield displacement, the consistency of the locus can be determined. Since the locus is derived under conditions ranging from pure tension to pure shear, biaxial loadings which produce compressive stresses at the interface are not considered. Thus the simulations are limited to only positive values of farfield longitudinal and transverse displacement(fig.5-2).

The biaxial tension test is simulated via a two dimensional plane strain finite element model. Through symmetry considerations, only one quadrant is considered(fig.5-3). The left boundary is constrained to only move in the y-direction. The bottom boundary is constrained to only move in the x-direction. The y-displacement of the top boundary is constrained to follow the y displacement of the top right corner node while the x-displacement of the right boundary is constrained to follow the x-displacement of the top right corner node. The ratio of longitudinal to transverse farfield displacement is varied by varying the ratio of y to x displacement imposed on the top right corner node.

The failure locus selected for these simulations is the ideal failure locus presented earlier(fig.5-4):

$$\sqrt{\left(\frac{\sigma}{\sigma_{max}}\right)^2 + \left(\frac{\tau}{\tau_{max}}\right)^2} = 1.$$

where

$\sigma_{max} = 85MPa$

$\tau_{max} = 90MPa$

As noted previously, this locus allows for a smooth transition from the experimentally observed failure stress in tension, 85MPa, to conditions of mixed normal and shear stress. Calculations with the purely normal stress based criteria are also performed in order to compare the relative energy release rates of both criteria. The model used to implement the criteria is the Lagrange multiplier model without the modified crack tip(i.e. the entire interface is constrained with Lagrange multipliers). A crack tip traction displacement relation is not used since the systems considered are ones with initially perfect interfaces. The absence of a singularity for these interfaces means that the effects of crack tip constraint will not be significant and hence reasonably accurate energy release rates can be obtained. As will be discussed later, the unstable nature of the simulations dictates that the initiation and nearly complete propagation of the interface flaw occurs within the same increment, thus limiting the amount of information which can be obtained about the flaw propagation process. The advantage of the unstable crack growth problem is that mesh density effects on the results are reduced. The absence of the singularity for the fully bonded interface reduces the differences in the initial stress/strain calculations found between coarse and fine meshes. The large flaw which is produced within the same increment as initiation ensures that the near crack tip strain energy which is attributed to crack tip constraint (which is sensitive to the mesh density) is small compared to the total energy released. However, it should be noted that the constraint conditions created by the use of Lagrange multipliers enhances the unstable nature of the crack growth process for these configurations and would in fact indicate more crack growth than physically possible for loading configurations which supposedly exhibit stable crack growth. The results of the simulations for both criteria are shown below in tables 5-1 and 5-2 for various ratios of farfield transverse to longitudinal displacement:

TABLE 5-1

Energy release rates from biaxial tension simulations for normal stress criteria -

ratio of transverse displacement to longitudinal displacement, $\frac{u_2}{u_1}$	energy release rate, J/m^2	angle of flaw initiation, ^{o} (measured from pole)
0.0	.353	0
.25	.324	0
.5	.358	0
.75	.410	0
1.0	.454	----

TABLE 5-1

Energy release rates from biaxial tension simulations for mixed stress criteria -

ratio of transverse displacement to longitudinal displacement, $\frac{u_2}{u_1}$	energy release rate, J/m^2	angle of flaw initiation, ^{o} (measured from pole)
0.0	.301	0
.25	.275	0
.5	.320	0
.75	.363	0
1.0	.383	----

The evolution of the interface normal and shear stress prior to failure for each case is shown in figures 5-5a through 5-5e. As the ratio of transverse to longitudinal displacement increases, the distribution of the interface stresses becomes increasingly uniform, leading to simultaneous failure of the entire interface for last case(i.e. ratio = 1.0). All other cases have failures which initiate at the pole of the particle. From figure 5-6, it's shown that the energy release rates for the purely normal stress failure criterion are higher that those of the mixed failure criteria. This is physically consistent since the mixed stress criteria generally allows for earlier failure of the interface, hence producing lower values of system strain energy and strain energy release. However, for both criteria, the calculated energy release rates increase with an increasing ratio of farfield transverse to longitudinal displacement and the magnitudes of the release rates for the

mixed stress criteria are significantly higher than the values derived for the interface energy, .1631 J/m^2.

The increase in interface energy calculated from the biaxial tension experiments may be due to the numerical difficulties present in the simulations. The simulations indicate that a majority of the total failure area of the interface is created within the first increment that failure initiates. Physically, this suggests that the tensile/tensile-shear process is inherently unstable. For unstable systems, quasi-static modeling may not be entirely appropriate[17]. Although the stationary crack analysis used to derive the interface energy and the failure locus explicitly removes the dynamic effects by constraining the crack to not propagate, the kinetic energy present during a real failure may be significant. The biaxial tension calculations seem to indicate that the portion of strain energy released during failure which should be channeled to kinetic energy is being directed towards creating new surfaces(fig.5-7), thus leading to an increase in apparent interface energy. By taking into account these kinetic effects, the calculated interface energy should be much closer to the value obtained from the quasi-static analysis.

Although these encouraging results appear to indicate that the amount of strain energy released during crack initiation and subsequent propagation is more than sufficient for creating the new surfaces, it is unclear whether this approach is applicable to arbitrary configurations. It should be noted however that these types of simulations may give an indication as to what types of experiments should be used to determine failure criteria and may aid in identifying relevant macroscopic interface failure trends.

5.2 Numerical Example: Indentation Test

Background on the Indentation Test

The indentation test is an old experimental configuration which has conventionally been used to probe the hardness of materials[62]. Recently, it has also been used to determine the modulus of thin films and the strength of thin film/substrate interfaces[55]. As a result, several studies using this setup have been conducted in an effort to rigorously quantify the properties of interfaces. Two major proponents of the indentation test have been Ritter and Matthewson[63, 64]. Their studies have incorporated various strength interfaces with different indenter geometries. In their work they have characterized the various failure initiation scenarios into three "types"[53]:

Type I - The interface flaw initiates in the region of the interface just outside the contact radius of a spherical indenter well before the film undergoes plastic deformation(fig.5-8). This type of failure is typical of relatively weak interfaces.

type II - The interface flaw initiates during film penetration of the spherical or Vickers type of indenter during or after significant plastic deformation of the film has occurred. This type of failure is typical of relatively strong interfaces(fig.5-9).

type III - The indenter penetrates the film so thoroughly that part of the indenter load is supported by the substrate. Significant plastic deformation of the film occurs before the initiation of an interface flaw. This type of failure is typical of high strength interfaces(fig.5-10).

Ritter and Matthewson go on to suggest that two quantities are sufficient to characterize the interface, namely the fracture toughness and the strength parameter which is a measure of the significance of strength-controlling defects(i.e. characteristic asperity dimensions, etc.) and the nature of the strength measurement technique(i.e. shear, tension, etc.)[54]. It should also be noted that the deformation patterns of the indentation test facilitate the approximation of an interface shear strength value albeit one which is strongly tied to the topology of the interface surfaces.

Present Study

In the present study, the analysis thus far has been limited to systems which are predominantly elastic. In order to test the general applicability of a stress based interface failure criteria, a comparison of results gathered from indentation experiments and an indentation simulation using a stress based interface failure criteria is performed. The indentation data cited is obtained through experiments performed by Dr. Andrew Zhuk. The indentation observations described below are a summary of Dr. Zhuk's results:

The indentation experiments performed by Dr. Zhuk on two different interface systems consist of 100 micron thick epoxy films mounted to a silicon substrate via monolayer interfaces. The radius of the indenter is 794 microns. One interface system consists of a 100%vol COOH monolayer with evaporated chromium and gold and is intended to be identical to the interface system created for the tension tests. The second system consists of a 50%vol CH3 and 50%vol COOH monolayer with evaporated chromium and gold and is intended to approximate a weaker interface. Several dead load tests are performed and the subsequent indenter displacements and final locations of interface cracks are observed. The 100%vol COOH monolayer interface

indentation tests fail to produce any flaw initiation or growth while the weaker interface system(50% CH3, 50% COOH) exhibits significant flaw formation and growth. A sample of some of the micrographs obtained from the 50% CH3/50% COOH tests is shown in figure 5-12 and a plot of the final indenter displacements vs. corresponding dead weight loads for both systems is displayed in figure 5-13.

For the moderate strength interface(i.e. the 50% CH3/50% COOH monolayer interface) the indentation process follows a frequently observed pattern[54]. Typically, the indenter penetrates the film, causing the material directly underneath it to undergo plastic deformation. The incompressible nature of the material during plastic deformation forces it out from underneath the indenter in a process similar to that of extrusion. The flowing motion of the material creates tremendous shear stresses near the interface. Interface flaws generally initiate in these regions of intense shear(fig.5-14) and simultaneously propagate towards and away from the center[54].

In order to utilize the information from the previously derived failure locus, one major modification must be made. The failure locus was previously derived under conditions ranging from pure tension to mixed tension-shear. The interface failures observed from the indentation experiments indicate that the failures typically initiate in locations which are subjected to large compressive stresses, conditions which are not accommodated by the failure locus. As a rough approximation, the allowance for interface failure during compression is incorporated by extrapolating the failure locus linearly to allow for higher shear stresses before failure(fig.5-15).

The indentation tests are simulated through an axisymmetric finite element model employing the same dimensions used for the experiments. The mesh used is shown in figure 5-16 and consists of bi-linear axisymmetric continuum elements for the epoxy film and rigid surface elements for the indenter. The left boundary is constrained only to move in the y direction. The indenter-epoxy interface is modeled as frictionless while the bottom interface is modeled as being frictionless with the extrapolated failure criteria being implemented through the Lagrange multiplier model without the modified crack tip(i.e. the entire interface is constrained with Lagrange multipliers) for simplicity. The epoxy is modeled as an isotropic, rate independent, elasto-plastic material characterized by the stress-strain data found from the previously shown compression test(fig 5-17).

Figures 5-18a-d show the deformed finite element mesh at various indenter depths ranging from 10 to 40 microns. The left and right arrows in figures 5-18c and 5-18d indicate the location of the inner and outer radii of the interface crack respectively. The equivalent plastic strain contours for the same indentation depths are shown in figures 5-19a-d. In figures 5-19c and 5-19d, it should be noted that the majority of the crack area is formed away from the plastically deforming region underneath the indenter, thus characterizing the failure as a type II

failure as defined by Mathewson and Ritter. Figures 5-20a and 5-20b show the evolution of interface shear and normal stresses respectively for the same indenter displacements. It can be seen that the crack initially forms in a region subjected to high compressive normal stresses, hence indicating that the flaw initiates through a shear failure of the interface. In the latter stages of the indentation, the inward growth of the flaw stops while the outer crack radius continues to grow while subjected to zero or slightly tensile interface normal stresses. As stated previously, the constraint conditions imposed by the Lagrange multipliers probably encourage more crack growth than would normally be possible.

Although the simulations fail to provide quantitative predictions about crack initiation and growth, the calculations qualitatively agree with indentation observations of "moderate" strength interfaces. A comparison of the 100% COOH interface simulation and the experimental load-displacement curve is shown in figure 5-21. The load-displacement curve from an indentation simulation without interface failure is shown in an attempt to provide an upper bound. The significantly higher load levels sustained during the experiments may be due to a combination of the constraint created by the non negligible friction present between the indenter and epoxy, the pressure dependent nature of the epoxy's post yield behavior, and a possible displacement offset in the experimental measurements(i.e. the experimental curve may be shifted by a constant displacement). A comparison of the crack inner and outer radius measurements for the 100% interface simulation and the 50% CH3/50% COOH interface is shown in figure 5-22. Although the 50%CH3/50% COOH interface physically corresponds to a lower strength interface than the 100% COOH system, the simulations using the failure locus derived from the 100% COOH interface produced flaws which initiated at load levels lower than the experiments on the 50% CH3/50% COOH system. There are several possible causes for the discrepancy. The extrapolation of the deduced criteria is probably inappropriate at the high pressure levels(fig.5-23) present during indentation. Since the criteria is derived under conditions ranging from high negative pressures to pure shear, the extrapolation may tend to underestimate the shear stress required to initiate the flaw. Secondly, it is possible that the failure criteria is not applicable to arbitrary geometries even as an approximation.(i.e. the interface can not be uniquely described by a stress criteria). The effects of plastic deformation may render the entire locus useless since the dissipative effects of plastic are neglected during the original formulation. Although it doesn't seem physically realistic that plasticity would alter interface strength, large pressures may affect the plastic behavior of the epoxy(i.e. possible increase in yield strength) in such a way that the apparent strength of the interface is affected. Also, the relatively slow application of the dead load combined with the inherent rate dependence of the epoxy might limit the amount of crack growth observed since low loading rates allow the material more time to absorb the energy which would otherwise be used to create new surfaces. Finally, the effects of surface roughness and friction,

coupled with the presence of large positive pressures, inhibits the initiation and growth of interface flaws. The inherent topology or surface roughness may act to increase the apparent strength of the interface by increasing the actual interface contact area or by affecting the local stress field in a way such that flaw initiation is more difficult. Friction reduces propagation of existing flaws subjected to high positive pressures since debonded surfaces, which are free of shear tractions in the negligible friction case do not allow the crack tip to feel the full effects of load shedding[36].

The friction inhibits the inward growth of the crack(where the pressures are very high) and has less of an effect on the outward growth since the pressures outside of the indenter in later stages of deformation actually become slightly negative. By observing that the majority of the crack area is created during the outward propagation of the crack and that this propagation takes place far away from the region dominated by intense plastic deformation, it is possible that for weak interfaces, the majority of the energy released by the film during propagation goes into creating the new surfaces and frictional dissipation instead of plastic dissipation(fig.5-24).

5.3 Conclusions

The goal of this work has been to investigate the applicability of several interface failure models and assess their ability to accurately describe the interface failure processes. The calculations performed in this thesis lead to several specific observations about interface modeling techniques:

• Explicitly using energetic feasibility to determine interface failure is highly impractical in that the probable history of the crack can only be obtained after probing many possible histories. For cases where the interface is initially flawless, invoking an energy criteria implies that the location of failure initiation is known a priori, which is not generally possible.

• There are several difficulties with using a potential to describe the interface. Essentially, using a potential dictates that a stiffness description and hence some dimension must be introduced to the interface. Although the method provides a very natural framework for the exploration of several relevant phenomena including characteristic material lengths, material interaction behavior, and interface energies, the property differences between the matrix and the interface make it extremely difficult to directly apply. For polymer systems, the relative difference in stiffness between the polymer matrix and the interface is so large that the approach becomes numerically unstable. Specifically, the ratio of the largest to smallest eigenvalues of the global stiffness matrix

becomes so high that the solution becomes very sensitive to small perturbations which include roundoff error. For systems where the interface is known to be very compliant or where the matrix is known to be extremely stiff, the approach has been successfully applied. Unfortunately, the range of parameters required to make this possible for the epoxy matrix-glass bead system are inconsistent with experimental observations.

• Kinematic constraints applied to the interface facilitate the use of a purely stress based criteria. The method is numerically stable because it circumvents the difficulties of a stiffness description. However, obtaining a proper stress failure criteria is difficult and there may not be a unique failure locus which guarantees satisfaction of energetics. Also, this method does not allow the explicit use of interface energy in determining failure and the sole use of kinematic constraints along the interface can create unrealistic constraints on existing flaws. This "pinning" of the crack tips can produce unrealistically high crack tip stresses which act to degrade the physical accuracy of the solution.

• A physically realistic stress failure criteria can be deduced indirectly from energetics. By assuming that the energy associated with the interface is independent of the mode of loading at the interface crack tip and that the systems investigated are predominantly elastic, the use of the J -integral can determine the value of the near crack tip stresses during crack propagation hence producing a failure locus. The locus is sensitive to several factors including location relative to the crack tip from which the stresses are measured, the effects of crack tip constraint, the effects of interface element density, and the effects of the apparent stiffness of the surrounding material. The relationship between these effects can be determined through a normalized measure of the tensile crack tip opening angle(CTOA). This normalized measure makes self consistent modeling of the interface behavior possible.

• It is unclear whether a unique stress based failure locus is applicable to arbitrary geometries since the effects of other energy dissipating mechanisms are difficult to quantify through a static analysis given that fracture is an inherently dynamic process.

Although we were unable to uniquely determine a consistent interface failure criteria, the above observations suggest that various techniques are available to model interface behavior depending on the phenomena involved, the level of detail required, the size scales involved, and the resources available. Specifically, the observations imply that in order to properly characterize the interface and understand its behavior, several pieces of information must be available:

1) Dominant Mechanisms - The behavior of the interface can be properly quantified only after the source of the inherent/apparent strength of the interface is identified. Possible dominant mechanisms include mechanical locking of the constituents, interface diffusion(i.e. finite interphase thickness), electrostatic forces, and energetic compatibility.

2) Relevant Features - Once the dominant mechanism is identified, the values of parameters pertinent to describing that mechanism must be determined. Relevant parameters can include lengths characterizing the topology of the interface, the diffusion/interphase thicknesses, surface/interface energy values, or electrostatic discharge gap distances.

3) Indirectly Related Phenomena - There may be features of the material system not directly related to the interface but can subtlely influence the behavior of the interface. Examples of these include the micro level behavior of the constituents near the interface(i.e. microscopic deformation behavior, damage accumulation) and long range interactions(i.e. surfactant or other impurity migration to the interface).

4) Selection of an Applicable Modeling Technique - The modeling technique used to analyze the interface must be robust enough to incorporate the relevant features and phenomena of the dominant mechanism while also being efficient enough to produce a fairly accurate and useful "picture" of the behavior in a reasonable amount of time. Models can range from continuum type formulations(i.e. finite/boundary elements, finite differences) to explicit molecular or atomic level characterizations(i.e. molecular dynamics, first principle calculations).

Each one of the above requirements relates to the interface at a different level. Improperly identifying the dominant mechanisms leads to improper selection of modeling techniques, hence producing an inaccurate "picture" of the interface behavior. Continuum techniques such as finite elements have been previously shown to provide reasonably accurate values of global interface fracture properties such as energy release rates and effective stress intensity values for systems with initially macroscopically observable interface flaws. The success of these approaches on "macroscopic" fracture problems is mainly due to the size scale of study required to obtain the parameters. That is, the properties such as energy release rate and effective stress intensity are not dependent on detailed knowledge of near crack tip stress and displacement fields. They are inherently "integral" quantities which can be computed from the "averaged" behavior of the surrounding medium. It is for these kinds of calculations that the finite element method is especially effective. Since these quantities are only meant to give a sense of

the "toughness" of the interface, and not a detailed description of the relevant phenomena and behavior of the interface, the finite element meshes can be designed specifically to obtain the desired parameter via special techniques(i.e. focus meshes, singular elements, etc.). The drawback of these special techniques is in their inability to monitor the interface behavior during crack propagation(its difficult to keep singular elements or a focused mesh in front of the crack as its moving).

Continuum models can be extended in a limited way to accommodate microscopic phenomena such as interface flaw nucleation and crack growth by explicitly incorporating interface constitutive models which attempt to accurately capture the dominant microscopic features of the interface behavior(i.e. interface potentials, incremental constitutive laws, etc.). Again, the difficulty of these approaches is that these models essentially furnish an equivalent continuum description of the microscopic behavior. A detailed description of such phenomena such as microscopic interface and constituent damage accumulation, topology evolution, and property gradient effects, is not possible. Although theoretically it is possible to explicitly incorporate the relevant parameters(i.e. characteristic lengths, interface energy, etc.) into the interface constitutive laws, the numerical stability of this approach for many systems is questionable. The results of this work illustrate this fact in their inability to obtain consistent detailed information about the interface(i.e. near crack tip stresses) which are affected subtlely by the microscopic behavior of the surrounding material, events not explicitly accountable via the continuum description of the surrounding material. In this work, the difficulty specifically manifests itself in the unreasonably high ratios of matrix to interface stiffness.

The underlying reason for the problems prevalent in finite element modeling of the interface is that the systems under study are generally characterized by more than one length scale. Away from the interface flaw, where displacement gradients are not very severe, the length scale characterizing the material is so large(i.e. specimen dimensions) that a continuum description of the system is adequate. However, near the interface, the system may be characterized by much smaller dimensions such as the diffusion distance of the constituent materials(i.e. interphase thickness), the average asperity height, or the electrostatic discharge gap distance. This mismatch in scale is the source of most of the numerical problems encountered in methods which attempt to explicitly and simultaneously incorporate both scales into one model.

A more effective and efficient approach would probably involve an indirect coupling of the various size scales. The models describing each scale would be evolved independently with information being transferred from one scale to another through a versatile basis which translates

conditions occurring at one scale to equivalent conditions to be applied at another. For example, a continuum description could be used to model material "away" from the interface while a "near" interface description could be provided by an independent model(fig 5-23). The stresses observed at the continuum/microscopic region boundary could be translated into farfield conditions to be applied to the microscopic model which would be used to explicitly evolve the behavior of the interface. The effects of interface evolution would then be translated and fed back as continuum boundary conditions, allowing the continuum model to adjust to changes in the interface. This indirect coupling, would eliminate the numerical difficulties prevalent in explicit scale coupling techniques and simultaneously provide a detailed description of the interface behavior.

5.4 Future Work

The relative significance of other mechanisms on the interface fracture process require investigation. Specifically, the region of material near the interface which has properties which are some average of the surrounding constituents should be explicitly modeled. The property gradients of this "interphase" probably govern the flaw nucleation and growth process and are probably largely responsible for the magnitude of the interface energy. Accounting for this region would probably eliminate some of the numerical instability of the interface potential description. The effects of interface topology which directly affect interface friction and actual interface contact area should also be investigated. Considering that friction is a large energy dissipation mechanism during compressive loading and that the interface contact area can determine the strength of the interface, a micromechanical study of these phenomena may be appropriate.

Finally, other dissipative phenomenal such as the rate and history dependence of the constituent materials, the possible rate dependent nature of the interface itself, the kinetic effects of the fracture process, the viability of multi scale modeling, and the development of experimental techniques to obtain relevant micro scale parameters should be explored.

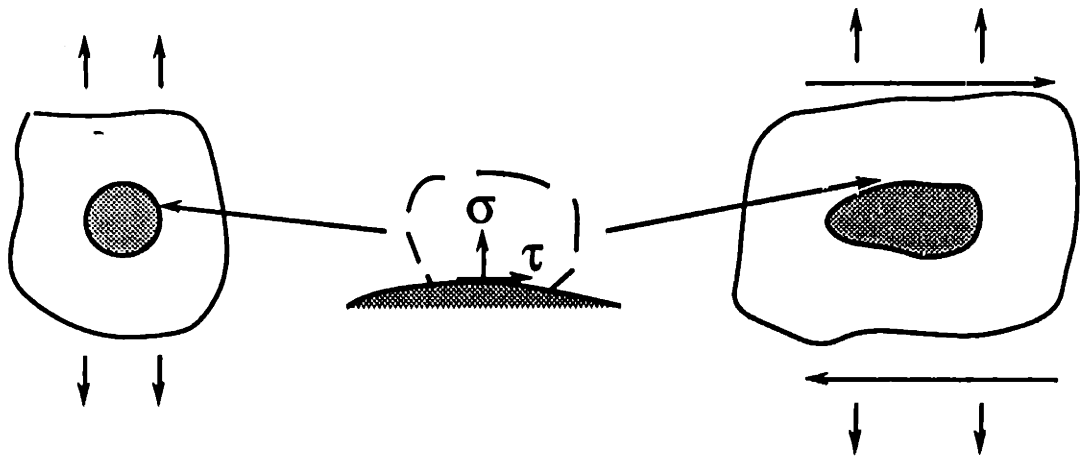

figure 5-1: Schematic of arbitrary geometry configurations. At the microscopic level, the interfaces are identical. Ideally, the energy release characteristics depend only on the stresses on or in the vicinity of the interface and are independent of the farfield loads and macroscopic geometry.

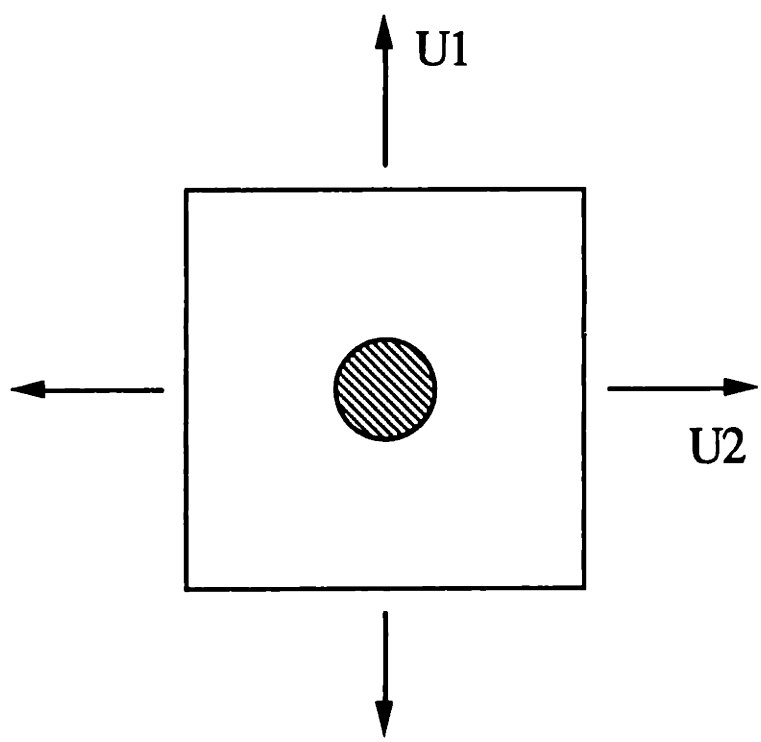

figure 5-2: schematic of biaxial tension test with various ratios of longitudinal displacement(u1) to transverse displacement(u2).

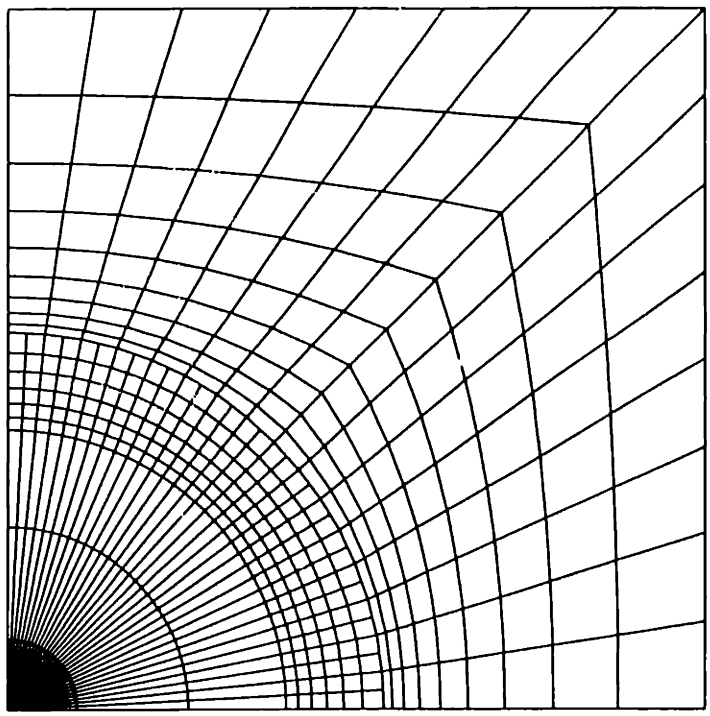

figure 5-3: finite element mesh of biaxial tension simulation

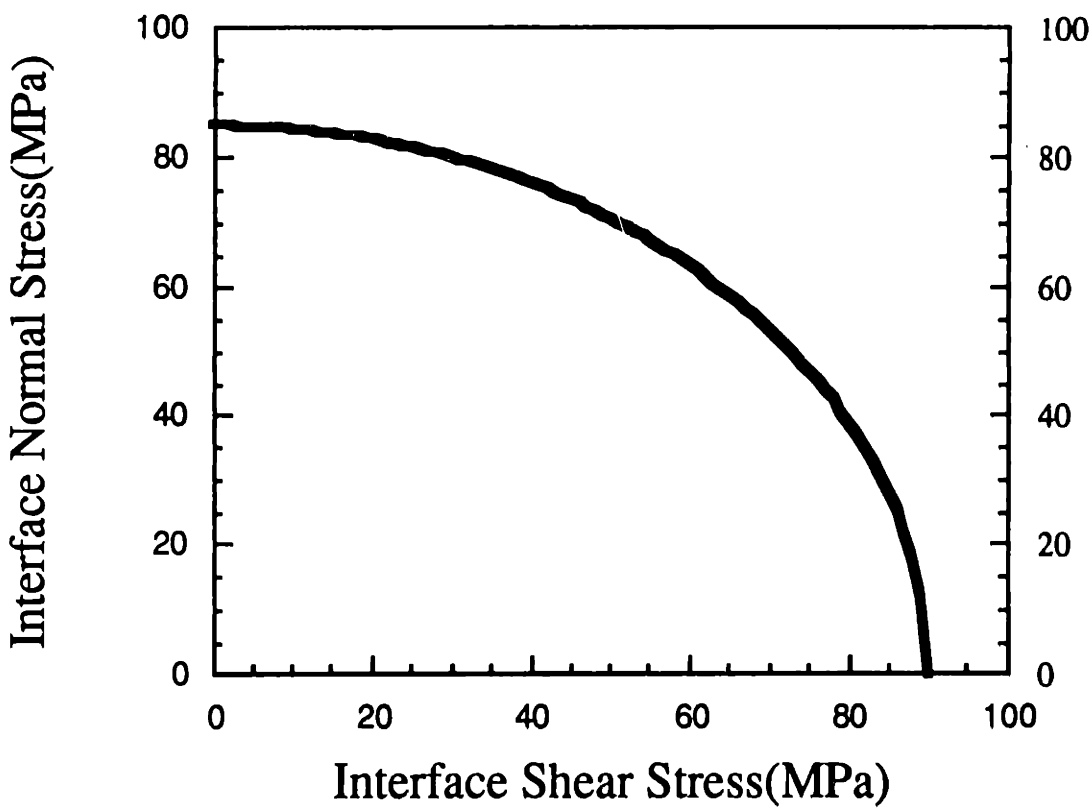

figure 5-4: previously determined failure locus

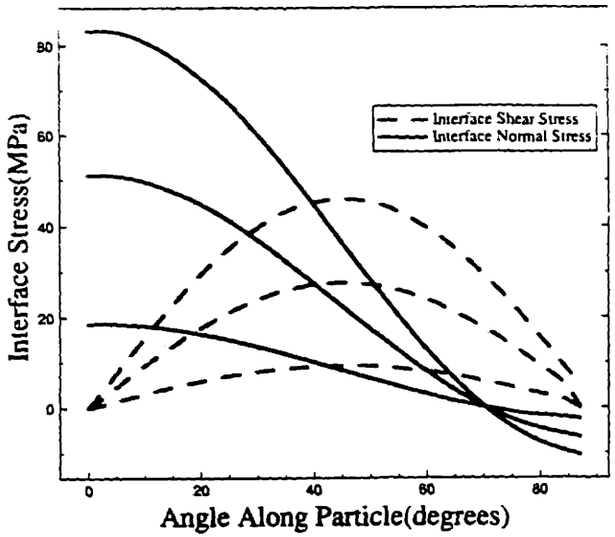

(a)

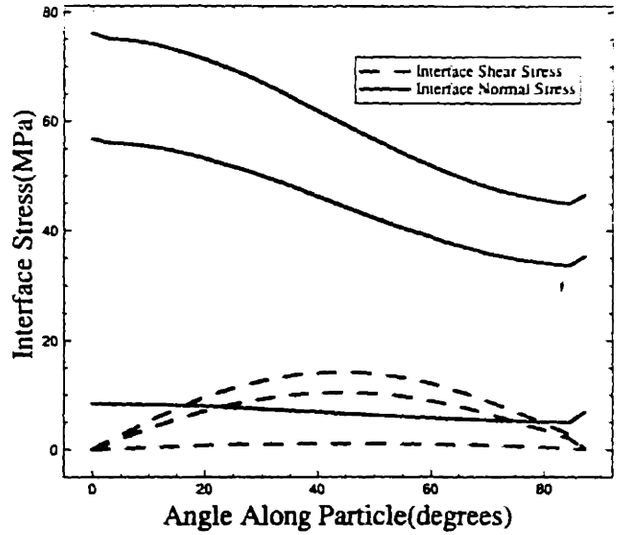

(b)

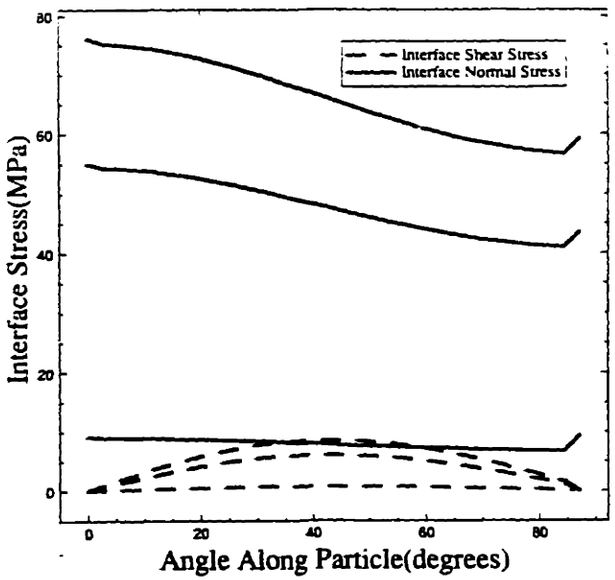

(c)

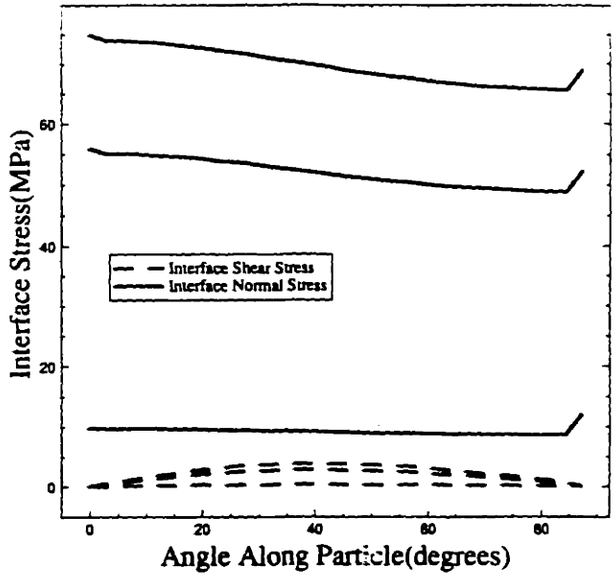

(d)

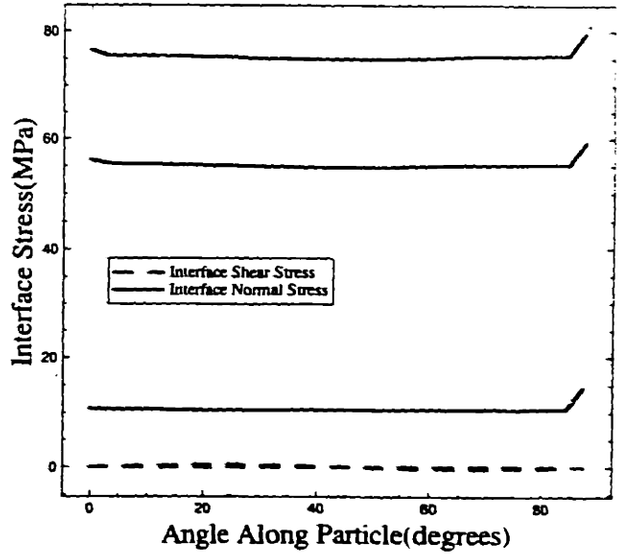

(e)

figure 5-5: evolution of interface stresses before failure for various ratios of longitudinal to transverse farfield displacement. (a) ratio = 0.0, (b) ratio = .25, (c) ratio = .50, (d) ratio = .75, (e) ratio = 1.0

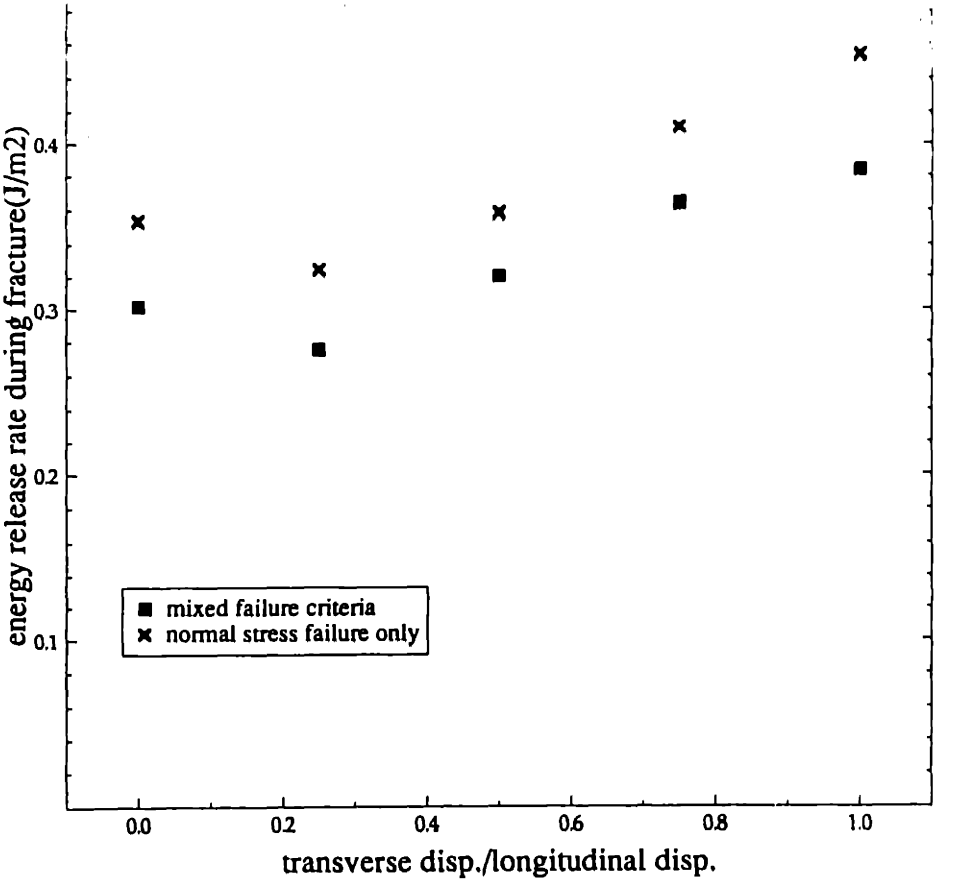

figure 5-6: energy release rates computed from biaxial tension simulations for various ratios fo transverse displacement to longitudinal displacement for the normal stress and mixed stress failure criteria.

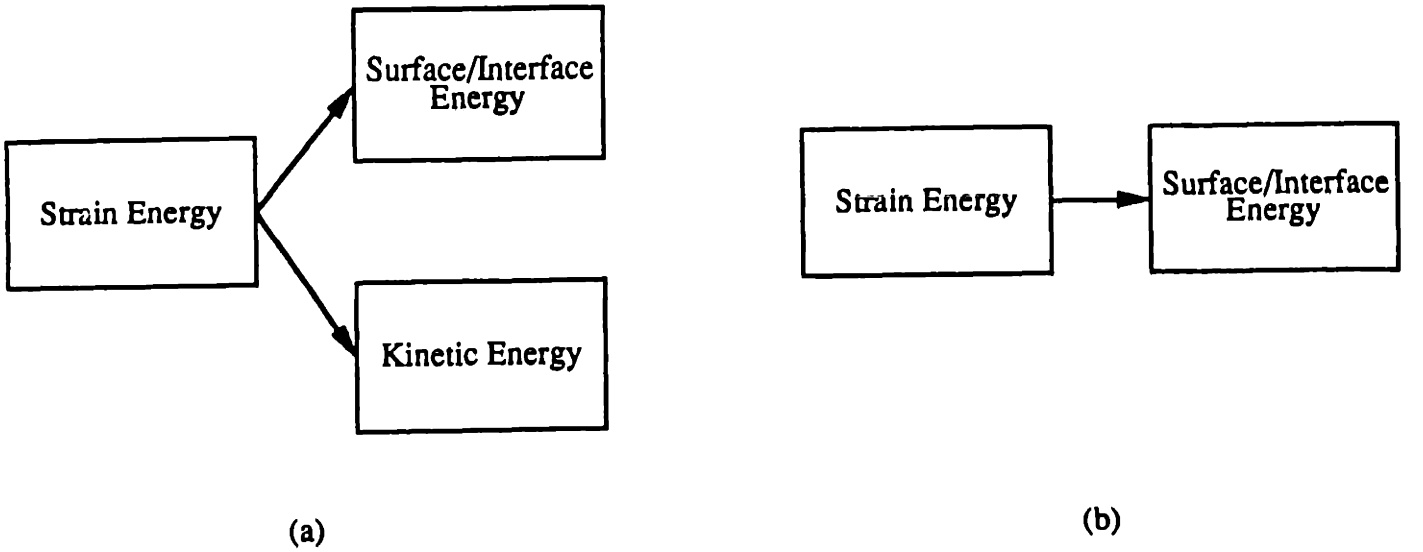

figure 5-7: (a) during an unstable elastic fracture, release strain energy is channeled towards surface creation and kinetic energies. (b) by modelling the process as quasi-static, the portion of strain energy which should be converted to kinetic energy is instead channeled into surface creation, hence producing an apparently higher measure of interface energy.

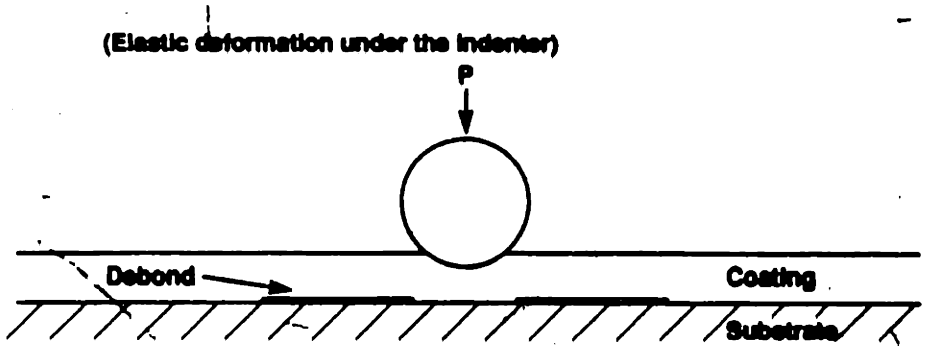

fig 5-8: schematic of type I failure

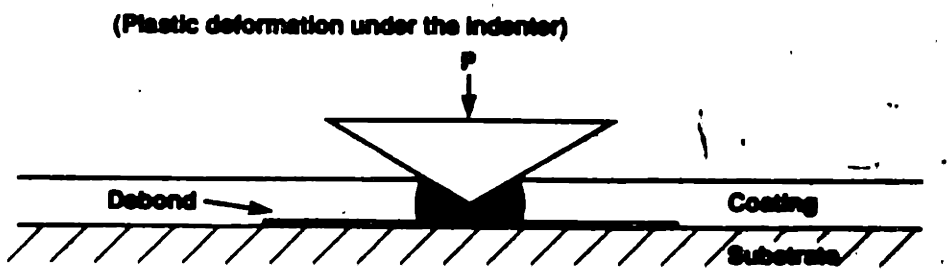

fig 5-9: schematic of type II failure

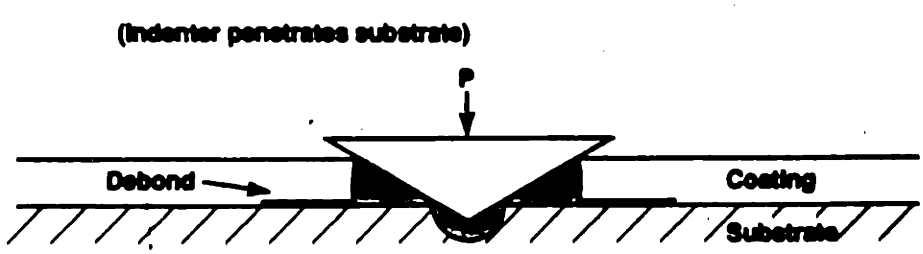

fig 5-10: schematic of type III failure

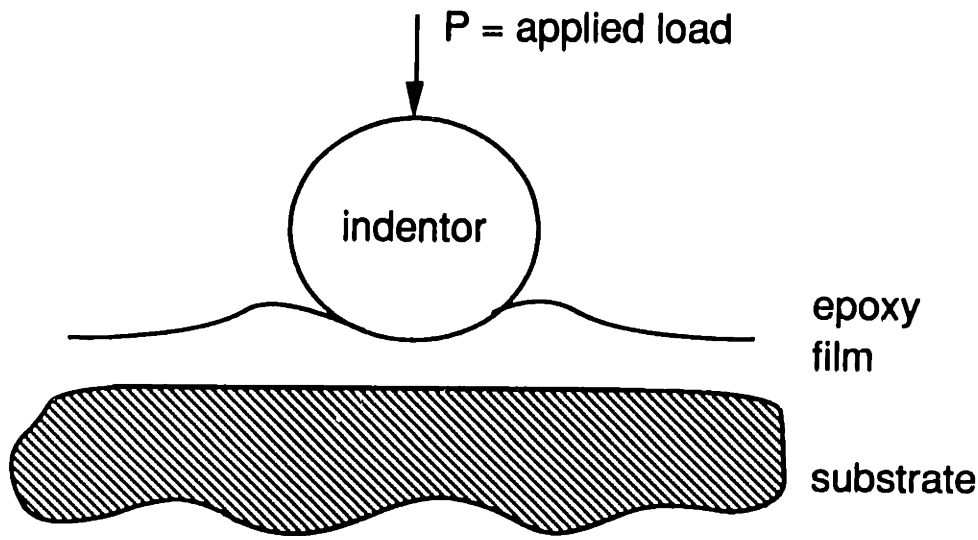

figure 5-11: schematic of indentation test

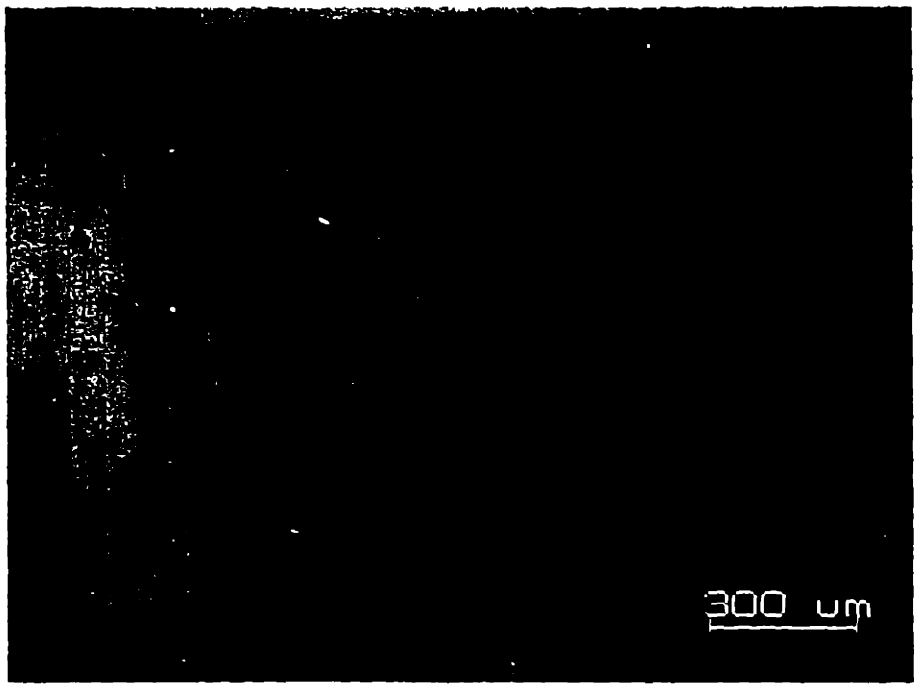

(a)

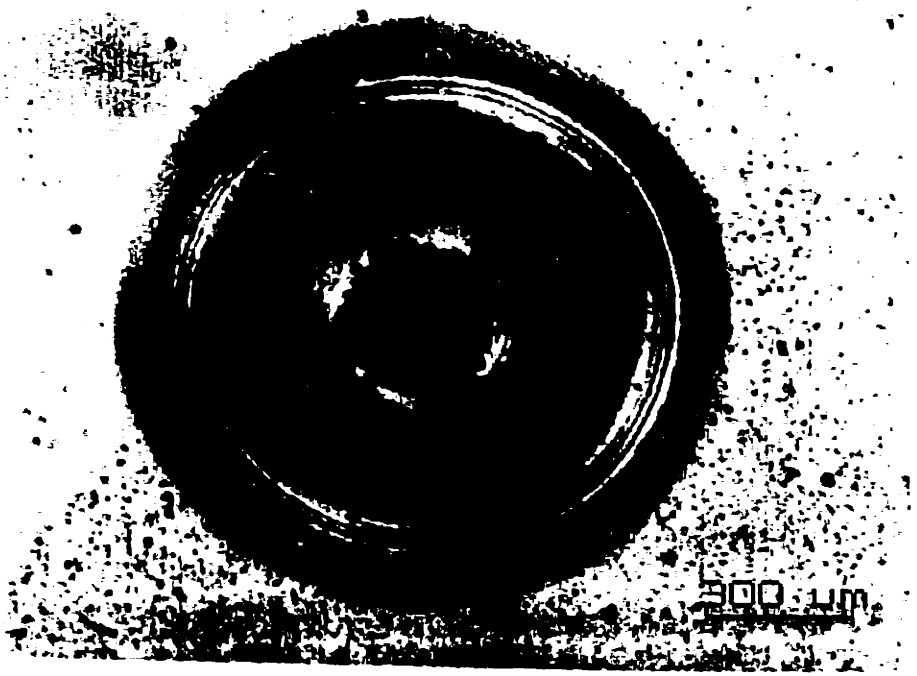

(b)

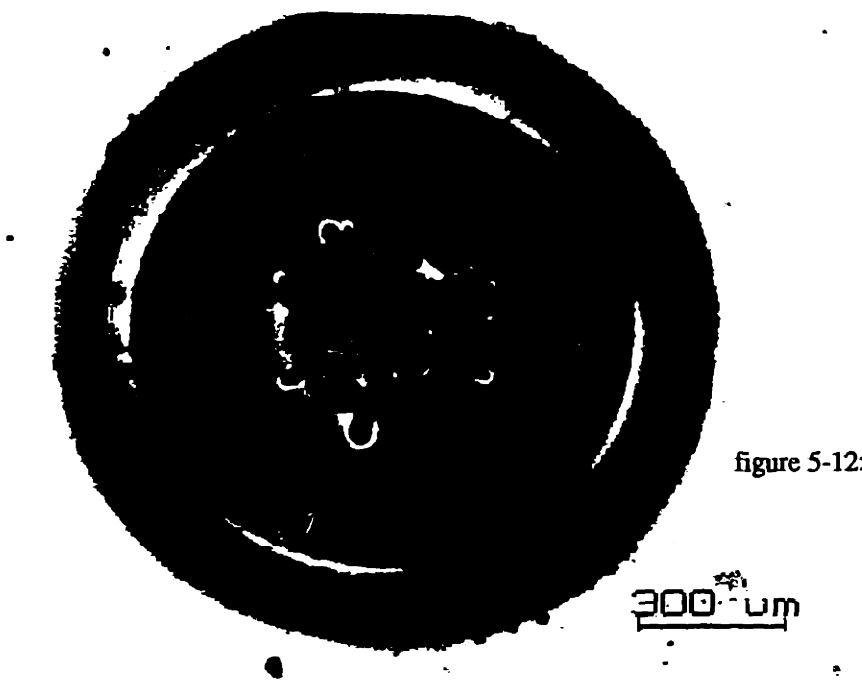

(c)

figure 5-12: micrographs of indentation crack for several dead loads for 50%CH_3/50%COOH interface. (a) load = 200N, (b) load = 250N, (c) load = 300N

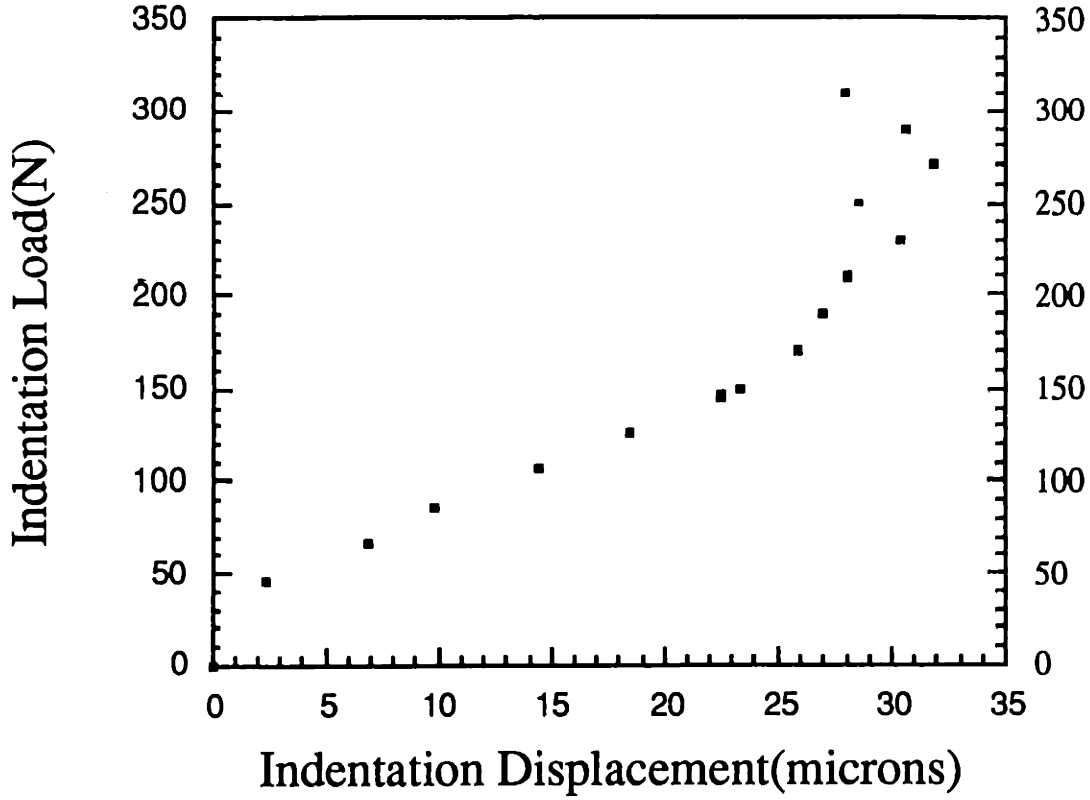

figure 5-13: plot of dead load vs. indentation displacement for 100%COOH interface.

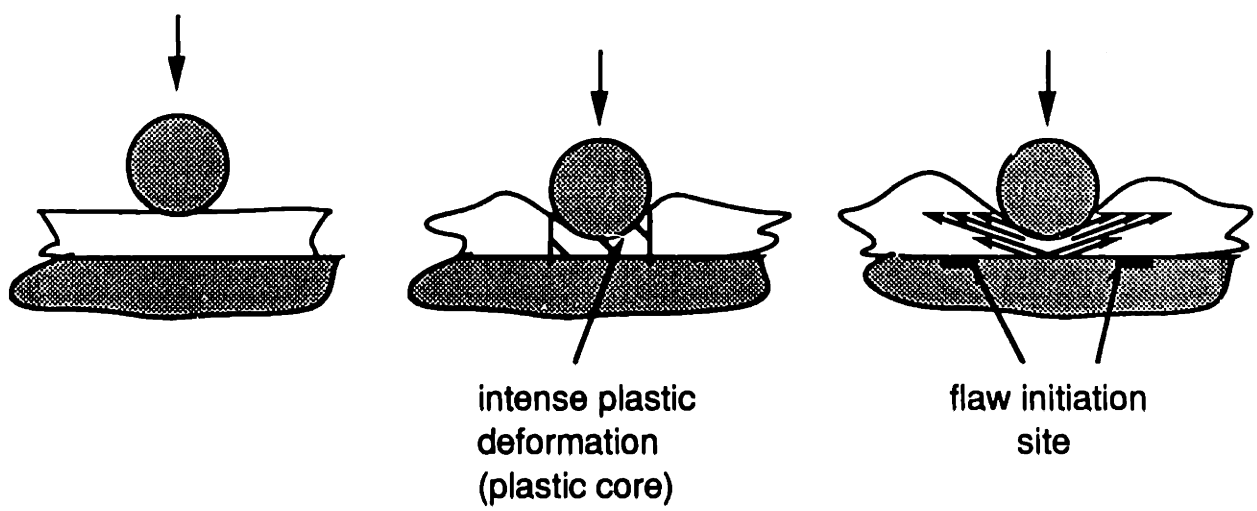

figure 5-14: Evolution of the indentation test. (a) Elastic deformation. (b) Intense plastic deformation underneath the indenter. (c) Flowing motion of plastic core creates high shear stresses at the interface which initiates flaws.

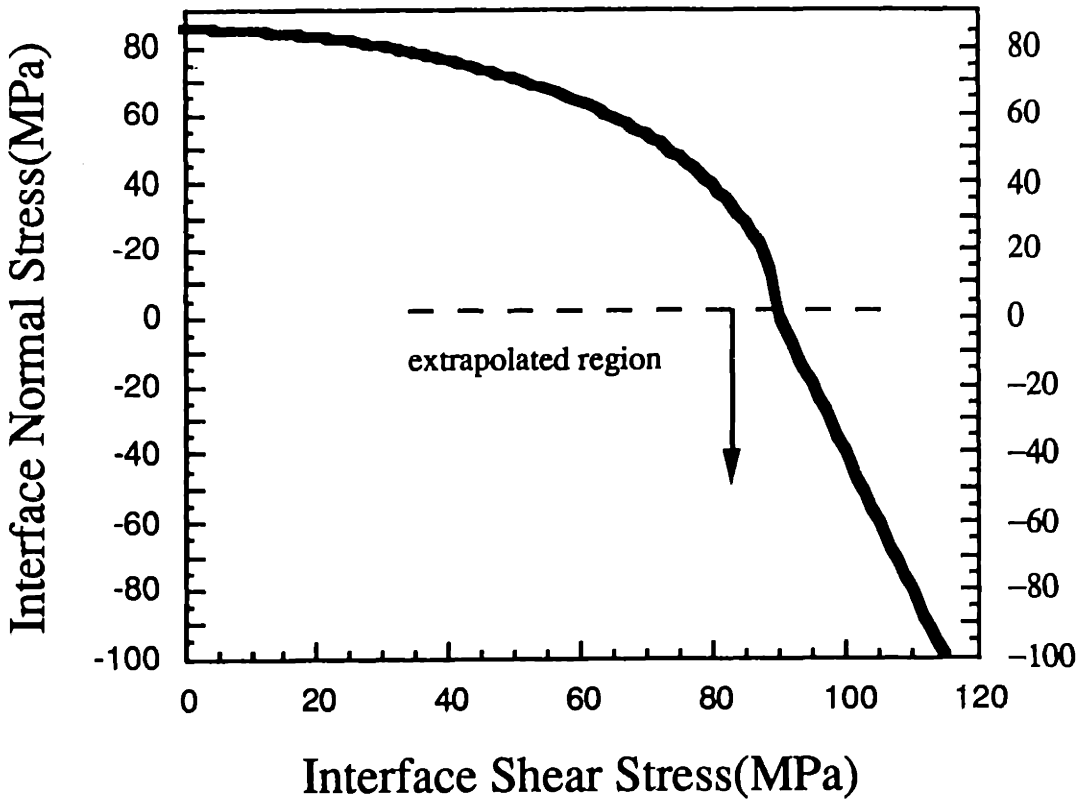

figure 5-15: The failure locus is extrapolated to allow for compressive failures

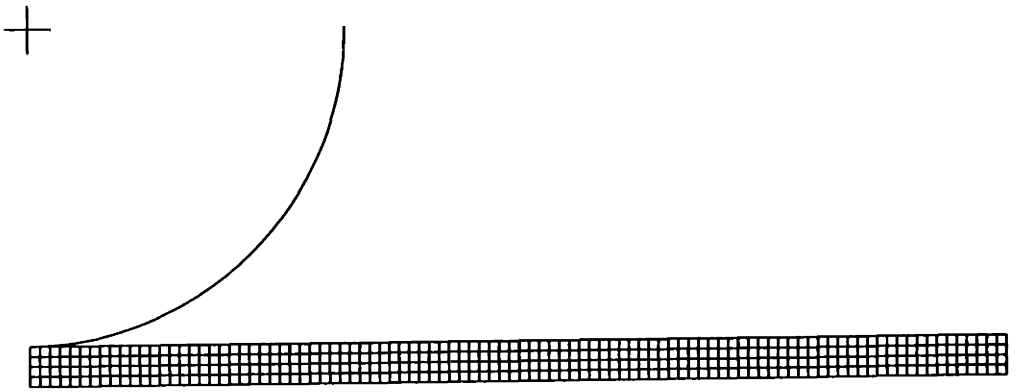

figure 5-16: finite element mesh used for indentation simulation

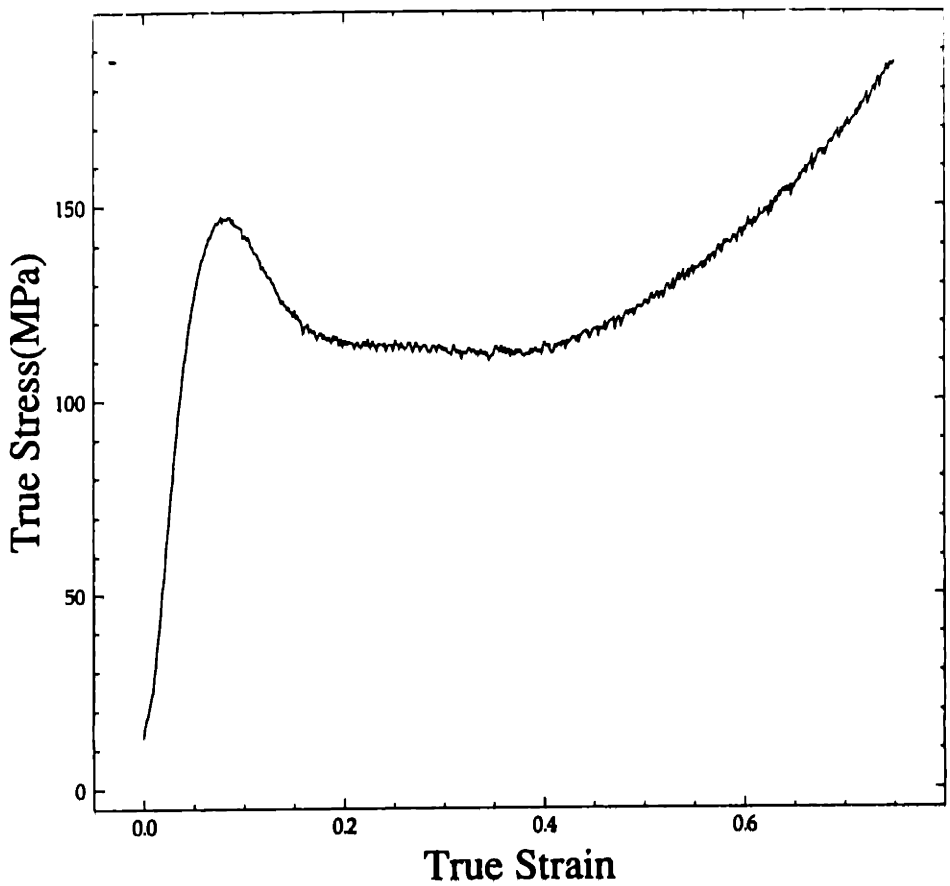

figure 5-17: stress-strain data from compression test

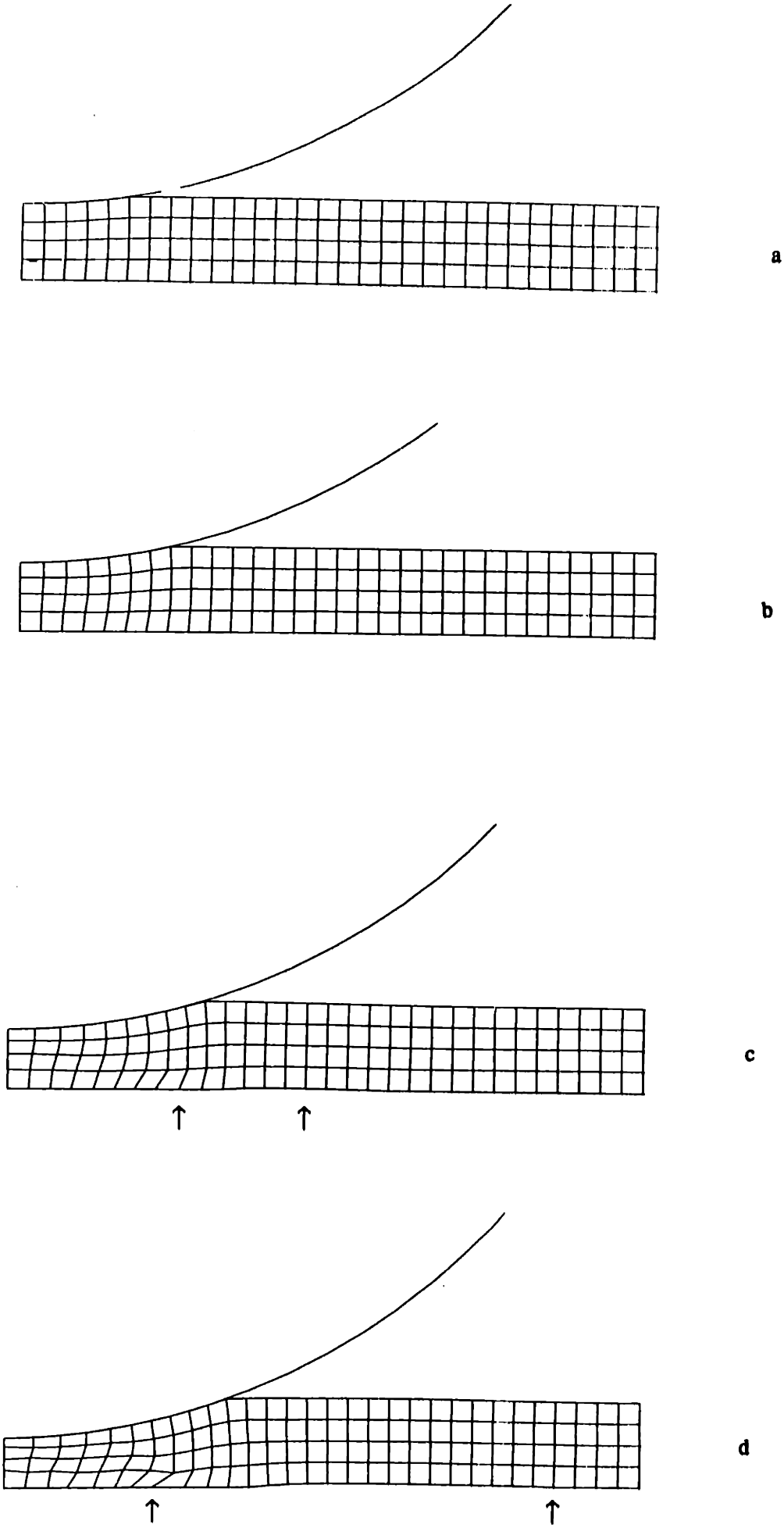

figure 5-18: Deformed finite element meshes from indentation simulations. Indenter displacement - (a) 10μm (b) 20μm (c) 30μm (d) 40μm (note: the arrows indicate the locations of the crack tips)

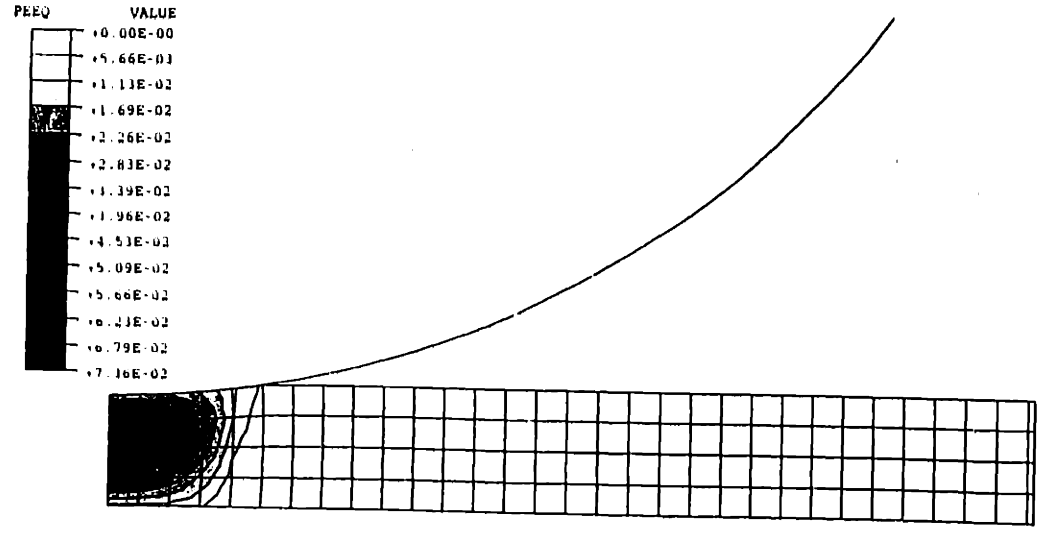

a

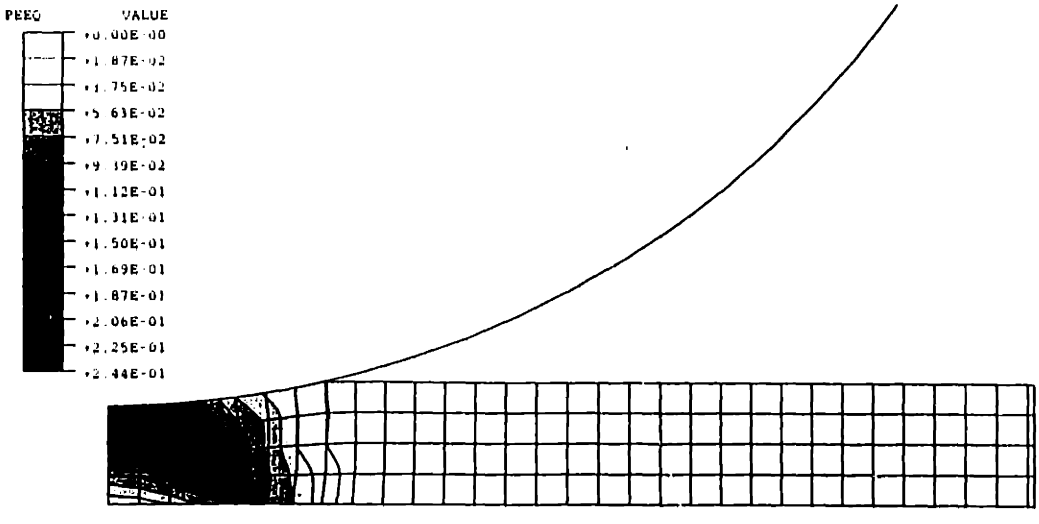

b

figure 5-19: Equivalent plastic strain contours for indenter displacement - (a) 10μm (b) 20μm (c) 30μm (d) 40μm

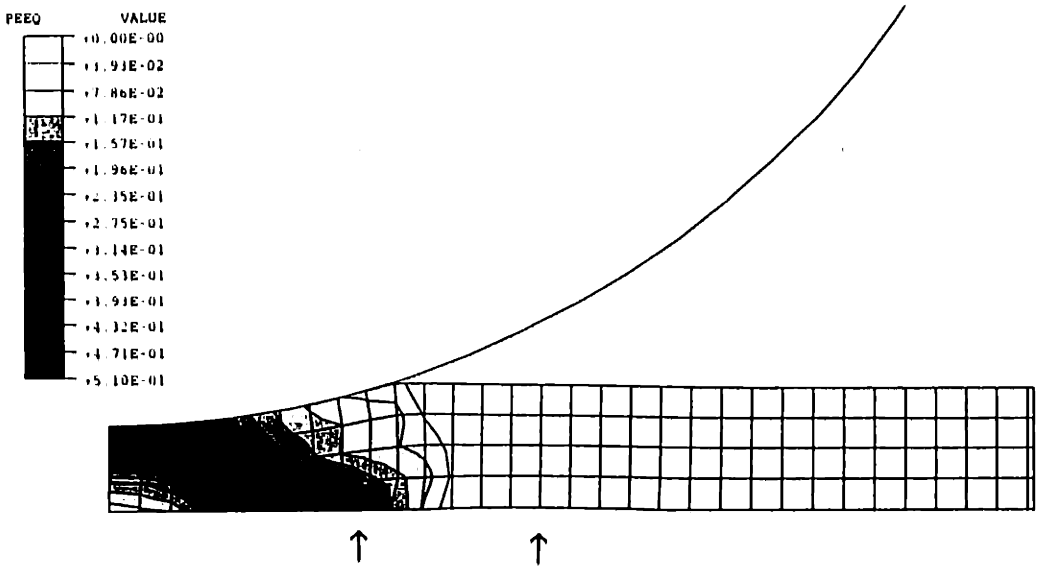
PEEQ
VALUE
+0.00E-00
+1.93E-02
+7.86E-02
+1.17E-01
+1.57E-01
+1.96E-01
+2.35E-01
+2.75E-01
+3.14E-01
+3.53E-01
+3.93E-01
+4.32E-01
+4.71E-01
+5.10E-01

c

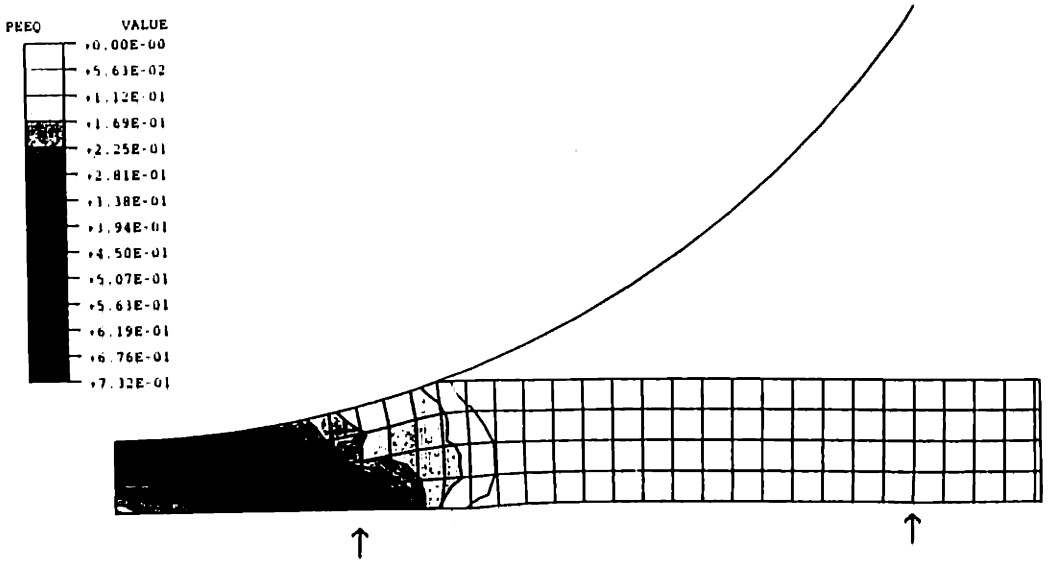
PEEQ
VALUE
+0.00E-00
+5.63E-02
+1.12E-01
+1.69E-01
+2.25E-01
+2.81E-01
+3.38E-01
+3.94E-01
+4.50E-01
+5.07E-01
+5.63E-01
+6.19E-01
+6.76E-01
+7.32E-01

d

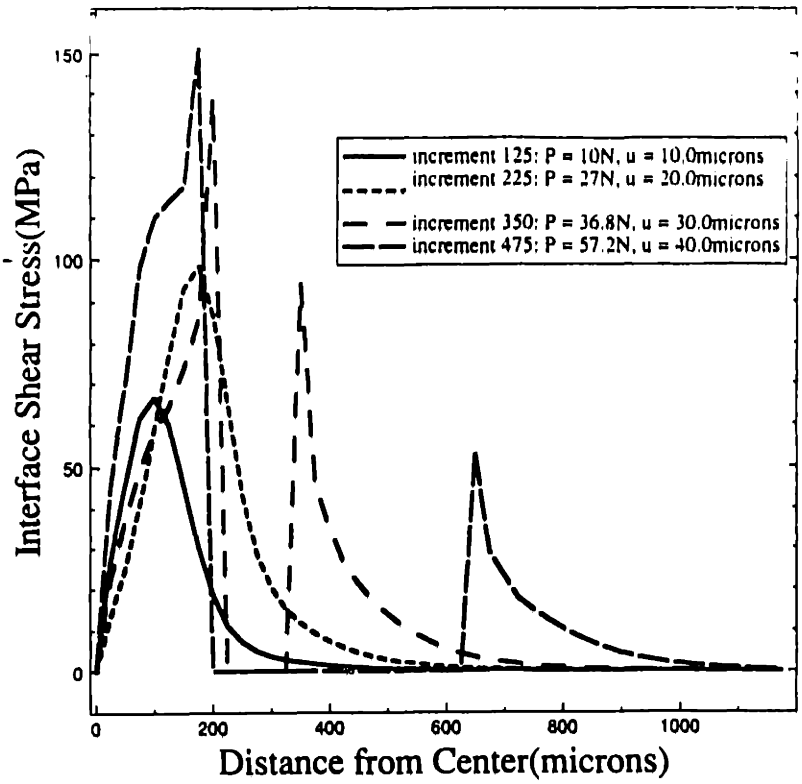

a

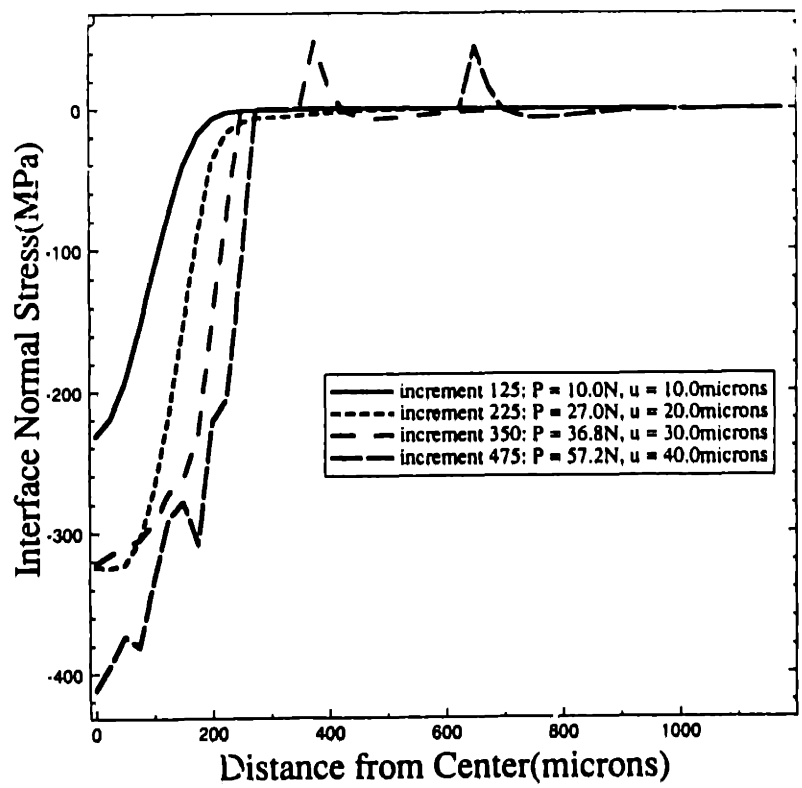

b

figure 5-20: (a) evolution of interface shear stress (b) evolution of interface normal stress

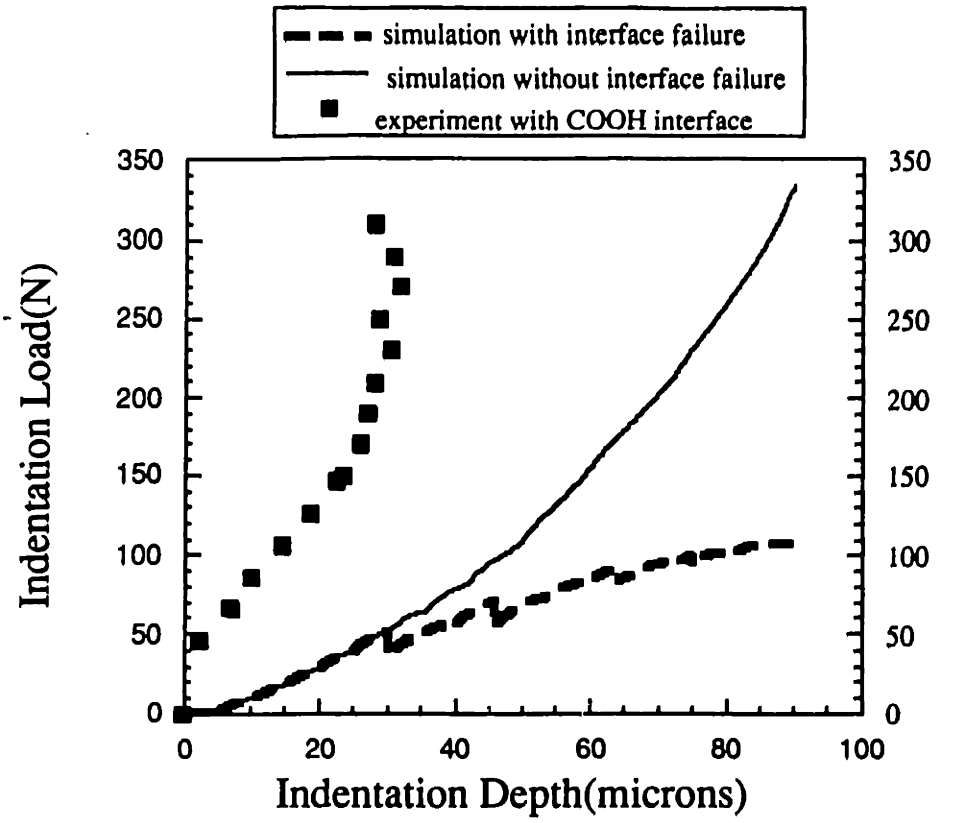

figure 5-21: comparison of load-displacement measurements between simulations with and without failure and experiments on the 100%COOH interface.

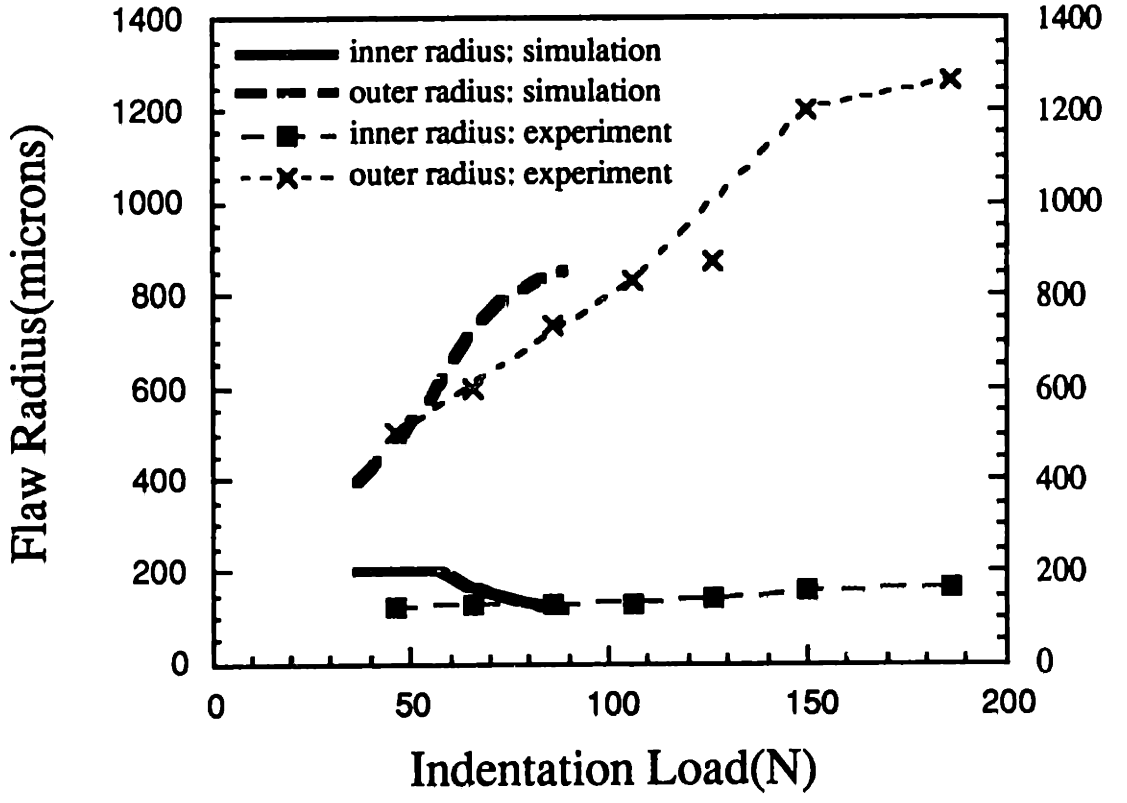

figure 5-22: comparison of inner and outer crack radii vs. load measurements between a simulation and experiments on the 50%CH_3/50%COOH

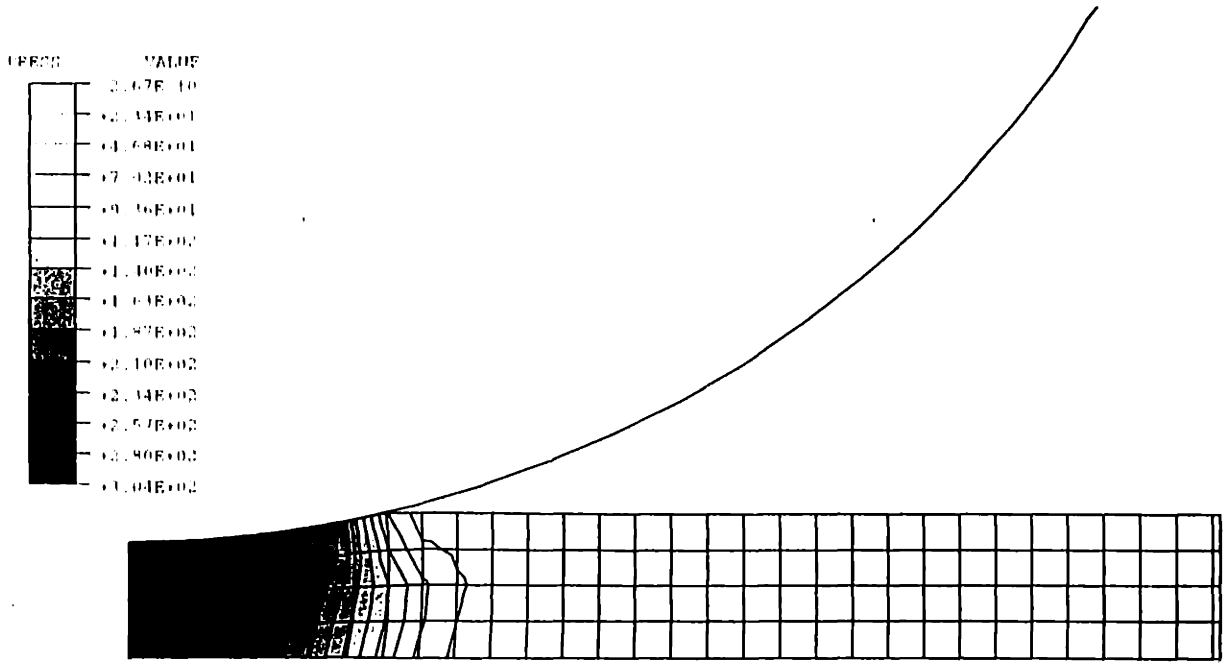

figure 5-23: sample pressure contour - indenter displacement = 20μm

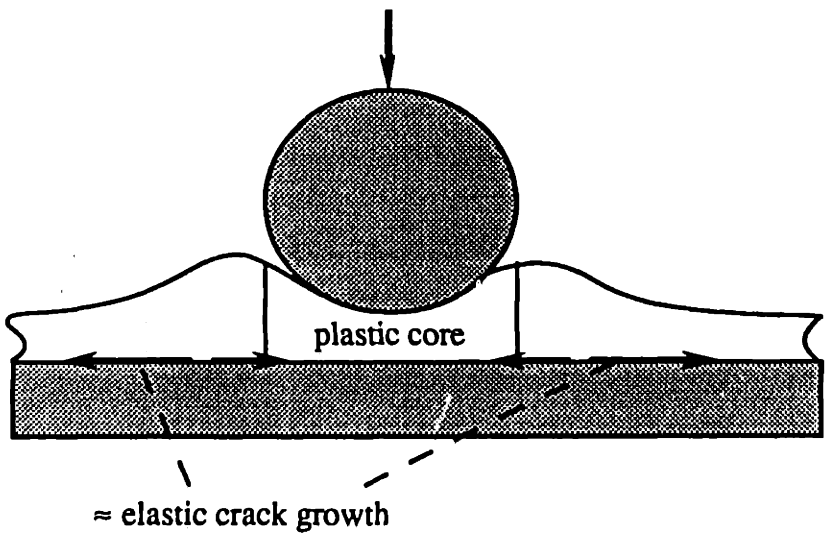

figure 5-24: The majority of the crack area is created within the elastically deforming portion of the film.

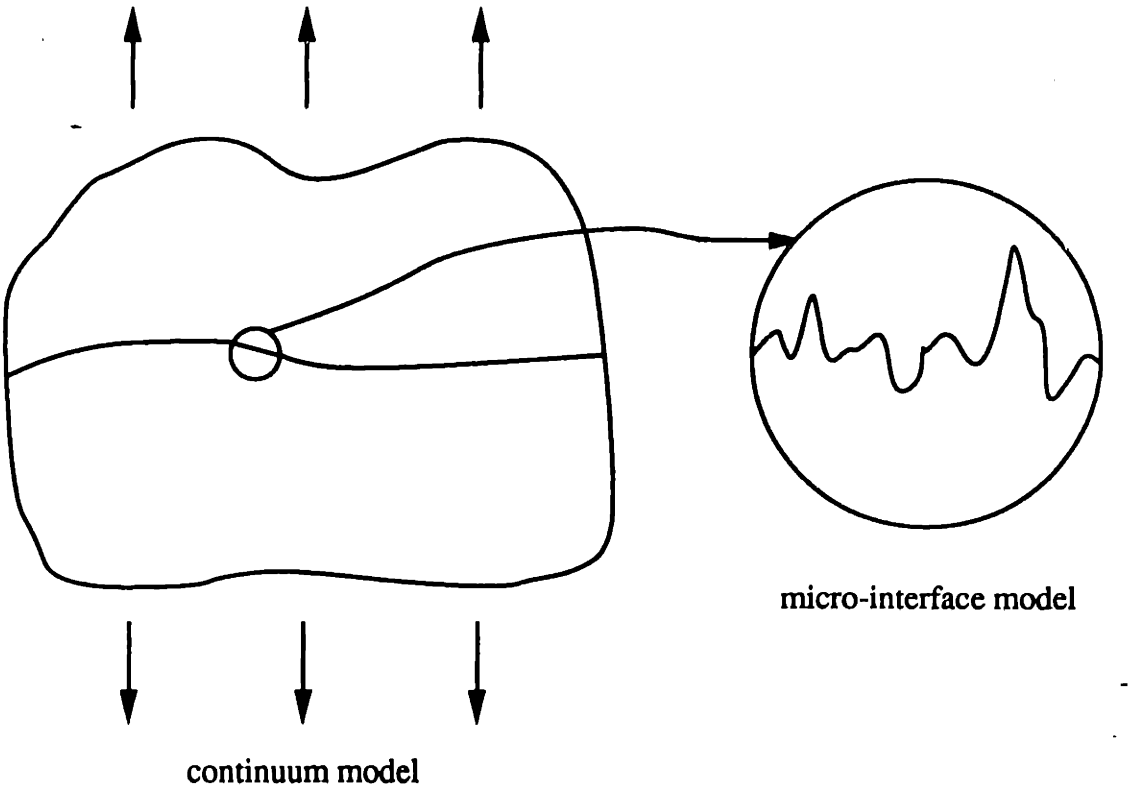

figure 5-25: Two size scales are indirectly coupled so that information from one scale is translated into conditions to be imposed at another scale.

References

[1] Griffith, A.A., The phenomena of rupture and flow in solids, *Phil. Trans. Roy. Soc of London*, A 221 (1921) pp. 163-197

[2] Griffith, A.A., The theory of rupture, *Proc. 1st Int/ Congress Appl. Mech.*, (1924) pp. 55-63. Biezeno and Burgers ed. Waltman (1925)

[3] Orowan, E., Energy criteria of fracture, *Welding Journal*, 34 (1955) pp.157s-160s

[4] Cherry, B.W., *Polymer surfaces*, (1981) Cambridge University Press.

[5] Kinloch, A.J., *Adhesion and Adhesives*, (1987) Chapan and Hall

[6] Bahchi, A., Lucas, G.E., Suo, Z., and Evans, A.G., A new procedure for measuring the decohesion energy for thin ductile film on substrates, *J. Mater. Res*, v9, n7 (1994) pp. 1734-1741

[7] McClintock, F.A., and Argon, A. S., *Mechanical Behavior of Materials*, (1965) Addison-Wesley Publishing Co.

[8] Wu, S., *Polymer Interface and Adhesion*, (1982) Marcel Dekker, Inc.

[9] Barber, J., R., *Elasticity*, (1991) Kluwer Academic Publishers

[10] Timoshenko, S.P., and Goodier, J.N., *Theory of Elasticity*, (1982) McGraw Hill

[11] Love, *A Treatise on the Mathematical Theory of Elasticity*, (1944) New York Dover Publications

[12] Sokolnikoff, I.S., *Mathematical Theory of Elasticity*, (1946) McGraw-Hill

[13] Dundurs, J., Discussion, *J. of Appl. Mech, v36,Trans. ASME*, v91, Series E (1969) pp. 650-652

[14] Williams, M.L., Stress singularities resulting from various boundary conditions in angular corners of plates in extension, *ASME J. Appl. Mech.*, 19 (1952) pp. 526-528

[15] Westergaard, H.M., Bearing pressures and cracks, J. *Appl. Mech.*, 61 (1939) pp. A49-53

[16] Broek, D., *Elementary Engineering Fracture Mechanics*, (1986) Kluwer Academic Publishers

[17] Kanninen, M.F., Popelar, C.H., *Advanced Fracture Mechanics*, (1985) Oxford University Press

[18] Irwin, G.R., Fracture, *Handbuch der Physik VI*, pp. 551-590. Flugge, Ed. Springer(1958)

[19] Hutchinson, J.W., Mixed mode cracking in layered materials, *Advances in Applied Mechanics*, 28 (1991)

[20] Hayashi, K., and Nemat-Nasser, S., Energy-release rate and crack kinking under combined loading, *J. Appl. Mech.*, 48 (1981) pp. 520-524

[21] Williams, M.L., The stresses around a fault or crack in dissimilar media, *Bull. Seismol. Soc. America*, 49 (1959) pp. 199-204

[22] Rice, J.R., A path independent integral and the approximate analysis of strain concentrations by notches and cracks, *J. Appl.Mech.*,(1968) pp.379-386

[23] Eshelby, J.D.,Calculation of energy release rate. In *Prospects of Fracture Mechanics*, pp.69-84, Sih, Van Elst, Broek, Ed., Noordhoff(1974)

[24] Erdogan, F., Stress distribution in bonded dissimilar materials with cracks, *J. Appl. Mech.*, v30 Trans ASME, v85 series E (1963) pp. 232-237

[25] England, A. H., A crack between dissimilar media, *J. Appl. Mech.*, v32 Trans ASME, v87 series E (1965) pp. 400-402

[26] Rice, J.R., and Sih, G.C., Plane problems of cracks in dissimilar media, *J. Appl. Mech.*, 32 (1965) pp. 418-423

[27] Comninou, M., The interface crack, *J. Appl. Mech.*, 44 (1977a) pp. 631-636

[28] Rice, J.R., Elastic fracture mechanics concepts for interfacial cracks, *J. Appl. Mech.*, 55 (1988) pp. 98-103

[29] Malyshev, B.M., and Salganik, R.L., The strength of adhesive joints using the theory of cracks, *Int. J. Fracture Mech.*, 5 (1965) pp. 114-128

[30] Evans, A.G., Ruhle, M., Dalgleish, B.J., and Charalambides, P.G., The fracture energy of bimaterial interfaces, *Mat. Sci. Eng.*, A126 (1990) pp. 53-64

[31] Zywicz, E., Parks, D., Elastic yield zone around an interfacial crack tip, J. of Applied Mech,v56(1989), pp.577-584

[32] Fraisse, P., Schmit, F., Use of J-integral as fracture parameter in simplified analysis of bonded joints, *Int. J. of Fract. Mech.*, v63(1993), pp.59-73

[33] S.E. Yamada, *Engineering Fracture Mechanics* 27(1987), pp.315-328

[34] G. Fernlund and J.K. Spelt, *Engineering Fracture Mechanics* 40(1991), pp.119-132

[35] Gent, A.N., Kinloch, A.J., Adhesion of viscoelastic materials to rigid substrates, III. Energy criterion for failure, *J. Polymer Science*, part A-2, 9 (1971) pp. 659-668

[36] Ballarini, R., and Plesha, M., The effects of crack surface friction and roughness on crack tip stress fields, *Int. J. Fracture*, 34 (1987) pp.195-207

[37] Evans, A.G., and Hutchinson, J.W., Effects of non-planarity on the mixed mode fracture resistance of bimaterial interface, *Acta Metall. Mater.*, 37 (1989) pp. 909-916

[38] Ungsuwarungsri, T., and Knauss, W.G., The role of damaged-softened material behavior in the fracture of composites and adhesives, *Int. J. Fracture*, 35 (1987) pp. 221-240

[39] Liang, Y.-M., and Liechti, K.M., Toughening mechanisms in mixed-mode interfacial fracture, (submitted to the *International Journal of Solids and Structures*, November 1993)

[40] Tvergaard, V., Hutchinson, J.W., The influence of plasticity on mixed mode interface toughness, *J. Mech. Phys. Solids*, 41 (1993) pp. 1119-1135

[41] Kardestuncer, H., *Finite Element Handbook*, (1987) McGraw-Hill.

[42] Suresh, S., *Fatigue of Materials*, (1991) Cambridge University Press

[43] Argon, A.S., Im, J., Safoglu, R., Cavity formation from inclusionsin ductile fracture, *Metall. Trans*, 6A (1975), pp.825-837.

[44] Strang, .G, Fix, J., *An analysis of the finite element method*, (1973) Prentice-Hall

[45] Bathe, .K.J., *Finite Element Procedures in Engineering Analysis*, (1982) Prentice-Hall

[46] Needleman, A., A continuum model for void nucleation by inclusion by inclusion debonding, *J. of Appl. Mech.*, v54(1987), pp.525-531

[47] Tvergaard, V., Effect of ductile particle debonding during crack bridging in ceramics, *Int. J. of Mech. Sci.*, v34 no.8(1992), pp.635-649

[48] Nicholson, D.W., On the detachment of a rigid inclusion from an elastic matrix, J. Adhesion, v10(1979), pp.255-260

[49] Gent, A. N., Hamed, G. R., Peel mechanics, *J. Adhesion*, v7(1975), pp.91-95

[50] Jensen, H.M., Cochelin, B., Fracture analysis of the constrained blister test, *Danish Center for Applied Mathematics an dMechanics* (1993)

[51] Bagchi, A., Lucas, G.E., Suo, Z., Evans, A.G., A new procedure for measuring the decohesion energy of thin ductile films on substrate, *J. Mater. Res.*, v9 no7(1994), pp.1734-1741

[52] Chalker, P.R., Bull, S.J., Rickerby, D.S., A review of the methods for the evaluation of coating-substrate adhesion, *Materials Science and Engineering*, A140(1991), pp.583-592

[53] Lin, M.R., Ritter, J.E., Rosenfeld, L., Lardner, T.J., Measuring the interfacial shear strength of thin polymer coatings on glass, J. Mater. Res., v5 no5(1990), pp.1110-1116

[54] Mathewson, M.J., Ritter, J.E., Adhesion measurement of thin polymer films by indentation, to appear as a chapter in the book *Characterization Techniques for Thin Polymer Films* (edited by L.T.Nguyen and H.M. Tong)

[55] Rickerby, D.S., A review of the methods for the measurement of coating-substrate adhesion, *Surface and Coatings Technology*, 36(1988), pp.541-557

[56] Zhuk, A.V., Knunyants, N.N., Oshmyan, V.G., Topolkaraev, V.A., Berlin, A.A., Debonding microprocesses and interfacial strength in particle-filled polymer materials, Journal of Materials Science, v28(1993)

[57] Goodier, J.N., Concentration of stress around spherical and cylindrical inclusions and flaws, *Trans. of the ASME*, v55(1933)

[58] Lanczos, *Variational Principles of Applied Mechanics*

[59] Wu, S., *Polymer Interface and Adhesion*, (1982) Marcel Dekker, Inc.

[60] Strang, G., *Linear Algebra and Its Applications*, (1982) Academic Press

[61] Voyutskii, S.S., *Autohesion and Adhesion of High Polymers*, (1963) John Wiley & Sons, Inc.

[62] Ashby, M.F., Jones, D.R., *Engineering Materials I*, (1980)Pergamon Press

[63] Ritter, J.E., Rosenfeld.R., Lin, M.R., Lardner, T.J., Interfacial shear strength of thin polymeric coatings on glass, *Mat. Res. Soc. Symp. Proc.*, v130(1989), pp.237-242

[64] Mathewson, M.J., Adhesion measurement of thin films by indentation, Appl. Phys. Lett., 21(1986), pp.1426-1428